Particle Formation of Smelt in a Fluidized Bed

A thesis submitted by

Jason C. Huff

B.M.E. 1994, Georgia Institute of Technology, Atlanta

M.S. 1996, Institute of Paper Science and Technology, Atlanta

in partial fulfillment of the requirements

for the degree of Doctor of Philosophy

from the Institute of Paper Science and Technology

Atlanta, Georgia

March 2001

COMMITTEE APPROVAL PAGE

PARTICLE FORMATION of SMELT IN A FLUIDIZED BED

(Dissertation Title)

Institute of Paper Science and Technology
Atlanta, Georgia

A dissertation submitted by: JASON Huff

Date: 3/22/01

Members of this Dissertation Defense Committee hereby affirm that the defense was successful and that all required corrections have been effected.

Defense Committee:

Member: [signature] Date: 3/22/01
(Signature)
Wolfgang Schmidl
(Typed full name)

Member: [signature] Date: 03/22/01
(Signature)
SEPPO KARRILA
(Typed full name)

Member [signature] Date: 03/21/2001
(Signature)
PREET M. SINGH
(Typed full name)

Advisor: [signature] Date: 03/22/01
(Signature)
H.J. Empie
(Typed full name)

Chair: [signature] Date: 3/22/01
(Signature)
Junyong ZHU
(Typed full name)

TABLE OF CONTENTS

LIST OF FIGURES

LIST OF TABLES

ABSTRACT

Experiments have been conducted to determine the effect of fluidization regime on particle formation in a fluidized bed molten smelt solidifier. Particle formation, as defined by this project, is the mechanism and rate of bed particle diameter change. Three particle-change mechanisms were considered in this project: attrition, coating, and agglomeration. Attrition is defined as particle shrinkage due to fluidized bed forces breaking them apart. Coating is defined as particle growth by layering and solidification of molten smelt onto individual particles, while agglomeration is defined as particle growth resulting from molten smelt binding and solidifying bed particles together.

The fluidized bed used in this project consisted of a known size distribution of solid model smelt particles fluidized in a 6.5 cm diameter by 43.2 cm high reactor, with the capability of feeding molten model smelt into the top of the bed. To avoid the high corrosivity of smelt, a eutectic mixture of $NaNO_3/KNO_3$ was used as a model smelt. A factorial design was used to determine the effect of fluidization regime on particle formation in the presence of changes in bed operation.

Fluidization regime was determined to have a significant effect on particle growth rate, but not the mechanism of particle growth. The growth rate of particles in the bed was determined to be the result of both agglomeration and coating, but the effect of agglomeration was determined to be dominant. Fluidization regime had an effect on the size of agglomerates formed, which resulted in differences in particle growth rate. These results were determined to be due to greater mixing and heat transfer of the turbulent bed,

which separated particles bound by molten salt and limited the amount of molten phase salt resident in the system by freezing it more quickly. Attrition of seed particles had no effect on particle formation.

NOTATION

D	Sampling position in bed
d_{bed}	Diameter of the bed
d_P	Equivalent spherical diameter
$\bar{d}_P$	Volume weighted mean particle diameter of bed (D_{43})
$\bar{d}_{Po}$	Mean particle diameter of seedbed particles
d_m	Sampler porthole size
d_s	Diameter of sampler
F_0	Mass feed rate of molten material to the bed
g_c	Dimensional constant used to represent force
H	Height of the fluid bed
h	Heat transfer coefficient
ΔH_f	Latent heat of fusion for salt.
J	Dimensional constant used to represent heat
k	Thermal conductivity
T_{mp}	Melting point temperature of the liquid feed
ΔT	Difference between T_{ms} and T_{mp}
u_0	Superficial gas velocity
u_1	Bubbling bed superficial gas velocity
u_2	Turbulent bed superficial gas velocity
m_{bed}	Mass of solid material in the fluid bed

Greek

ε	Void fraction
μ	Fluid viscosity
ρ	Density
σ	Surface Tension

Subscripts

L, g	Denotes property of the liquid feed or gas
0, 1, 2	Denotes overall value, into bed, out of bed
ms	Property of the molten stream
s	Surface property of molten particle or solid
G	Denotes particles that grew
F	Denotes particles that formed
Upper	Denotes upper sampling position
Lower	Denotes lower sampling position

INTRODUCTION

The flow of molten smelt from the recovery boiler into the smelt-dissolving tank is extremely hot and corrosive, making the control of that flow impossible with traditional valves. One of the main benefits of controlling this flow would be to control the resulting concentration of green liquor produced in the smelt-dissolving tank. This controlled concentration could then be used to increase the effectiveness of downstream unit operations by providing them with a steady state concentration as opposed to one that is constantly fluctuating.

A patented process has been developed to control the flow of smelt into the smelt-dissolving tank.[1] This process uses a fluidized bed to solidify the molten smelt leaving the recovery boiler making it much easier to handle. This solid smelt can then be added to the bottom of the smelt-dissolving tank with conventional solids conveying equipment. A further benefit of this process is the elimination of exhaust steam generated from injecting the hot smelt into the top of the dissolver.

The extremely high rates of mixing and heat transfer of a fluidized bed are used to break up the entering stream of molten smelt and then solidify it into particles.
The size of these particles is important to the effective operation of the bed. If particles form too small then they will be blown out of the bed. If they form too large and too fast then the fluid bed will collapse.

Current fluidized bed processes are able to predisperse sticky material to form relatively even and controlled particle growth through either coating or controlled

agglomeration. This process however, because of the extremely corrosive nature of smelt, is not able to do this. It is therefore the purpose of this dissertation to determine the rate and mechanism of particle formation, whether by coating or agglomeration, of a fluid bed in the presence of a concentrated stream of molten salt. Three key operating variables related to mixing and heat transfer have been isolated for study in this project. The first, fluidizing regime, is an indication of the overall mixing and heat transfer in the bed. Flow rate and temperature of the molten salt stream were also chosen because of their relationship to bed size and operability.

A bench scale fluidized bed has been constructed for this project with the capability to inject molten salt into the top of the bed. Samples are taken with the use of an in-bed sampler simultaneously from the upper and lower sections of the bed. These samples are then analyzed using optical microscopy and image analysis to determine their size and mechanism of formation.

LITERATURE REVIEW

Overview of Fluidization

Fluidization is the mixing of small solid particles by a flowing fluid (gas or liquid) in such a way that the entire mixture behaves like a fluid. A fluid bed starts as a pile of solid particles stacked on top of one another (fixed bed) with gas flowing up through the pile. As the flow of gas increases, pressure builds up along the pathways of the gas through the fixed bed. This pressure is eventually large enough to separate the particles from one another, which expands the pathway of the gas through the bed. This is the onset of fluidization. Pressure across the bed will remain constant with increasing fluid velocity as seen in Figure 1. [1-4]

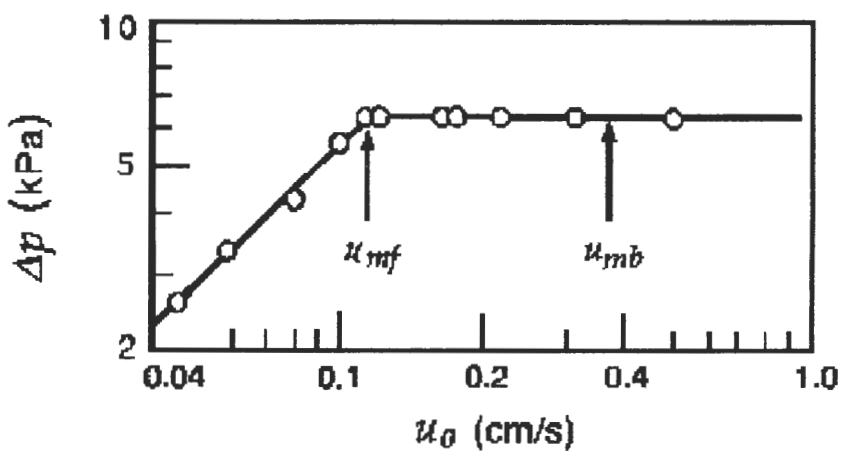

Figure 1. Relationship of pressure and gas velocity in fluidization. Where ΔP is the pressure drop of the gas across the bed, u_0 is the superficial gas velocity, u_{mf} is the minimum fluidizing velocity, and u_{mb} is the onset of a bubbling bed.[2]

The state at which particles are just suspended by the stream of fluid is referred to as an incipiently fluidized bed or a fluidized bed at minimum fluidization . This fluid

velocity is referred to as the minimum fluidization velocity (u_{mf}). At this time the pressure drop across the bed is equal to the weight of the fluid and particles in the bed.[2,6]

Fluid Bed Mixing

Mixing in fluid beds may be broken down into two scales, macro and micro mixing. Macro mixing deals with flow patterns and turbulence of the fluid while micro mixing deals with molecular transport phenomena. The larger scale particle motions in the bed are caused by vertical velocity profiles.[7] These vertical gas velocities induce mixing on a much smaller scale by turbulent motions such as eddies. These turbulent motions create a smaller scale mixing in the lateral direction. The greater the turbulence, the smaller the concentration differences seen in a cross section of the bed due to these eddies.[8]

Heat Transfer in Fluidized Beds

Heat transfer in a fluidized bed is a function of convective and radiation mechanisms. Heat is introduced into the bed via material introduced to the bed or by generation such as in combustion. Heat may also be absorbed due to endothermic reactions such as carbonate formation or the reduction of sodium sulfate in black liquor recovery.[9] Fluidized beds have excellent heat transfer characteristics due largely to the high amount of surface area available for heat transfer and the large amount of fluid with which this surface comes into contact.[10]

Convection

Convection is the process by which gas collisions impart their heat to the surface of a solid by momentary conduction and are then carried away by a bulk flow. In the case of a fluidized bed without generation where the fluid is well mixed, the heat capacity of the fluid is far less than that of the particles (three orders of magnitude) and therefore the temperature of the fluid moves quickly toward the temperature of the particles.[3] The rate of heat transfer in the bed is related directly to the velocity of the fluid stream for smaller particles[3] but has been found to be essentially independent of rate of heat transfer with large particles.[11] Therefore, small particle fluidized beds will be more affected by fluid velocity than larger ones.

Convection may further be broken down in a fluidized bed by either particles or gas. The two are similar in that they both deal with momentary contact between two objects in order to transmit heat energy. Particle convection, however, is heat transfer by the contact of particles on a surface while gas convection is the contact of gas molecules.[3]

Radiation

Radiation is the transfer of energy via electromagnetic waves and needs no direct contact with the object being heated. It is a function of the temperature and the emissivity or the ability of the body to absorb, transmit, reflect or store radiated heat energy. All objects in the bed, which are visible to another object, may heat or be heated by those objects. Heat transfer in a bed by radiation is not determined to be appreciative until the temperature of the bed is 600°C.[3]

Elutriation

There are size distributions seen in fluid beds that are affected differently by the fluidizing gas. A fractionation of particle size occurs within the bed referred to as elutriation.[12,13] This is the result of fluidizing gas reaching the terminal settling velocity of the elutriated particle where the drag on the particle caused by the fluidizing gas is greater than the weight of the particle, which allows the particle to be carried up and out of the bed (pneumatic conveying). This preferential fractionation according to particle size as a function of fluid velocity may be seen in Figure 2.[2]

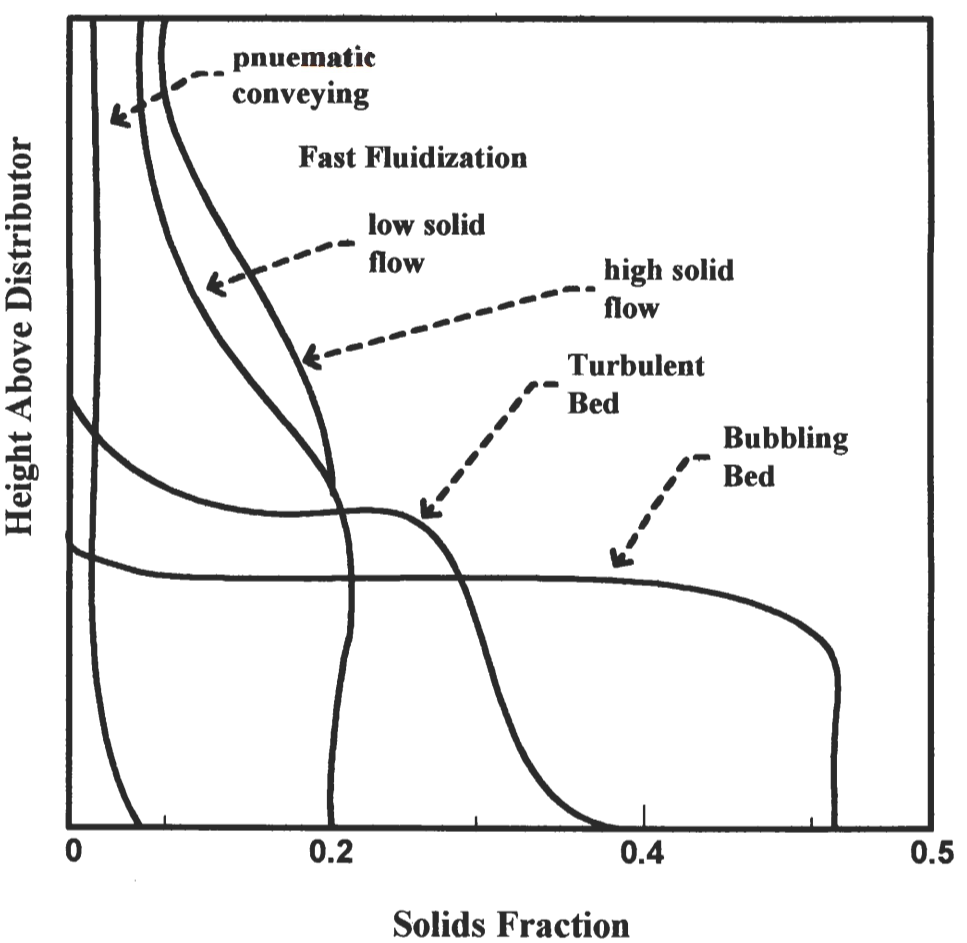

Figure 2. Preferential fractionation of particles a different fluid regimes [2]

Fluidization Regimes

Homogeneous Fluidization Regime

This region of fluidization is limited to a lower velocity very close to the minimum fluidizing velocity and is limited to fluidization with smaller, lighter particles. This regime is the homogeneous mixture of solid particles and gas with the absence of bubbles. Concentrations of particles and gas are uniform throughout this regime with little mixing occurring.[14, 22]

Bubbling Bed Regime

As fluidizing gas velocity continues to increase to the minimum bubbling velocity(u_{mf}), bubbles begin to form in the bed. This marks the beginning of bubbling bed regime.[2]

Fast Bubbles

This phase is shown to mark the onset of bubbling in which a small rapid succession of bubbles flows up through the bed. The overall velocity of the gas through the mixture of particles in this regime is slower than the velocity of the bubbles.[15] Mixing in this phase is accomplished by motion of the particles in the bubble wake and cloud.[16,17] Bed material is swept around the bubble and caught up in its wake to then be drawn partially into the bubble as seen in Figure 3.[15]

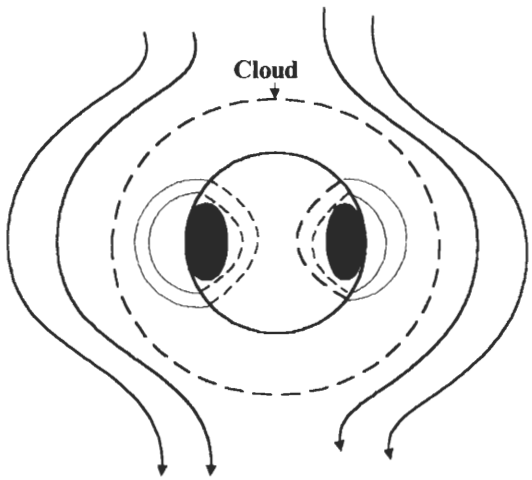

Figure 3. Flow of bed relative to fast bubble [16,17]

Slow Bubbles

Large bubbles moving slower than the interstitial fluid velocity of the fluidizing gas mark the slow bubble regime. The interstitial fluid flows rapidly through the void space of the bubble, as can be seen in Figure 4.[15] Bubbles increase in size as particle size increases and bubble growth size increases until the onset of turbulance.[22]

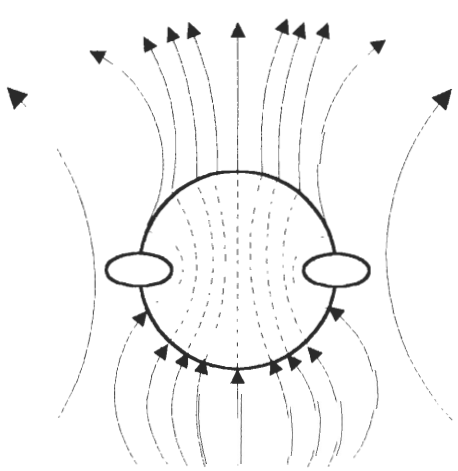

Figure 4. Flow of bed relative to a slow bubble [15]

Large bubbles may lead to the loss of bed material as they break the surface of the bed and throw bed material into the freeboard area above the bed. Fine particles within the fluidized bed will decrease the occurrence of these large bubbles by acting as a lubricant between the larger particles thus giving smoother fluidization.[18]

Turbulent Bed

The turbulent bed is characterized by regions of high and low particle concentrations on a scale much smaller than that seen in the bubbling bed.[19,20] The back mixing of particles seen in the bubbling bed is reduced in the turbulent regime where mixing is performed at a smaller scale.[22] This reduction of back mixing of particles is a transition to the fast fluidization regime.[2]

Fast Fluidization

Fast-fluidized beds are characterized by the high rate of elutriation or entrainment of smaller particles. These smaller particles are carried up through the fluid bed through larger bed particles. These particles are eventually circulated back to the bottom of the bed where they are again entrained through the bed and out the top. The larger, denser particles fractionate as in a bubbling bed, while the smaller, less dense particles in the rest of the bed are essentially uniform.[6,21] The use of a cyclone cleaner helps in the removal of the material from the gas during this circulation.[2,3]

Fluid Bed Design

Gas Distributor

Although there are variations on geometry and size, a fluid bed is essentially a tube with a perforated plate at the bottom. This plate or gas distributor is important because it determines how gas flows into the fluidized bed and thus the properties and uniformity of gas flow within the bed. It also provides a lower limit for travel of bed particles. Distributors have three basic designs. Examples of these designs can be seen in Figure 5.[3]

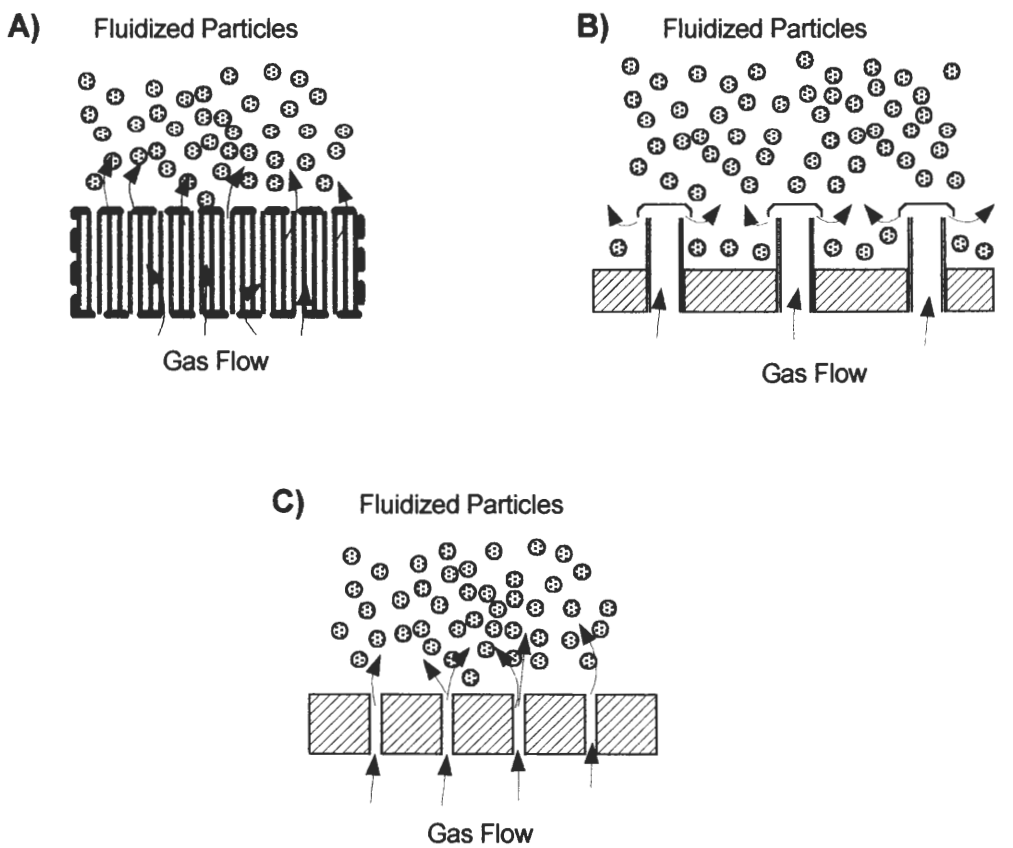

Figure 5. Various distributor designs [3]

These designs vary in complexity and are chosen to suit the particular application of interest. For example, distributor B or a stand pipe distributor, is useful in high

temperature applications where it allows particles to accumulate on top of the distributor thus shielding it from the heat in the bed. Distributor A is a porous material and provides very uniform gas flow but a high pressure drop which limits the overall flow of gas through it. Distributor C is a plate with holes making it cheap and easy to produce. [2,3]

Seed Bed Particle

A system of particle description has been devised by Geldart in which particles are categorized by their size, density, and the behavior of that size particle in a fluidized bed.[2] This system is summarized in the following:

Group A ($\rho < \sim 1.4$ g/cm3) These materials have a small average particle size and/or a low density. These particles fluidize easily. Bubbling is controlled with small bubbles at fast gas velocities.[2,3,4]

Group B ($1.4 < \rho < 4$ g/cm3) These particles fluidize well with vigorous bubbling action and bubbles that grow large.[2,3,4]

Group C Cohesive properties make these particles difficult to fluidize. Very fine powders represent them.[2,3,4]

Group D Representative of large and/or dense particles. Deep beds of these particles are difficult to fluidize. They behave erratically, giving large exploding bubbles or severe channeling, or spouting behavior if the gas distribution is uneven.[2,3,4]

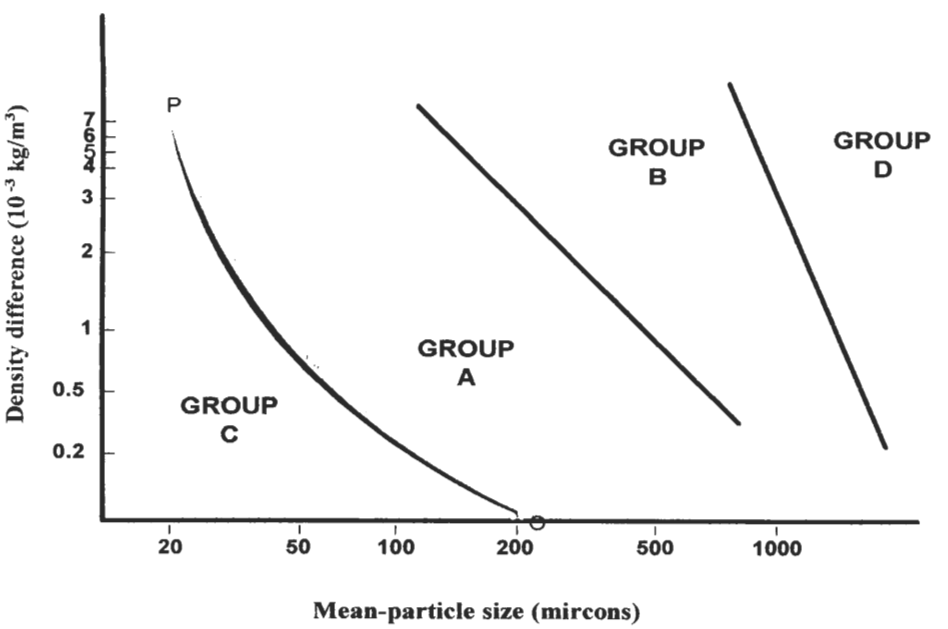

Figure 6. Relative size density of particles according to the Geldart system [3]

Effect of Particle Size on Fluidization Regime

The fluidization regimes discussed previously are not only a function of the fluidizing gas velocity (superficial gas velocity) but also of the type of particles fluidized in the bed. The following diagram (Figure 7) explains the relationship between the Geldart particle classification and superficial gas velocity (u_o) in determining the type of fluidization in the bed.[8,22]

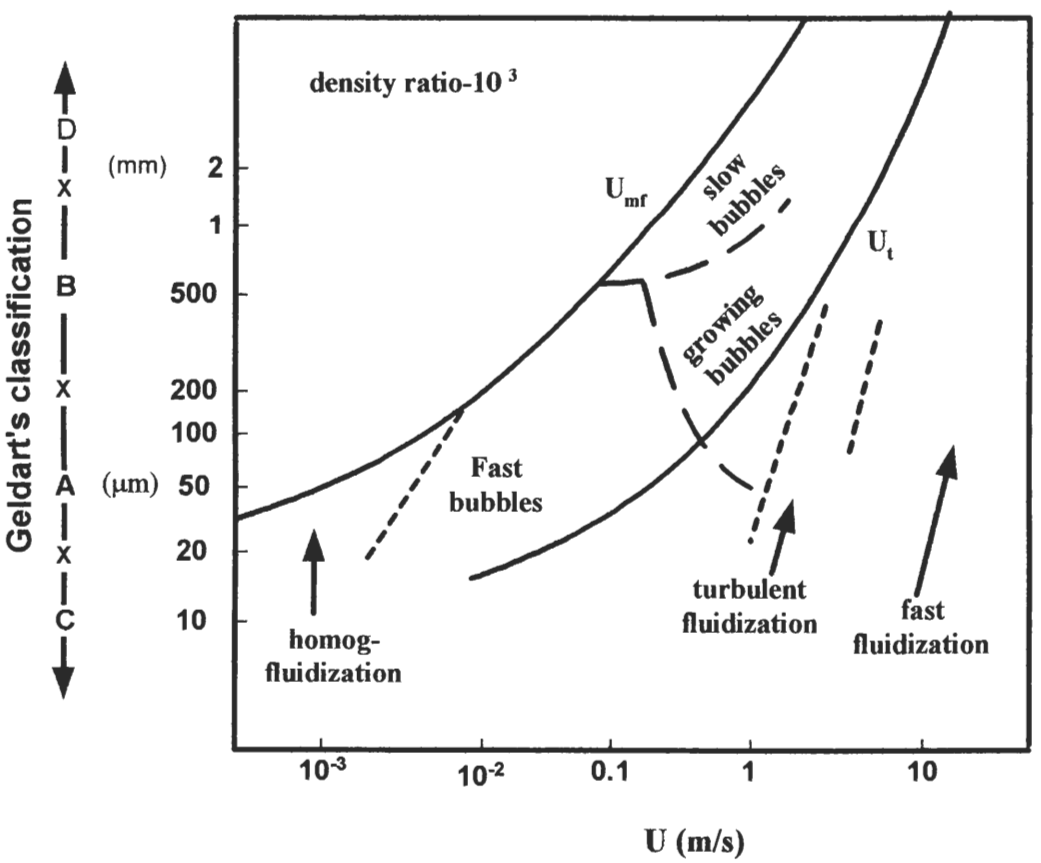

Figure 7. Fluidization Regimes as a Function of Particle Size and Fluid Velocity [8]

Particle Formation

The forces that bind and strengthen particles and those forces that wear away and break up particles determine particle formation. In a continuous operation, any change to the particle size distribution in the bed due to particle shrinkage or growth can be adjusted by the addition and removal of material in order to maintain the desired particle size distribution and bed volume as seen in Figure 8.[2,23] The rate of growth or shrinkage must be known to establish the rate of material removal of over and undersized material and the rate of introduction of the desired size particles.

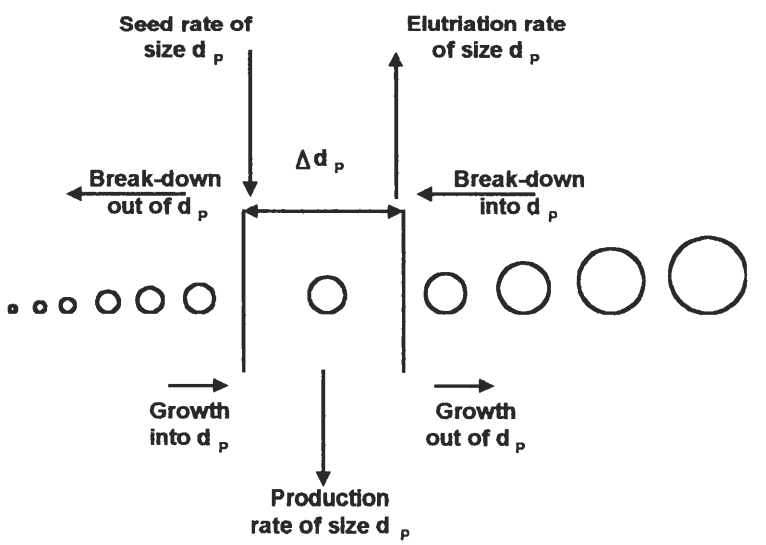

Figure 8. Mass balance of particles[23]

Particle Growth

In order for particle growth to occur, sticky bed material must combine with seedbed particles. Particle growth is a function of the stickiness of the material, the amount of available area for bonding, and time of contact.[24] These variables may occur in different routes for particle growth to occur, which are discussed later in this section.

Particle stickiness and available bonding area are strongly affected by the viscosity and surface tension of material in the bed.[25] Viscosity and surface tension decrease as the temperature of the sticky material increases. This decrease in viscosity with temperature increases the ability of the molten drops to spread over solid particles at contact thereby increasing the surface area of contact. This increased contact surface area enables more bonding to take place between the particle and sticky material resulting in a stronger final particle.[26]

The temperature of sticky material is a function of the amount of heat transfer in the bed. The amount of heat transfer is a function of the velocity and mixing of fluidizing gas (increased velocity leads to increased convection), the available surface area on which heat transfer can take place and the ability of the fluidizing gas to absorb and hold heat. A faster rate of heat transfer away from the molten smelt particles will lead to a faster increase in the viscosity and the surface tension[27] of the sticky material until finally the solid and no longer sticky. The increase in the rate of molten salt solidification will decrease the overall amount of molten salt in the system and may therefore decrease the number of particles that are able to agglomerate. This, in turn, may lead to a decrease in particle growth rate.[26,28]

Other factors that influence particle growth rate, include the fluidizing velocity and the initial particle size.[26] Velocity of gas provides excess kinetic energy, which will break particles up (Figure 7).

Growth Mechanisms

Particles may grow by one of two routes. The first route is the agglomeration or combination of particles by a sticky material resulting in a single particle. The second route is coating or layer growth of sticky material on the surface of individual particles. An example of the relative growth rates of each mechanism with respect to fluidizing velocity can be seen in Figure 10.[40]

Agglomeration

Agglomeration is the combination of multiple seed particles in order to form a much larger particle.[29] The agglomeration of particles leads to rapid particle growth due to the large amounts of volume that are added with each new particle addition as compared to coating. The potential for this rapid particle growth can be seen in Figure 11[40] where the agglomerated particle size increases as multiples of the smaller particle sizes.[20-23] This may be accomplished by a wet (having a liquid surface, possibly molten) particle drawn together to another particle by surface tension forming one large particle. This mechanism may also occur if one or more particles plastically deform over one another.

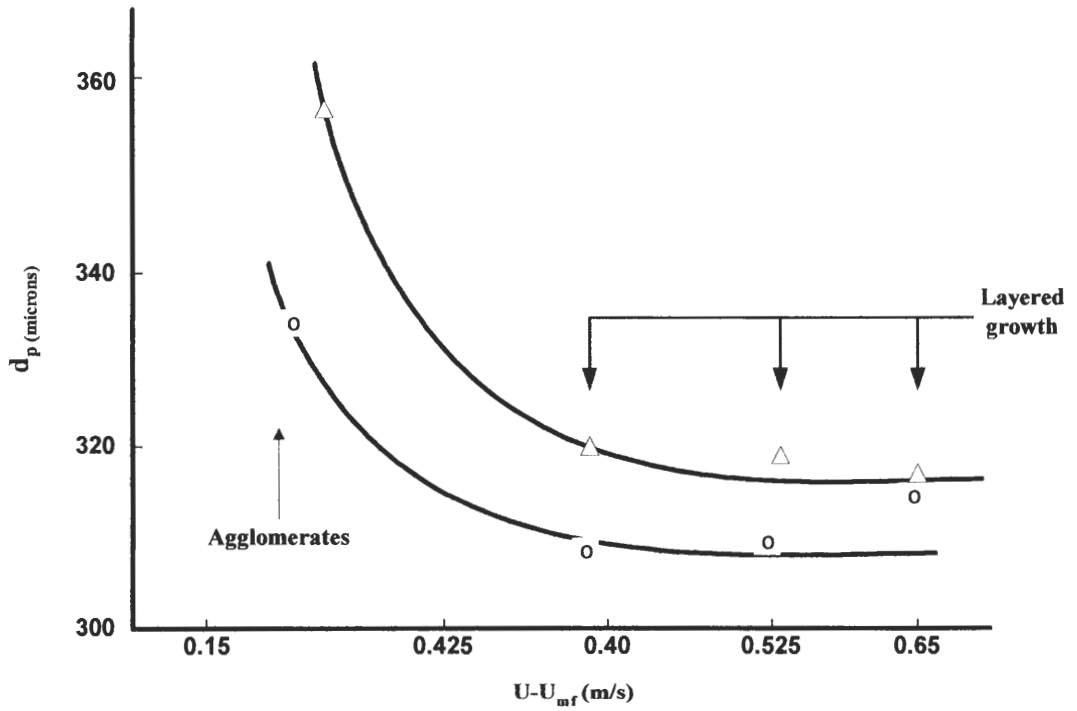

Figure 9. Relative areas of agglomeration and layer growth with respect to velocity[29]

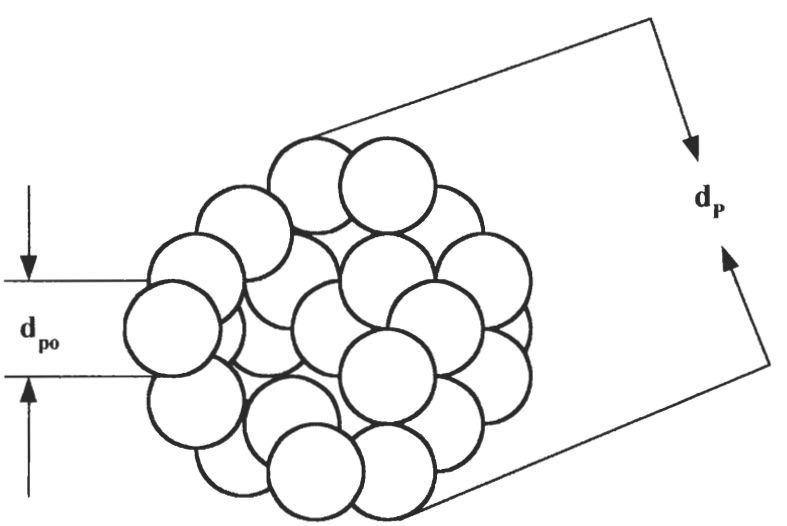

Figure 10. Fast rate of particle growth through agglomeration [3]

The mechanisms by which particles agglomerate is a function of the surface condition and area of contact available between agglomerated particles. These mechanisms are described in Table 1.

Table 1. Mechanism of Particle Agglomeration[34]

COMBINATIONS	DESCRIPTION
Eutectic	**Two solid particles are held together by a patch of molten material between them**
Plastic Deformation	**Solid particles contact and conform to one another at their common interface due to the viscous flow of the high temperature molten material**

Agglomerate Strength

Particle strength or green strength is increased by the amount of bonding at the interface of agglomerated particles. This interfacial bonding is increased by the plastic deformation of the particles together or by sintering. The impact of either of these processes is enhanced with temperature and time.

Plastic Deformation

Plastic deformation increases the amount of surface available for contact between two particles by allowing a particle to flow into and over the surface of another. This allows for intimate joining of the surfaces and therefore the potential for strong bonding. Plastic deformation is mainly a function of viscosity. As a particle's viscosity decreases with increasing temperature, it is easier for the particle to flow over other particles.

Sintering

Sintering strengthens bonding by molecular diffusion across the interface of agglomerated particles. It occurs at approximately 2/3 of the melting point and increases until the melting point. Molecular diffusion causes the formation of a common grain between agglomerated particles. An entire particle may diffuse into another particle (smaller particles will diffuse into larger ones due to surface tension effects).[36]

Sintering may be defined as the "consolidation of a powder by means of prolonged exposure to elevated temperatures which are, below the melting point of any phase" of the solid.[24-27] Sintering is accomplished via three mechanisms: (1) Transport by lattice diffusion or from within the particle to the intersection of both particles, (2) Transport by evaporation and condensation or from the surface of the particle to the intersection of both particles, (3) A liquid in which the particle or particles dissolves the surface material of the particles and then evaporates leaving a solid bridge between the two particles.[35] These different mechanisms may be seen in Figure 12 and 13. Material migrates to the interface between the two particles both through the lattice inside the particle and as a gas condensing at the particle intersection.

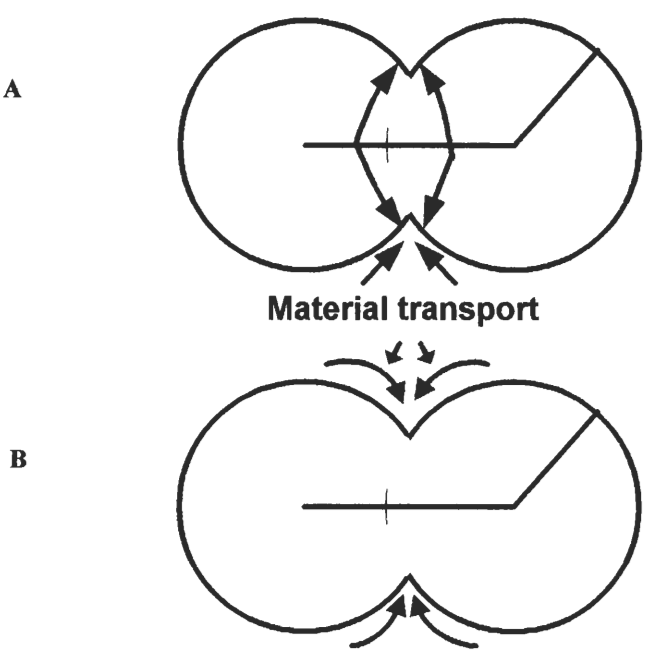

Figure 11. Sintering of particles by (a) lattice diffusion and (b) evaporation condensation[7]

As the liquid bridge between the particles evaporates, a solid bridge is formed by the material dissolved in the solvent, thus binding the particles together.

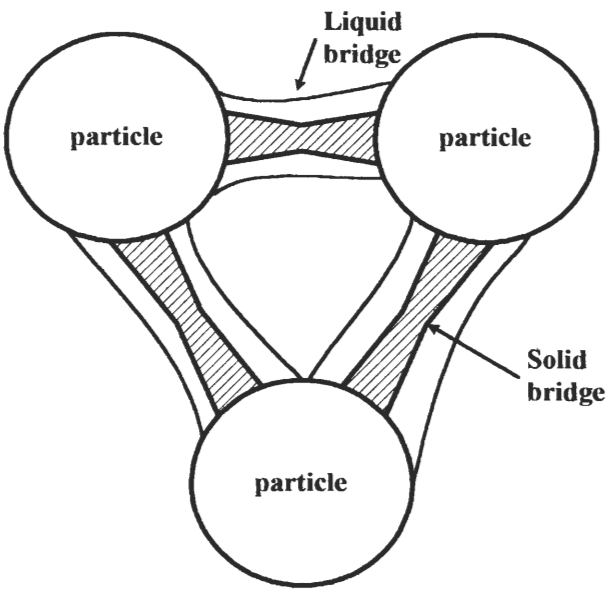

Figure 12. Sintering of particles by liquid phase[29]

Coating

Coating or layer growth is caused by a sticky material bonding to the outside of a single seed particle and then losing its sticky properties before it has an opportunity to form an agglomerate by attaching to another seed particle. The size of this layered or coated particle grows in proportion to the amount of sticky material collected on the surface of that particle. In the case of this project, molten salt droplets act as the sticky material and coat the outside of a cool particle and freeze on the surface forming a layer.[29,38,40]

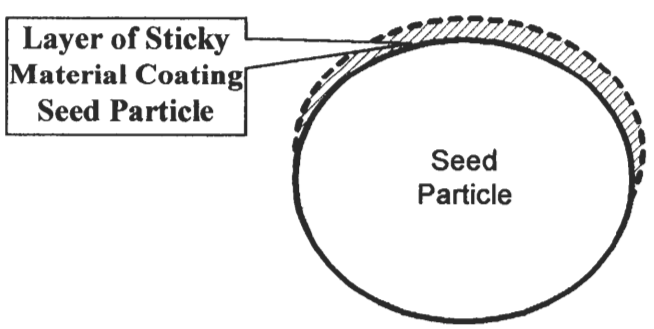

Figure 13. Seed particle coated with solidified molten salt

Particle Shrinkage

Particle Attrition

Attrition is the result of kinetic energy in the system breaking up particles balanced against the strength of those particles to resist breakup. Attrition has a greater effect on the larger agglomerates as opposed to the seedbed. This can be seen in Figure 14 where gas velocity and particle size are plotted with time. Kinetic energy increases as a result of increases in the superficial velocity of the system. If particles are uniformly and vigorously mixed (such as in a turbulent or a fast bed), then particle growth is slowed.[40,41] This is further shown in Figure 14 where particle growth rate is greater for the particle formed in a bed with a lower superficial velocity.

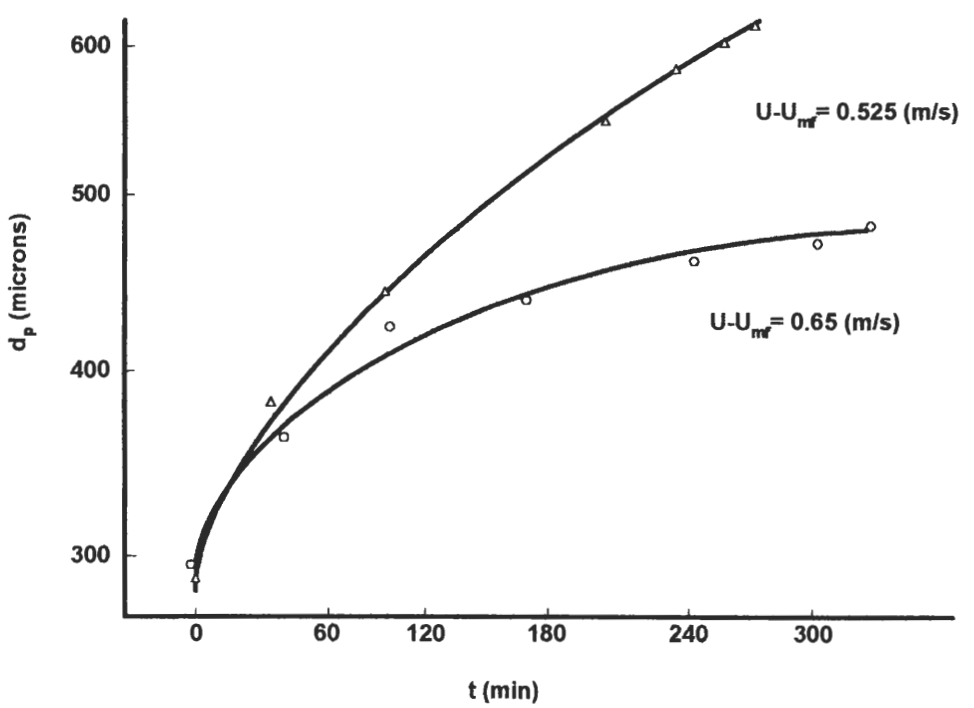

Figure 14. Negative effect of velocity on particle size over time[19]

Mean Particle Diameter

In order to define mean particle diameter, particle diameter must first be defined. Particle diameter, as used here, is the equivalent spherical diameter or the diameter of a sphere with the same volume of the particle being represented.[42] Mean particle diameter is a way to represent the total mass of particles.[43] Mean particle diameter can be defined many different ways. Listed below are a few.

1. Number Weighted Mean Diameter (D_{10}) [43,44]

This term gives the average diameter of the distribution, based on the number of particles in the distribution. This term can be used to determine the probability of a particle of a certain diameter occurring in a distribution of particles. The calculation can be observed in Equation 1.[43,44]

$$D_{10} = \frac{\sum n_i d_i}{\sum n_i} \qquad \textbf{Eqn 1}$$

2. Area Weighted or Sauter Mean Diameter (D_{32}) [43,44]

This term gives the moment about the origin as determined by the surface area of particles in the distribution. It is very often used in spraying where evaporation or combustion is involved due to its strong emphasis on surface area (A) of the particles for mass transfer. This makes sense, because combustion and evaporation take place at the surface of the particle, which means that it would have a strong effect on both of these operations. The calculation for this mean diameter can be seen in Equation 2.[43]

$$D_{32} = \frac{\sum n_i d_i^3}{\sum n_i d_i^2} = \frac{\sum_1^N A_i d_i}{\sum_1^N A_i} \qquad \textbf{Eqn 2}$$

3. Volume Weight Mean Diameter (D_{43}) [43]

This term gives the moment about the origin as determined by the volume of particles in the distribution. This calculation for this mean diameter can be seen in Equation 3 (c.f. p. 72).[43]

$$D_{43} = \frac{\sum n_i d_i^4}{\sum n_i d_i^3} = \frac{\sum_1^N (V_i) d_i}{\sum_1^N V_i} \qquad \textbf{Eqn 3}$$

Defluidization

In order for particles to remain fluidized in the bed, they must remain within a given size range. If particles become too small, they are elutriated out of the bed; if they become too big, they become too heavy for the bed to support and fall out of the bed.[2] It is for this reason that an understanding of the effects of bed operation on particle size distribution is important.

Defluidization as a Result of Particle Growth

When the weight of a particle, as a result of growth, exceeds the upward force that the gas exerts on it to keep it fluidized, the particle will fall out of the bed. The rate that this occurs affects the stability of the bed. If this rate is relatively slow, then material that has grown too large can be removed and new seedbed material can be put in its place in order to preserve the bed volume. If growth occurs too quickly, it can result in a particle that is too large to remove from the bed or the defluidization of the fluidized bed.[29,40]

Defluidization as a Result of Particle Shrinkage

Attrition of Particles

When the fluidizing velocity exceeds the terminal velocity of a particle formed as a result of particle attrition, the particle will be carried up and out of the bed, or elutriated.[2] The rate that this occurs, as with particle growth, affects the stability of the bed.

Current Technology

Overview of Recovery Process

The kraft recovery process has two basic purposes. The first purpose is to recover the inorganic components of black liquor, which are regenerated and used for cooking wood chips for pulp production. The second is to recover thermal energy through the combustion of the organic component of black liquor. The recovered pulping chemicals can then be used to pulp more wood chips, and the recovered thermal energy can be used elsewhere in the mill.[9,45]

In order to accomplish these two purposes, black liquor is sprayed into the high temperature environment of the recovery boiler where the organic portion burns and produces thermal energy which, in turn, drives chemical reactions that begin to regenerate the inorganic portion of the black liquor back into a usable form for pulping. This thermal energy also melts the salts present in the black liquor. These molten salts, or smelt, are mainly composed of Na_2CO_3 and Na_2S. Smelt collects on the bottom of the recovery boiler at approximately 760°C where it spills out of the boiler and directly into the smelt-dissolving tank forming green liquor. A representation of this process can be seen in Figure 15.[45]

There are three main disadvantages to this process design. First, smelt flow into the smelt-dissolving tank is uncontrolled, therefore making the concentration of green liquor uncontrolled. Second, injection of the molten smelt into the top of the tank produces steam laced with TRS (total reduced sulfur), which must be scrubbed, and

finally, the contact of extremely hot molten salt with water has the potential for a smelt water explosion.[9]

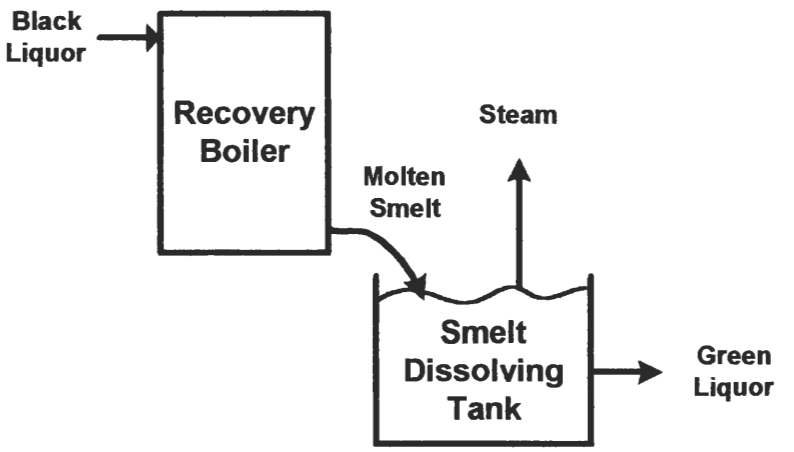

Figure 15. Conventional recovery process handling of molten smelt.

The proposed smelt solidifier would be placed between the recovery boiler and the smelt dissolving tank in order to solidify the molten smelt before it enters the smelt dissolving tank as can be seen in Figure 16.[46]

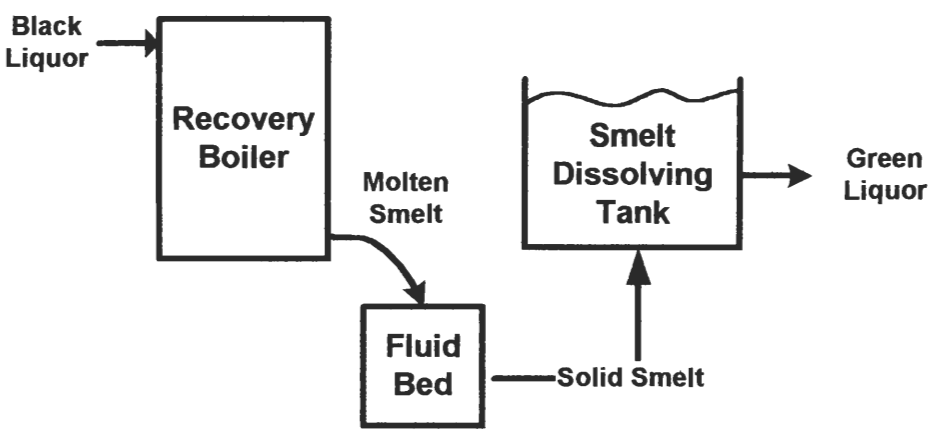

Figure 16. Proposed setup of fluid bed as a smelt solidifier

This process addresses all three of the disadvantages of the current design. The first is the control of smelt flow into the smelt-dissolving tank. Solid smelt can be fed in

by preexisting technology such as a screw feeder, which would allow for the concentration of green liquor to be controlled. The second is the elimination of steam from the smelt-dissolving tank vent due to the introduction of solid smelt at the bottom of the smelt-dissolving tank.[46] The elimination of steam by bottom-of-the-tank introduction was determined in previous research by Reeves to be the result of heat transfer from the steam bubbles formed at the point of particle introduction, which then condensed and collapsed before they reached the surface.[47] Finally, there is no contact between molten smelt and water thereby eliminating the potential for a smelt water explosion.[9]

Current Uses of Fluidized Beds in Recovery

There are several different fluidized bed-based processes that have been developed for use in black liquor recovery processes. These technologies can be broken down into three applications; fluid bed calciners, combustors, and gasifiers. Fluid bed calciners will not be discussed here because they do not handle black liquor and therefore have no smelt.

Fluid bed combustion involves the burning of black liquor in a fluidized bed composed initially of an inert medium such as silica or iron oxide, which is used to create the particle seedbed. Black liquor is sprayed into the fluidized bed where it spreads throughout the bed while burning. Though the overall temperature of the bed is maintained below the melting point of smelt to avoid defluidization, there are localized pockets of high temperature created by the combustion of black liquor droplets that result in small pockets of molten smelt. These pockets of molten smelt coat the cooler inert seed particles and solidify on them.[48-53] The population of the seed bed is controlled by removing larger particles that have grown for further processing.[55]

Fluid bed gasification is the process by which black liquor is heated in an oxygen deficient atmosphere until the volatile organic compounds are pyrolyzed and recovered as combustible gases. This can be accomplished by partially combusting the black liquor in an oxygen depleted atmosphere as seen in a patented process by Shick and further developed by others, where substoichiometric amounts of oxygen are fed into the fluidized bed in order to provide enough oxygen to partially burn the black liquor injected into the bed which provides the energy necessary to gasify the rest.[50] Another method available for gasification is the indirect addition of thermal energy to the bed as can be seen in the ThermoChem process where pulsed heat exchangers efficiently provide the thermal energy for pyrolysis of volatile organic compounds to a bed fluidized by steam. As the volatile organic compounds are removed by gasification, inorganic residue from the black liquor remains on the surface of the particle making it grow over time. As with the fluidized bed combustor, these particles must be removed for further processing.[54]

Differences Between Proposed Method and Current Technology

The greatest difference between current technology and the proposed fluidized bed smelt solidifier is the distribution of molten smelt in the fluidized bed. The current technologies are characterized by molten smelt generated locally in small, dispersed pockets[55] while the proposed smelt solidifier will have to handle a large, sustained, and centralized in-flux of molten smelt into the top of the fluid bed. The effect that these differences have on particle formation, and thus the stability of the bed itself, is unknown and must be understood before this proposed technology could be used to solidify smelt commercially.

Thesis Objectives

The overall objective of this research is to determine the effect of fluidization regime on particle formation in a fluidized bed smelt solidifier. The effect on particle formation, in the context of this research, is the rate of change of mean particle diameter with time and the mechanism responsible for that change. Particles can either grow, shrink, or stay the same size. Two basic growth mechanisms are considered in this project. The first, coating, involves the buildup of layers of solidified molten salt on the surface of seedbed particles. The second, agglomeration, is the result of molten salt binding multiple particles together. It is hypothesized that the dominant mechanism will shift from agglomeration at lower fluidizing velocities (bubbling bed) to that of particle coating at higher fluidizing bed conditions (turbulent bed) due to the increase in the rate of mixing and heat transfer in the fluidized bed. Specific objectives include:

1. Design and build a bench scale fluidized bed solidifier with the capability to control critical bed parameters, such as molten salt feed rate, type of fluidization and bed volume.

2. Determine the particle size distribution and growth rates of fluidized bed seed particles removed from fixed points in the fluidized bed.

3. Microscopically evaluate bed particles taken in Objective 2 in order to determine the dominant mechanism of particle growth.

EXPERIMENTAL

Equipment

There were several pieces of equipment needed to fulfill the objectives of this dissertation. This section contains explanations of their design and function. The individual equipment and their relationship can be seen in Figure 17.

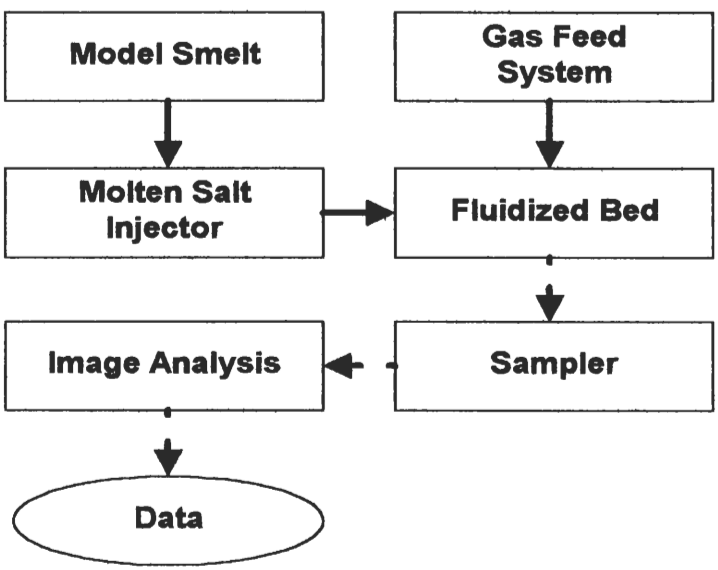

Figure 17. Overall relationship of equipment in model smelt solidifier

Model Smelt

A eutectic combination of KNO_3 and $NaNO_3$ was used as a model smelt in this project due to the high temperature and corrosiveness of smelt.[56] An extensive search has been performed on thousands of chemicals in order to find a model chemical that best suits the requirements of this project. These requirements are analyzed in this section.

Properties

In order for a model smelt to be used effectively in this project, it is necessary to compare the values of properties that affect particle growth between the model and real system. These properties can be seen in Equation 4.

$$\frac{d\bar{d}_P}{dt} = f\left(C_{Pg}, C_{Pms}, \mu_g, \mu_{ms}, k_g, k_{ms} d_{Po}, u_0, \rho_g, \rho_{ms}, \rho_P, \Delta T, F_o, \sigma, \Delta H_f, h\right) \quad \textbf{Eqn 4}$$

Only some of the properties for the real system are currently defined, those being the properties for smelt and steam seen in Table 2 and Table 3 and compare very well.[46]

Table 2. Properties of eutectic combinations of Na_2CO_3-Na_2S (Smelt) and $NaNO_3$ - KNO_3 (model smelt) [25,55-58]

PROPERTIES	SMELT	MODEL SMELT
T_{mp} (°C)	762	222
ρ_S (kg / m^3)	1892	2170
ρ_L (kg / m^3)	1892	1867
μ_L (Ns / m^2)	0.0031	0.0047
σ_L (N / m)	0.211*	0.122
k_L (W / mK)	0.45*	0.51
ΔH_f (kJ / kg)	142*	143
C_P (kJ / kgK)	1.05*	1.78[62]
Newtonian Fluid	yes	yes

A close comparison of the properties of steam and air can be seen in Table 3.

* Values Calculated from 100% Na_2CO_3

Table 3. Properties of steam (Proposed fluidizing gas) and model fluidizing gas (Air)[63]

PROPERTY	PROPOSED (STEAM)	MODEL (AIR)
ρ_g (kg / m^3)	0.64	1.16
μ_g (Ns / m^2)	1.2X10^{-5}	1.85X10^{-5}
k_g (W / mK)	0.025	0.026
C_{Pg} (kJ / kgK)	2.0	1.0
T_g (°C)	110	25

Several properties of the proposed system were not defined specifically by the patent[46] on which this work is based, but ranges for the variables can be assumed. The properties and their assumed ranges can be seen in Table 4.

Table 4. Assumed property ranges

PROPERTIES	RANGES		AVERAGES	
	Proposed	Model	Proposed	Model
u_o (mm/s)	700-2500	1000-2000	1600	1500
ΔT (°C)	100-200	40-60	150	50
d_{Po} (mm)	0.5-0.75	0.63	0.63	0.63

These assumed values represent the potential operating conditions of the proposed smelt solidifier. These values are also used for comparison in dimensionless terms generated through dimensional analysis.

Dimensional Analysis

Dimensional analysis was performed on the variables in Equation 4 in order to further compare the proposed and model systems. These dimensionless groups and their respective meanings can be seen in Table 5.

Table 5. Dimensionless Groups

DIMENSIONLESS GROUP	DEFINITION
$\frac{\frac{d\bar{d}_P}{dt}\bar{d}_{Po}\rho_L}{\mu_L}$	**Dimensionless rate of particle growth**
$\frac{\bar{d}_{po}u_0\rho_g}{\mu_g}$	**Ratio of inertia and viscous forces [63] Indicates flow regime of the bed (Reynolds number)**
$\frac{h\bar{d}_{po}}{k_g}$	**Dimensionless temperature gradient at the surface of particles Gives an indication of the amount of heat transfer at the particle surface[63] (Nusselt number)**
$\frac{C_P\mu}{k}$	**Represents the ratio of the momentum and thermal diffusivities of the fluid [63] (Prandtl number)**
$\frac{\sigma_L\bar{d}_{po}\rho_g g_c}{\mu_L^2}$	**Indicates the thickness of the layer to be formed on the surface of the bed particles.**
$\frac{\Delta T\bar{d}_{Po}^2\rho_L^2 k_L g_c J}{\mu_L^3}$	**This term is a combination of two terms and is representative of the potential of the particle to agglomerate**
$\frac{F_0\Delta H_f\bar{d}_{Po}^2\rho_L}{\mu_L J}$	**Represents the rate of heat transfer to bed particles**

The values for each of the respective variables of the two systems seen in Tables 2, 3, and 4 were then used to calculate these dimensionless groups. A more detailed explanation of the development of these terms can be seen in Appendix 1. A comparison of these values can be seen in Table 6.

Table 6. Comparison of smelt and model systems using dimensionless groups

DIMENSIONLESS GROUP	SMELT SYSTEM	MODEL SYSTEM	*Smelt System* / *Model System*
$\frac{\bar{d}_{po} u_0 \rho_g}{\mu_g}$	**54**	**59**	**0.92**
$\frac{h \bar{d}_{po}}{k_g}$	**6.3**	**6.12**	**1.0**
$\frac{C_{PL}\mu_L}{k_L}$ (molten salt)	**7.2**	**16.5**	**0.44**
$\frac{C_{Pg}\mu_g}{k_g}$ (gas)	**0.96**	**0.71**	**1.4**
$\frac{\sigma_l \bar{d}_P \rho_g g_c}{\mu_l^2}$	**26200**	**6500**	**4.0**
$\frac{\Delta T \bar{d}_{Po}^2 \rho_L^2 k_L g_c J}{\mu_L^3}$	**3.22×10^9**	**4.1×10^8**	**7.9**
$\frac{F_0 \Delta H_f \bar{d}_P^2 \rho_L}{\mu_L J}$	**76**	**50**	**1.52**

These comparisons are good. All are within an order of magnitude and five out of the seven are within 55%. These dimensionless numbers and actual comparisons of the data indicate a good comparison between the model system and the proposed system.

Hazards

Both KNO_3 and $NaNO_3$ are used as food additives making them safe and easy to work with in this project.[67-70] There are two notable exceptions however. The first is that the mixture should not be heated above 500 °C because it will decompose into NO_2, which is hazardous.[64,65] The second potential hazard is that both chemicals are

oxidizers.[66,67] This however, should never be a problem because neither should ever come in contact with combustible materials in this project.

Melting Temperature

The melting point is a big factor in the selection of a model smelt. The difficulty in building and operating equipment safely and effectively decreases significantly as the operating temperature decreases, making a low temperature molten salt extremely attractive.

The eutectic combination of sodium nitrate and potassium nitrate has a melting point of 222°C, which is much lower than the 762°C melting point of eutectic sodium carbonate-sodium sulfide.[58] The estimated change in heat loss through the wall due to radiation has been determined to be minimal as can be seen in Appendix 1.

Corrosion

The mixture of $NaNO_3$-KNO_3 does not corrode SS316 as shown in preliminary corrosion tests performed in this dissertation and in the literature.[70,71]

Fluid Bed

The actual fluidized bed is the particles and gas mixture, but the term will be used here to describe the equipment that supports fluidization. Each piece of equipment that supports fluidization is discussed in this section. A diagram of their relationship to one another can be seen in Figure 18.

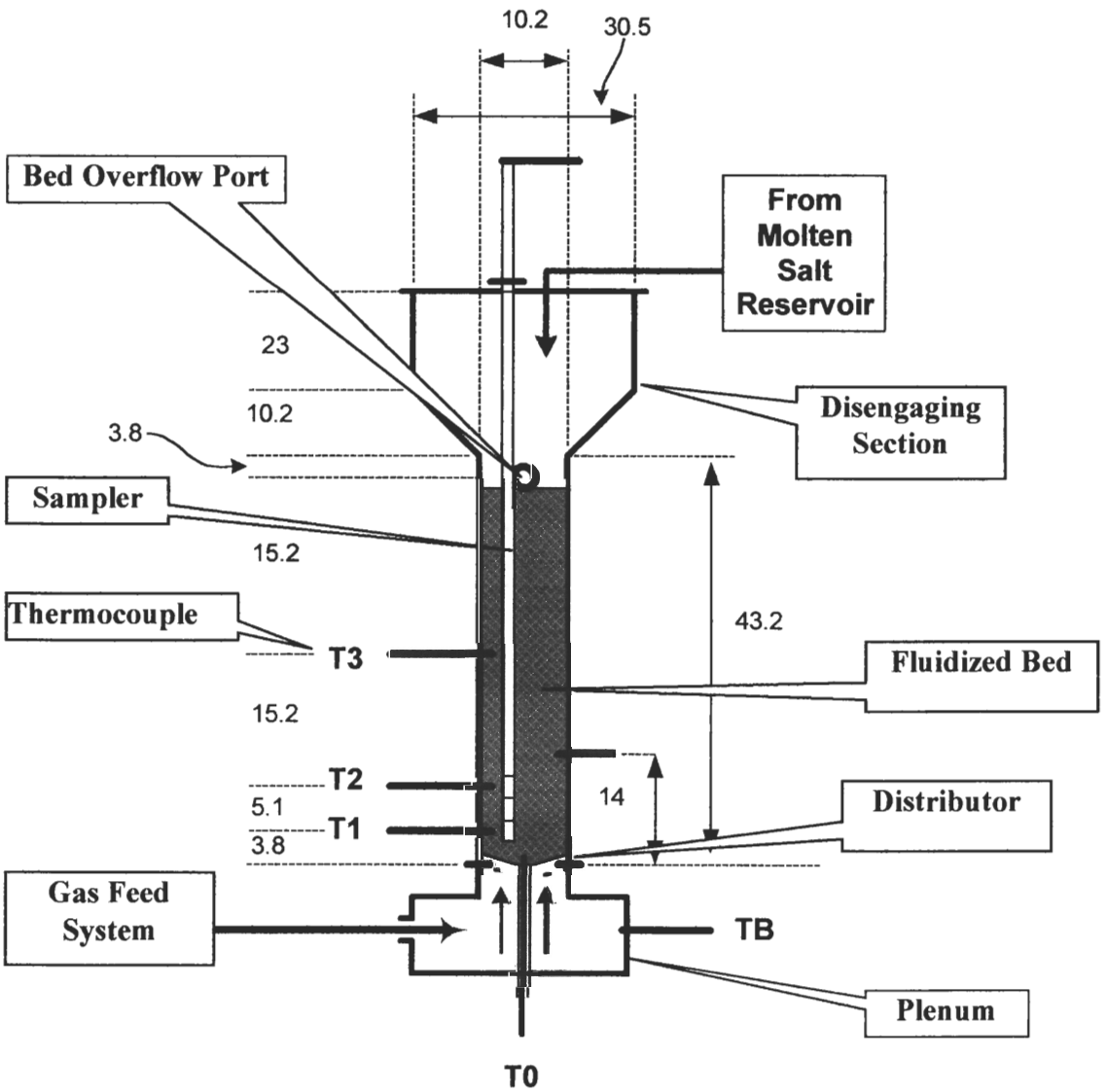

Figure 18. Overall diagram of fluidized bed. All measurements in centimeters.

Distributor

The distributor is used to control the flow of gas into the fluidized bed. There are two different gas distributors used in this experiment. Each is used to provide similar flow characteristics at their respective superficial gas velocity. The high and low velocity distributors can be seen in Figure 19 and Figure 20 respectively.

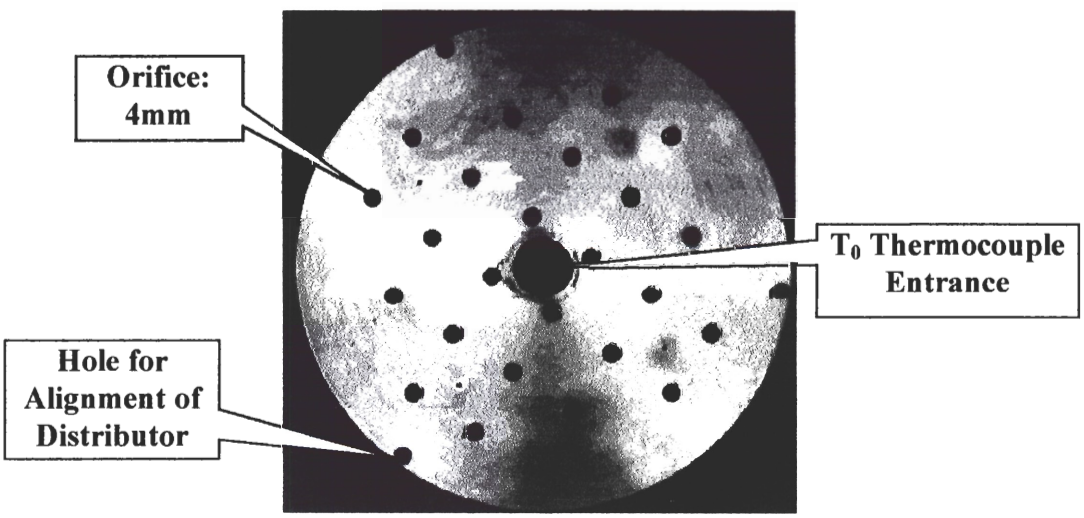

Figure 19. High superficial velocity distributor. There are 24 holes for gas flow and 3 on the edges for alignment with the reactor and plenum.

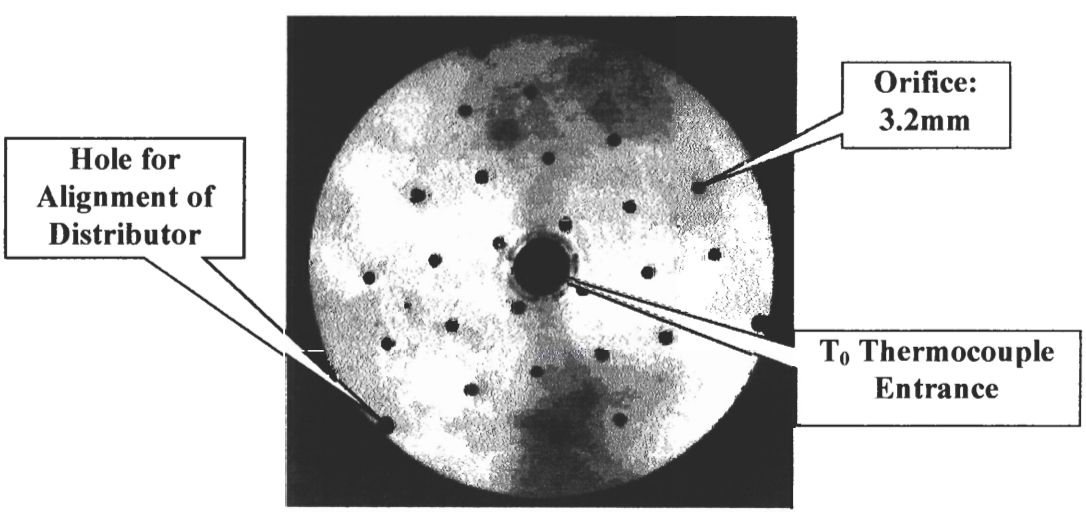

Figure 20. Low Superficial Velocity Distributor. There are 24 holes for gas Flow and 3 on the edges for alignment with the reactor and plenum.

The holes in both distributors used in this project are made to produce the same orifice velocities (u_{or}) at their respective superficial gas velocities (u_o) . This is important because the use of the same plate for each superficial gas velocity would produce different gas jet lengths and orifice velocities through the distributor by squeezing a different amount of gas through the same size holes. This would result in a difference in conditions between the two fluidizing regimes that are independent of the fluidizing regime itself, which would introduce error to the experimental design.

It is also desired to reduce the impact of gas jets on the fluidized bed so that particle formation can be evaluated more in terms of superficial gas velocity. This was accomplished by maximizing the number (N_{or}) and size of gas orifices (d_{or}) across the face of the distributor. The maximum number of orifices that could be fit evenly on the surface of the distributor is twenty-four. This upper limit on the number of gas orifices is determined by the size of the hole for the T_o thermocouple entrance in the center of the distributor as can be seen in Figure 19 and Figure 20.

The size of the orifices is then determined by using the following relationships.[2] The pressure drop across the distributor is determined by Equation 5.[2]

$$\Delta P_{distributor} = (0.3)\,\Delta P_{bed} \qquad \textbf{Eqn 5}$$

This equation is a rule of thumb measurement established by the literature.[2] The pressure drop across the bed is determined by the weight of the bed divided by the surface area of the distributor. The pressure drop across the bed is 6.9kPa which results in a 3.1kPa pressure drop across the distributor.

This pressure drop across the distributor can then be related to gas velocity through the distributor orifices (u_{or}) with Equation 6.[2]

$$u_{or} = C_{d,or}\left(\frac{2\Delta P_{distributor}}{\rho_g}\right)^{1/2} \qquad \textbf{Eqn 6}$$

Where $C_{d,or}$, coefficient of drag, is determined from tables in the literature for these conditions as 0.6.[2] The gas orifice diameter (d_{or}) can then be determined for each superficial gas velocity (u_o) by using Equation 7.[2]

$$d_{or} = \left(\frac{4}{\pi}\frac{u_o}{u_{or}}\frac{1}{N_{or}}\right)^{1/2} \qquad \textbf{Eqn 7}$$

The results for both distributors can be seen in Table 7.

Table 7. Properties of the two distributor plates used in this project

PROPERTY	TURBULENT BED DISTRIBUTOR	BUBBLING BED DISTRIBUTOR
u_0 (mm / s)	2000	1000
N_{or}	24	24
d_{or} (mm)	3.97	3.175

Bed

The bed itself is defined here as the vessel that actually contains the particles during fluidization. The vessel without the fluidized particles can be seen in Figure 21.

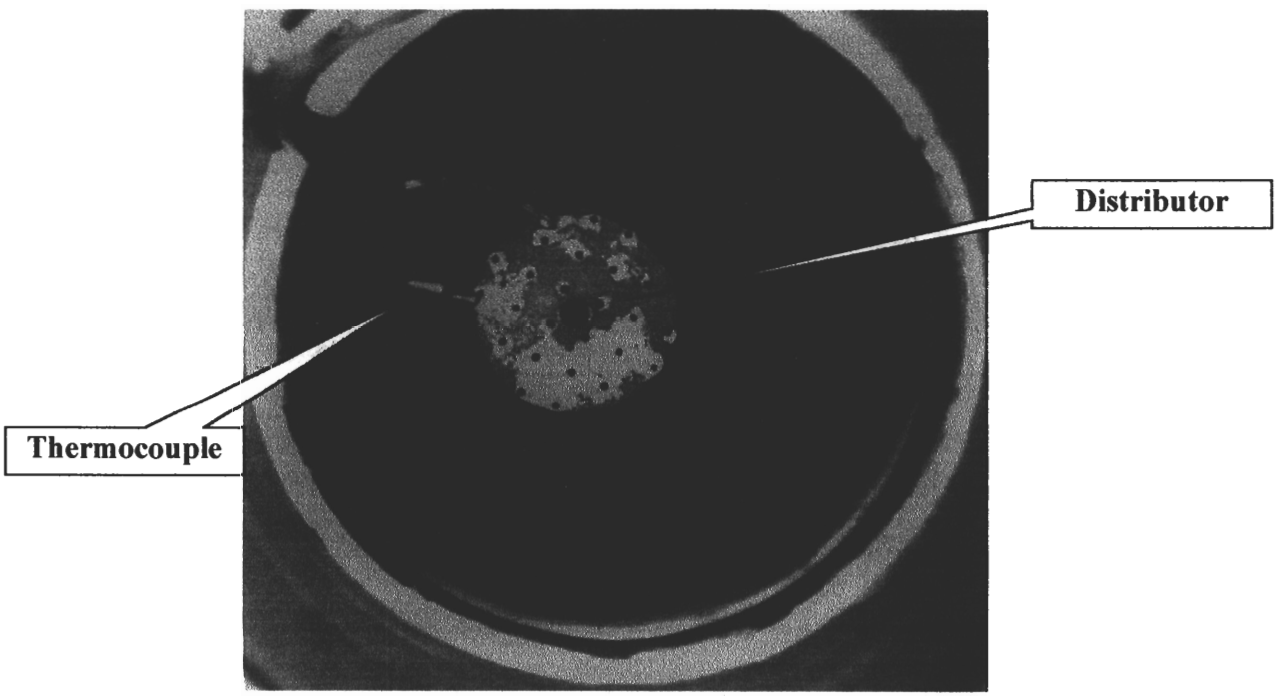

Figure 21. Inside of fluidized bed reactor vessel

Bed Dimensions

The dimensions of the bed were designed more out of convenience than any engineering consideration. It is desirable to have a bed at a standard size that is just large enough to place a hand or an arm inside. It is also not desirable to have the bed too large because this increases the amount of material that is needed for an experimental run.

Diameter

The diameter of the bed is 10.2 cm. This diameter is used because it is a standard pipe size and therefore easier to construct. It also has a relatively low surface to volume

ratio, which helps to maximize the particle surface area within the bed relative to the wall of the reactor. This is important because heat transfer at the wall is not being investigated but rather heat transfer in the bed.

Height

The height of the bed is 43.2cm above the distributor and is determined by the bed overflow port as seen in Figure 18. This particular height has no particular effect on this project and was chosen because the port was already present in the side of the reactor. This port limits the height of the bed the same way that a hole in the side of a bucket of water would limit the height of that water.

Thermocouples

Thermocouples are used to monitor the overall temperature of the bed and the uniformity of that temperature. Thermocouples protrude into the bed from the wall approximately an inch up the side of the reactor vessel as indicated in Figure 18. One thermocouple protrudes through the center of the distributor into the bed and monitors the temperature at the distributor.

Plenum

The plenum is used to create a high-pressure stagnant region before the distributor. This is to insure that gas flowing through the distributor is even over all of the holes of the distributor. A picture of the plenum can be seen in Figure 22.

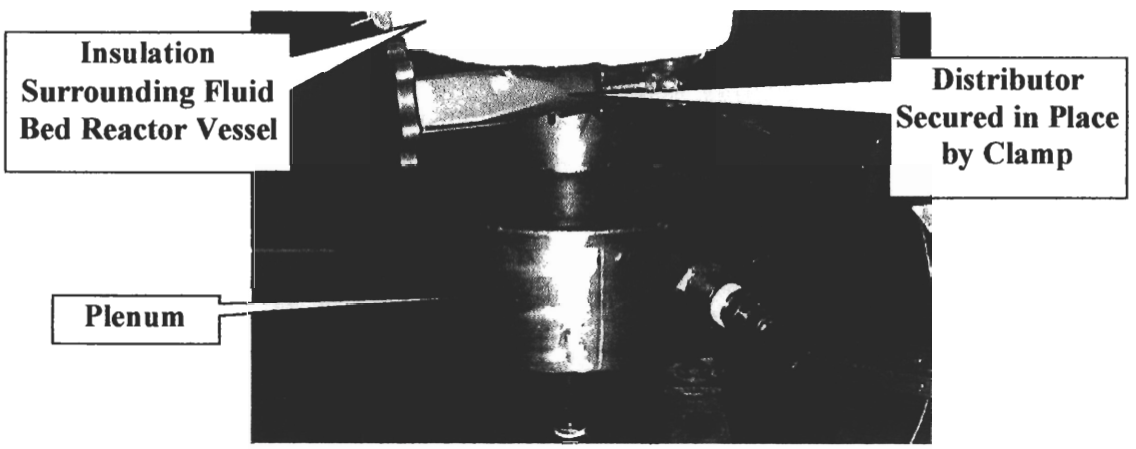

Figure 22. Plenum attached to bottom of fluid bed reactor vessel. It is necessary to remove the plenum and distributor before each experiment to calibrate the flow as discussed in Experimental Procedures

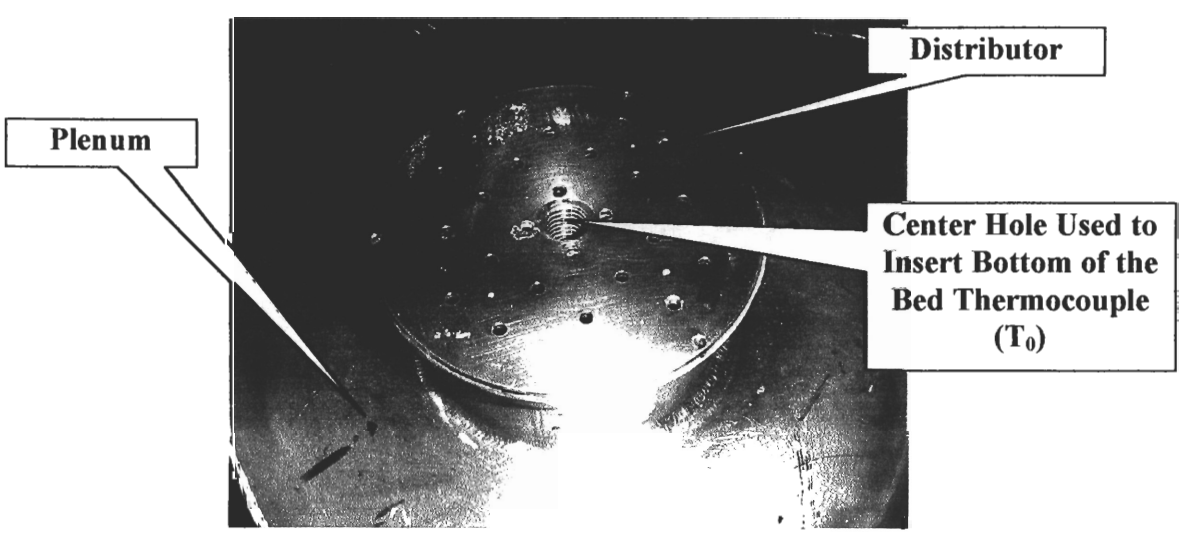

Figure 23. Top view of plenum detached from fluid bed reactor vessel. The distributor, pictured here, is sandwiched between the plenum and the fluid bed reactor vessel as pictured in Figure 22

Disengaging Section

The disengaging section is a wide section over the top of the bed that reduces the superficial gas velocity. This reduction of superficial gas velocity causes some of the larger elutriated material to fall back into the bed therefore reducing the overall height requirement of the bed. The disengaging section used in this project (seen in Figure 24) was made from as piece of 30.5cm diameter pipe for ease of construction.

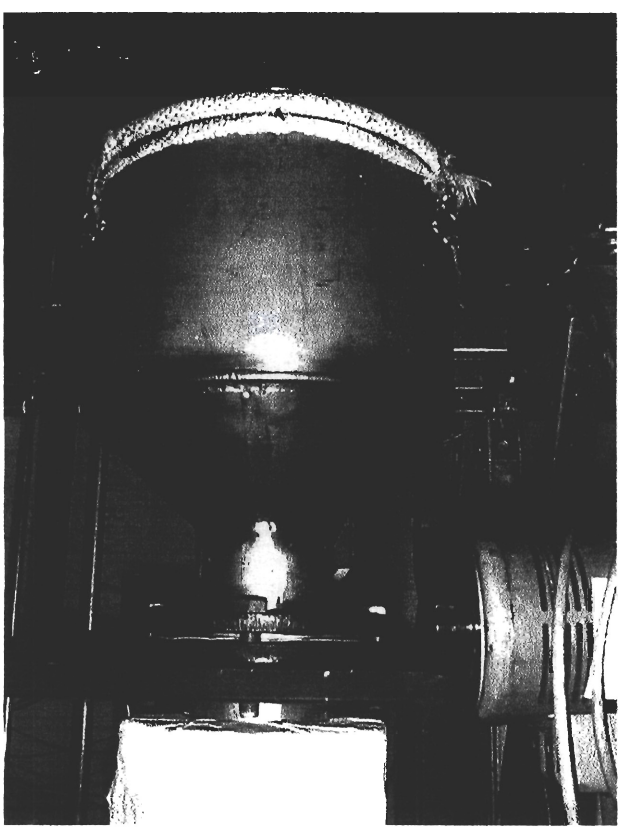

Figure 24. Disengaging section

Molten Salt Injection

The purpose of the molten salt injection system is to meter the molten salt into the top of the bed at a fixed temperature. This section outlines the parts of this system and their purpose.

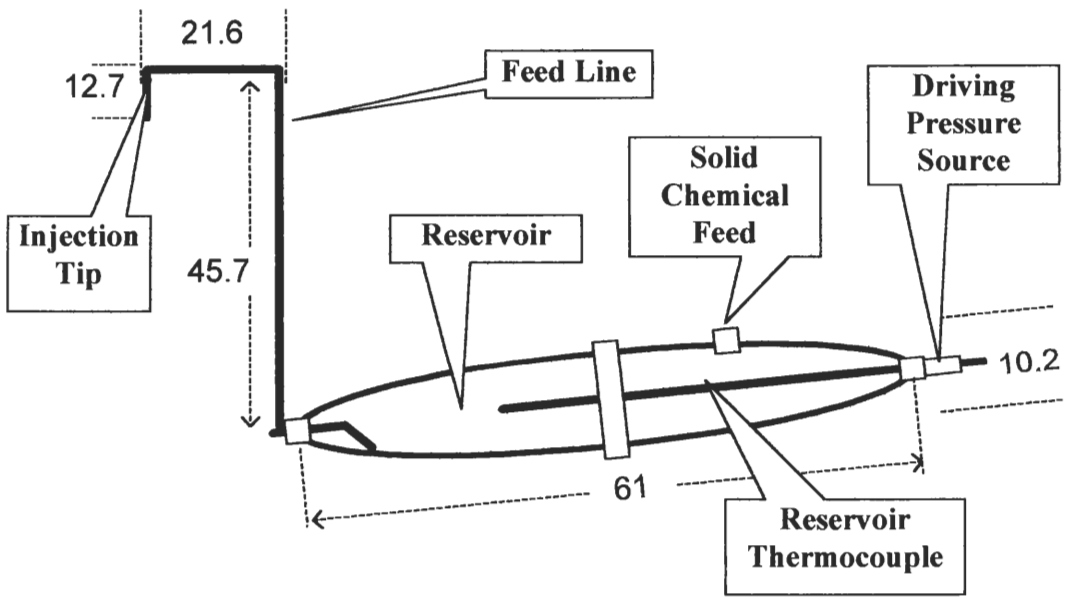

Figure 25. Molten salt injection system. All measurements in centimeters

Reservoir

The molten salt reservoir is a vessel that melts and pumps the molten salt. The temperature of the salt is controlled by heating tape[72] wound around the outside and is pumped by pressurizing the air pocket above the salt with approximately 10-21kPa.

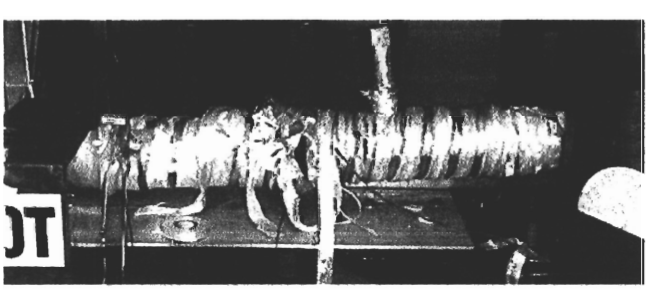

Figure 26. Side view of molten salt reservoir

Feed Line

The molten salt feed line has two purposes. The first is to deliver molten salt to the injection tip at a constant temperature, and the second is to provide a pressure drop to act against while forcing salt into the bed. It is also traced with heating tape to maintain the temperature of the molten salt.

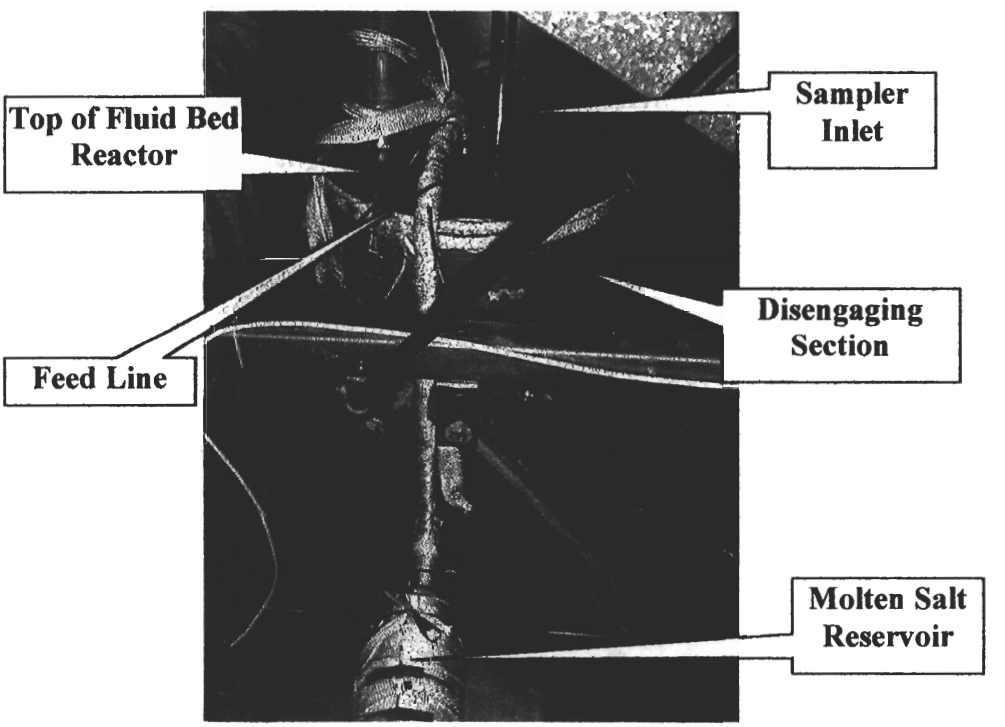

Figure 27. Molten salt feed line entering the top of fluid bed. The line is 6.4mm diameter tubing leaving the molten salt reservoir and converts to 3.2mm diameter tubing after approximately 22.9cm.

Injection Tip

The injection tip directs the molten feed into the top of the bed. A cartridge heater is used because of its high heating capacity. This high heating capacity is important because the injection tip is exposed to airflow inside the reactor, which makes the molten salt susceptible to freezing.

Gas Feed System

The purpose of the gas feed system is to provide air as fluidizing gas at a constant mass feed rate. This is accomplished through the use of a mass flow controller.[73] The mass flow controller used in this project has a maximum flow of 500 SLPM, which led to a problem when a design change required that the gas feed system supply up to 760 SLPM. House air was then added to the overall flow to make up the difference as can be seen in Figure 28.

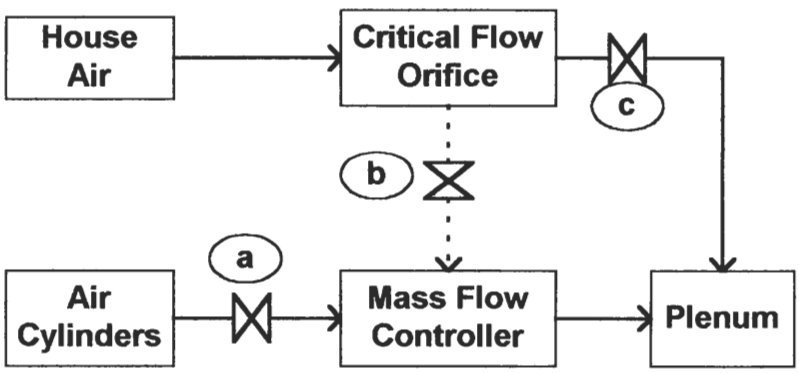

Figure 28. Gas feed system

House Air

The flow of house air is initially calibrated by closing valves ***a*** and ***c*** while opening ***b***. In this way the critical flow rate of house air can be easily adjusted before each experiment. The use of the critical flow orifice allows for a constant mass flow rate of gas so long as the pressure and density on the positive side of the orifice remains constant and the pressure drop across the orifice remains greater than two fold. After the flow of house air is calibrated, valve ***b*** is closed, and ***a*** and ***c*** are opened. The mass flow rate being directed into the plenum is now known.

Cylinders and Manifold

Four compressed air cylinders are connected to a manifold; the outlet is then run through the previously mentioned mass flow controller and into the plenum. The mass flow controller is set to allow the desired flow rate minus what is being provided by house air.

Sampler

The purpose of the sampler is to take a representative sample simultaneously from the upper and lower halves of the bed. This is accomplished by allowing the bed to flow into void cavities in the sampler opened at the desired locations in the bed. These cavities can be seen in Figure 29.

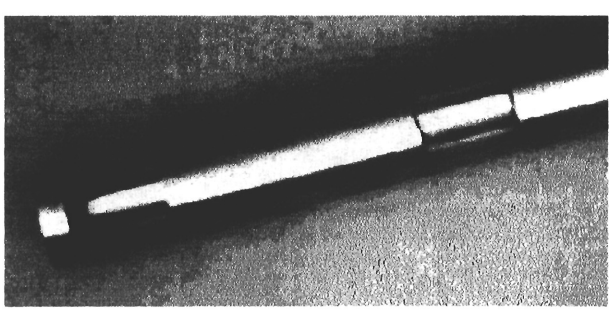

Figure 29. Sampling ports in the open position.

The sampler is made of two concentric stainless steel tubes with identical holes cut in the sides of each tube. This allows the tubes to be closed when set in one position and open when rotated 180° counter to one another to the opposite position. The handles on top of the sampler are used to rotate the two tubes counter to one another and also indicate whether the sampler is opened or closed as can be seen in Figure 30 and Figure 31.

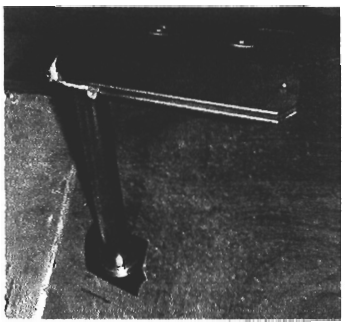

Figure 30. Closed sampler with 0° of rotation. Both sampling ports are oriented in the middle of the bed and facing out towards the wall.

Figure 31. Open sampler with 180 ° of rotation. The position and orientation of the sampling ports has not changed in relation to the closed position.

As mentioned earlier in this section, one of the main goals of the sampler is to minimize the disturbance to the bed in order to get an representative sample. This is accomplished by two means. The first is to insert the sampler along the direction of flow of fluidizing gas and the second is to minimize the cross sectional area of the sampler to avoid significantly increasing the superficial gas velocity in the bed.

The size of the desired sample (1/2 % of bed volume), as well as the size of the openings (3.5X the maximum expected particle size) in the probe, is determined by a maximum expected particle size of 1.6mm. This value is thought to be the extreme possibility of conditions and should offer a safety cushion for proper bed sampling. The

validity of using these criteria in the building of the sampler has been verified by the accuracy of experimental results.

Image Analysis

The purpose of image analysis in this project is to photograph and analyze images of particles created in experiments. Unfortunately, a large size distribution of particles was created in the experiments, making them impossible to photograph with one piece of equipment.

Large Particle Imaging

Large particles are referred to here as all particles not going through a 1.4 mm sieve. These particles cannot be properly analyzed on microscope equipment because of their large size where a single particle may take up the entire field of view. These particles are analyzed instead on a photographic table, which has a much larger field of view.

Small Particle Microscopy

Small particles, or those going through a 1.4 mm sieve, are analyzed at 6X magnification on a microscope.

Image Analysis Software

OPTIMAS 5.2 is used in this project to analyze images by the previous two processes in order to convert images into meaningful data.

SEM

Scanning electron microscopy (SEM) has been used in this project to take three-dimensional pictures of individual particles.

Procedures

This section provides an overview of the general purposes of the procedures involved in running experiments of this project. For a list of detailed operational instructions, please see Appendix 2.

Setup of Experiment

Sieve Seed Bed Particles

The seedbed is composed of a monodisperse distribution of a eutectic mixture of $NaNO_3$-KNO_3 particles. The size range of the particles was determined by sieving them between 0.71 mm and 0.425 mm. The particle size distribution of the material received from the manufacturer was too large and had to be broken down into this size range by a blender. This was a very labor intensive and time consuming part of the experiment. More detail on the particle seedbed is contained in the Design section.

Molten Salt Injection System

Preheat Reservoir

After the reservoir is filled with model chemical, it must be heated slowly over time to avoid exceeding the safety temperature of 500°C. The reservoir holds approximately 2.1 kg of model chemical and takes approximately 3 to 3.5 hours to reach operating temperature. LabView(C) software is used to control the two heating tapes used to heat the molten salt reservoir.

Preheat Molten Salt Feed Line

The molten salt feed line is heated up after the molten salt reservoir has reached its operating temperature. This reduces the wear and tear on the heating tape tracing the feed line. It has been found to be very difficult to achieve uniform heating over the entire length of the line when rewrapping this heating tape. Each new setup of heating tape results in a new set of operating conditions, which must be defined and adjusted through trial and error. The molten salt feed line is heated by one heating tape, which is controlled with a potentiometer and measured with three thermocouples.

Molten Salt Injection Tip

The molten salt injection tip heater is controlled by a potentiometer and monitored by two thermocouples. Because the tip is heated by a high-density cartridge heater, it should be noted that it's temperature should not exceed 400°C. The specific settings of the potentiometer are determined through an overall calibration of the molten salt injection line.

Calibration

Molten Salt Flow Rate

The molten salt flow rate is calibrated at the beginning of each experiment by controlling the air pressure placed in the headspace of the molten salt reservoir. This pressure is controlled through a pressure regulator on a compressed air cylinder. Due to the low operating pressures required to transfer the molten salt, a needle valve has been installed to bleed off pressure after the regulator and therefore allow the pressure regulator to be set at a higher, more stable operating pressure. The flow of molten salt can be

controlled by changing the regulator pressure or by changing the opening in the needle valve, as can be seen in Figure 32.

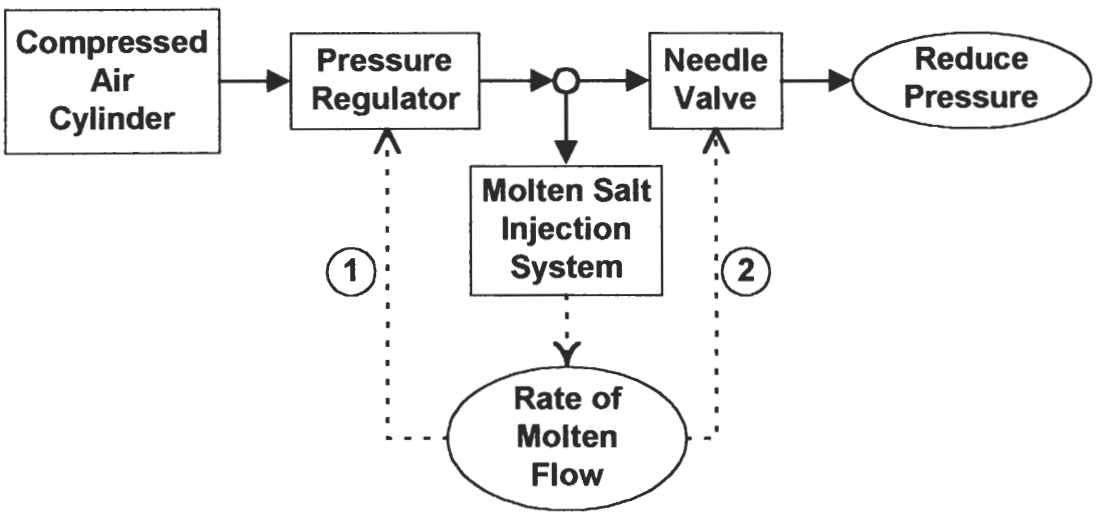

Figure 32. Flow chart of molten flow rate calibration

Molten salt flow rate is measured by collecting the molten stream leaving the injection tip in a preweighed stainless steel pan held under the reactor vessel (plenum and distributor removed). This pan is then weighed and the increase in weight divided by the collection time is the molten salt flow rate. Each sample is taken for approximately 15 to 30 seconds. This flow rate is rechecked for accuracy and found to change by no more than plus or minus 5%.

Temperature of Molten Flow

The temperature of the molten salt flow is calibrated by changing the temperature of either the molten salt feed line or the injection tip depending on the severity of the adjustment required. Larger adjustments are made on the entire line because of the greater residence time of the salt.

Molten salt temperature is measured with a thermocouple as the salt falls through the reactor vessel and out the bottom of the fluidized bed (plenum and distributor removed) in the same position the weight is taken. It should also be noted that any changes to the temperature will cause changes to the molten salt flow rate. After this is done, the plenum and distributor are replaced at the bottom of the fluid bed reactor.

Gas Feed System

House Air

The house air is set at its maximum stable pressure of 538 kPa in order to gain the highest flow possible. Pressures above this lead to an unstable flow rate due to compressor operation. This air is calibrated at the beginning of each run by redirecting the house airflow at 538 kPa through a mass flow meter to determine the mass flow rate. After the mass flow rate of house air is determined, the flow is redirected back to a line going straight into the plenum. More information can be obtained in the section on Equipment.

Compressed Air Cylinders

Four compressed air cylinders supply the rest of the air needed to meet the desired experimental conditions. The pressure regulator and mass flow controller are set to provide the additional flow rate of air. At the low gas flow rate (bubbling bed) the compressed air cylinders provide 100% of the fluidizing gas to the bed, namely 380 SLPM (Standard Liters per Minute). At the high gas flow rate (turbulent bed) the compressed air provides approximately 490 SLPM of the 760 SLPM needed.

Fill Seed Bed

The particle seed bed is poured into the fluid bed reactor through the sampling port at the top of the disengaging section after the correct fluidizing gas flow rate is set. The seedbed consists of 2300 grams of seedbed particles. After the seedbed has been poured into the fluid bed reactor, the computer is set to collect data.

Running Experiment

Starting Experiment

A valve controlling the flow of air into the headspace of the molten salt reservoir is turned on to start the flow of molten salt into the bed. A clock is simultaneously started. This is used to determine sampling times.

Sampling

Samples are taken after the experiment has run for thirty seconds and at one-minute intervals thereafter. This is continued until the sampler cannot be inserted fully into the bed due to a buildup of particles that have fallen out of the bed. These particles that have fallen to the bottom of the bed have grown beyond the size where they can be fluidized.

Samples are taken by inserting the closed sampler into the sampling inlet in the top of the fluid bed reactor with the sampling ports facing the outside wall of the fluidized bed reactor. Once the sampler is in place, both sampling ports are opened up for 5 seconds and closed again. With the samples (upper and lower) secure, the sampler is withdrawn from the bed and the samples are placed into separate containers for analysis. A quick

check of each sampling port is made to insure that all material has been removed and the next sample is ready to be taken. There was no evidence of any salt scale on the outside of the sampler wall.

End of Experiment Procedures

Shutting Down Equipment

The molten flow is shut off as soon as the experiment is complete in order to avoid wasting material. The data collection and control software program is then shut down and the molten salt reservoir is allowed to cool. The fluidizing gas from the compressed air cylinders is shut off to preserve the air in them for later use while the house air is allowed to continue. Allowing the house air to continue cools down the bed.

Recover and Resieve Seed Bed

After the bed has been allowed to cool, the plenum is detached from the rest of the reactor, and the material left over from the experiment is removed. This material is then resieved to obtain particles from the original seedbed that have not been agglomerated for use in future seedbeds.

Digitizing Samples

Separating Particles

Particles are separated by size into large and small particle groups due to the difficulties of effectively photographing large and small particles at the same magnification with good definition. This is discussed further in the Equipment section under image analysis. The masses of the large particle and small particle fractions are recorded.

Mounting Small Particles

In every sample there are many times more small particles than large ones. Approximately half of these small particles are mounted on a sheet of transparent contact paper while the other half is stored. The contact paper provides a secure medium where the particles can be held securely in place for imaging. Particles are dispersed evenly over the surface of the contact paper using a small paintbrush. This helps to prevent clumps of particles from being mistaken as a single particle during image analysis.

Photographing Particles

Small Particles

Because of the large area of the contact paper covered with small particles and the relatively small field of view of each photograph of the microscope, ten random pictures are taken across the surface of the contact paper. This is accomplished by laying a transparency of twenty evenly spaced numbered squares over the top of the of the contact paper. Ten of these twenty squares are randomly chosen for each sample and photographs are taken in the center of each. This setup can be seen in Figure 33.

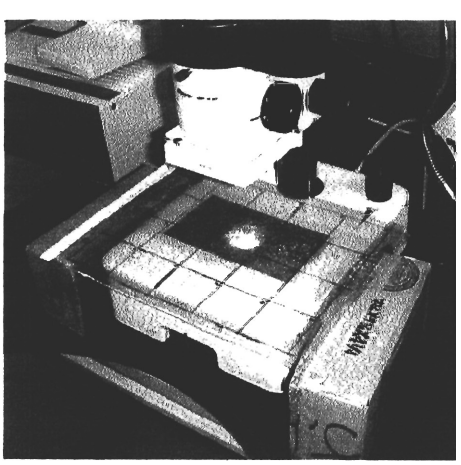

Figure 33. Small particle image analysis equipment

Large Particles

The small number of larger particles allows them all to be taken in one picture. These particles are placed in a petri dish and photographed using a standard camera stand. This setup can be seen in Figure 34.

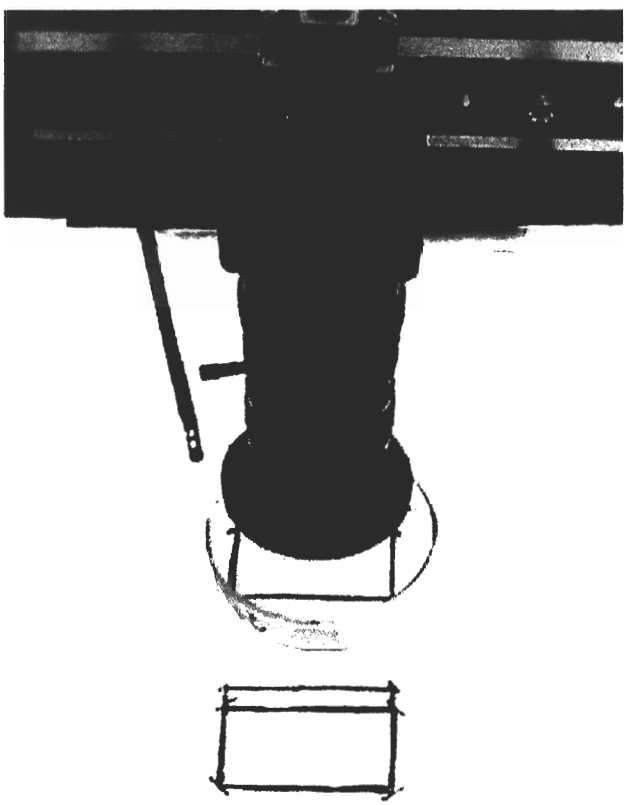

Figure 34. Large Particle Imaging Setup

Image Analysis

The purpose of image analysis is to determine the distribution of three-dimensional particles from two-dimensional images.

OPTIMAS 5.2

OPTIMAS 5.2 is image analysis software used to convert the images of particles into useful data. Examples of these images can be seen in Figure 35 and Figure 36.

Figure 35. Small particle Image. The frame width is approximately 15mm

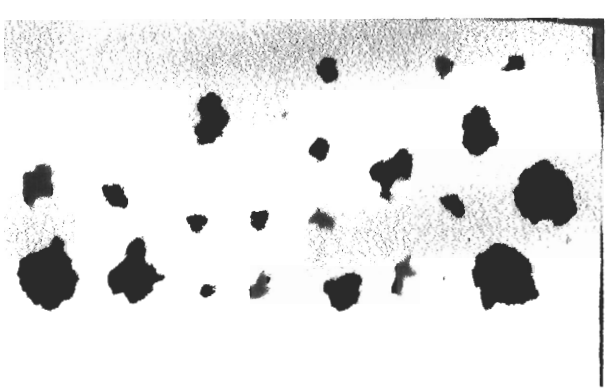

Figure 36. Large particle image. The frame width is approximately 70mm

Data Measured

Two main values determined using image analysis are area and shape factor. Area, as defined here, is the projected area of the particle. Shape factor (S) is defined as the perimeter of the particle image outline (P) squared divided by the area of the particle image (A).[51,75]

$$S(Shape\ Factor) = P^2 / 4\pi A \qquad \textbf{Eqn 8}$$

As the shape of the particle image becomes more irregular, the perimeter increases relative to the area which increases the value of the shape factor as can be seen in Figure 37 and Figure 38.

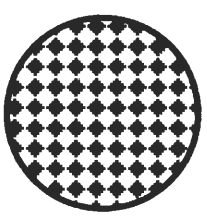

Figure 37. Shape factor for circle is 1

Figure 38. Shape factor > 1

Determining Particle Volume

There are two methods used to determine the volume of particles in this project. The first method (Method I) and the method predominantly used determines the volume of a cylinder with the same shape factor and image area as the particle being analyzed.[74,75] The second method (method II) determines the volume of a slab with the same shape factor and image area as the particle being analyzed and is used for particles which are relatively wide and flat, making them difficult to compare to a cylinder.

These wide and flat particles were found only in the large particle analysis when a difference was determined between the volume of the sample calculated by its weight and density and, the volume calculated using method I. This difference resulted from an assumption made by method I that the unseen depth of the particle is equal to the width. This results in larger volumes calculated for broad flat particles than are actually present.

Method I **Pill Method**

The volume (V) is determined by considering the particle as a cylinder with hemispherical ends. This is shown in Equation 9. This method was used on all small particles and on most large particles with some exceptions, which will be discussed in Method II.

$$V = \frac{4}{3}\pi R^3 + \pi R^2 L \qquad \textbf{Eqn 9}$$

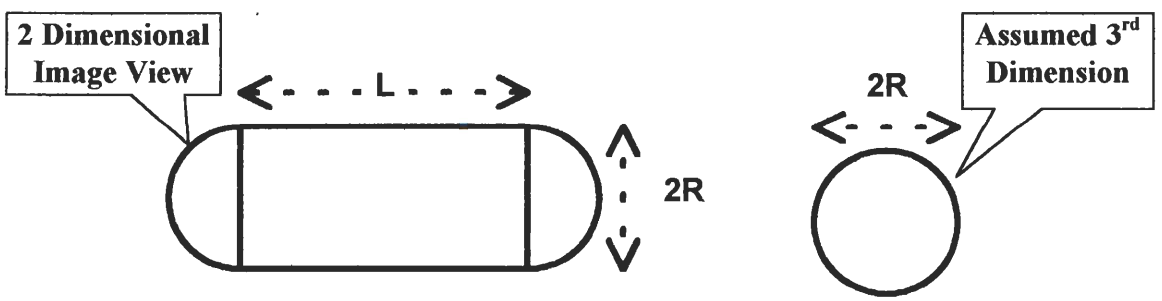

Figure 39. Method I

The shape factor is used to determine R and L through the following relationships found in the literature.[74,75]

$$\frac{L}{R} = \pi[S - 1 + \sqrt{S(S-1)}] \qquad \textbf{Eqn 10}$$

$$R = \sqrt{A \Big/ \left(\pi + 2\frac{L}{R}\right)} \qquad \textbf{Eqn 11}$$

$$L = \left(\frac{L}{R}\right)R \qquad \textbf{Eqn 12}$$

Method II **Slab Method**

Applying Method I to some large flat particles resulted in huge errors when comparing the estimated volume of the particle to the known volume of the particle calculated from its mass. This led to the development of Method II. This method is a modification of the pill method and is used to approximate the volume of particles whose depth is approximately 40-70% of their breadth.

$$V = \left(\pi R^2 + (2R)L\right)\left(F(2R)\right) \qquad \textbf{Eqn 13}$$

The variable F is the ratio of the height over the width of the slab and is chosen to express the unknown height in terms of the known width of the slab. Experience and light transmittance through the particle guided the selection of slab particles and their depth.

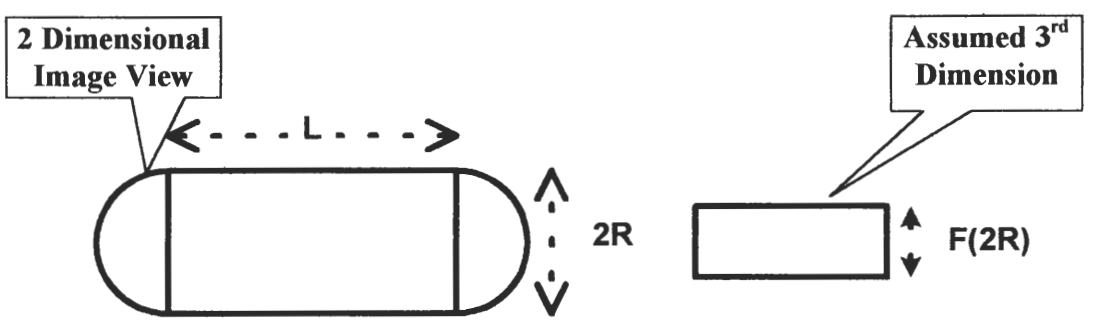

Figure 40. Method II. Used to approximate the volume of large flat particles

This use of method II is very subjective but there are very few particles (average of 0-3 Method II particles) in the overall sample that require Method II, making it easy to adjust the value of F to each particle according to the approximate volume of that particle as determined by the mass and density. The value of F tends to be between 0.4 and 0.7. Adjustment of F was also aided by the fact that particles were backlit during

photographing, which indicated the relative thickness of the particles to one another. A smaller value of F would be used to determine the volume of a particle with light shining through relative to a particle with no light shining through. Values of F were adjusted until the calculated volume of the large sample matched the measured volume as determined by the mass and density.

Particle Data Integration

The large and small particle size distributions cannot be combined in their present form because the volumes of the small (V_1) and large (V_2) particle samples do not accurately reflect the population of the bed. This is because only a portion of the small particles from the sample is actually measured during small particle image analysis while all of the large particles are measured in large particle analysis. Adjusting the small particle size distribution to reflect its actual size relative to the sample taken enables them to be combined into one distribution (Equation 21).

The following relationships were used to determine the particle size distribution that represents the bed. The volume of both the small (V_1) and large (V_2) particles were determined by dividing the respective measured masses (M) of each set of particles by the particle density of the salt which was assumed to be uniform throughout the particle (Equation 14 and 15).

$$V_1 = V_{Small\ particles\ sampled} = \frac{M_1}{\rho_p} \qquad \textbf{Eqn 14}$$

$$V_2 = V_{Large\ particles\ sampled} = \frac{M_2}{\rho_P} \qquad \textbf{Eqn 15}$$

The sum of these two volumes equals the volume of the sample and the volume of the resulting distribution to be analyzed as can be seen in Equation 16.

$$V_{Distribution} = V_{Sample} = V_1 + V_2 \qquad \textbf{Eqn 16}$$

Because all of the large particles sampled were photographed and analyzed, the volume of the large particles sampled equals the volume of the large particles determined by particle analysis (Equation 17). The volume of individual large particle size ranges is defined here as V_j.*

$$V_2 = \sum_{N+1}^{O} V_j \qquad \textbf{Eqn 17}$$

All of the particles taken in the small sample, however, are not photographed and analyzed as is represented by Equation 18. The volume of each particle size range that was photographed and analyzed is represented by V_i.*

$$V_1 \neq \sum_{1}^{N} V_i \qquad \textbf{Eqn 18}$$

Adjusting the volume of each particle size range by the ratio of the volume of the entire small particle volume (V_1) relative to the volume of the small particles analyzed ($\sum V_i$) results in a modified volume of the particle size range that can be combined with the particle size range volumes of the large particle distribution (Equation 19).

$$V_i^* = \left[\frac{V_1}{\sum_{1}^{N} V_i} \right] V_i \qquad \textbf{Eqn 19}$$

This sum of these modified volumes over the range of small particle sizes equals the volume of the small particles sampled (Equation 20).

$$V_1 = \sum_1^N V_i^* \qquad \textbf{Eqn 20}$$

This means that the volume of each distribution now amounts to a continuous distribution where the sum of the volumes of large and small particles analyzed represents the entire distribution (V_{Dist}). This can be seen in Equation 21.

$$V_{Dist} = \sum_{N+1}^{O} V_j + \sum_1^N V_i^* \qquad \textbf{Eqn 21}$$

---

* Large particles defined as those particles w/ diameters ranging from (N+1) to O. Small particles size ranges are defined as diameters ranging from (1) to (N).

Data Analysis

Mean Particle Diameter

The mean particle diameter was determined by calculating the equivalent spherical diameter (ESD). Using Equation 22 and histograms, such as the one seen in Figure 41, mean particle sizes were determined.

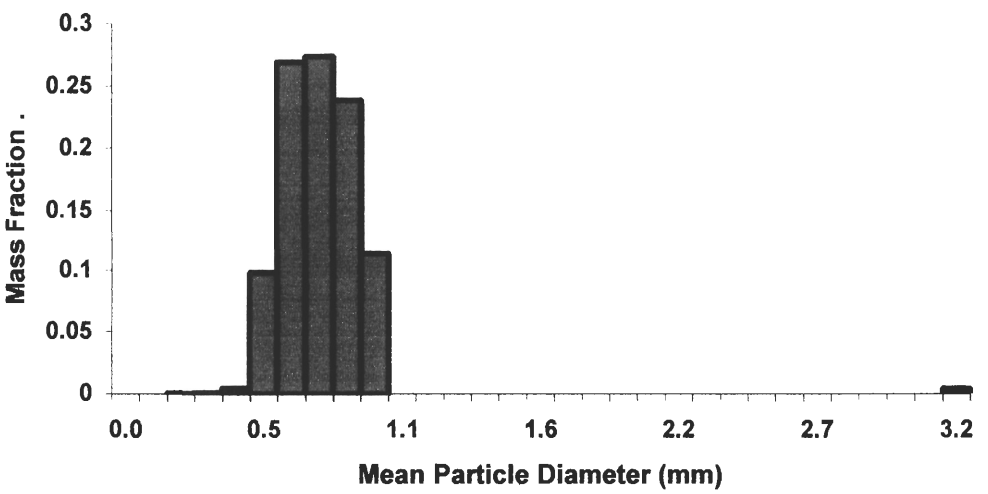

Figure 41. Distribution of particles in bed Experiment 3.1 at 30sec

Image and data analysis were used to produce histograms for each sample taken and for each of these histograms, a volume weighted mean particle diameter was calculated using Equation 22.[76] All references to mean particle diameter in this dissertation refer to Equation 22 where the actual calculated diameter of each particle is the equivalent spherical diameter.

$$\bar{d}_P = D_{43} = \frac{\sum n_i d_i^4}{\sum n_i d_i^3} = \frac{\sum_1^N (V_i) d_i}{\sum_1^N V_i} \qquad \textbf{Eqn 22}$$

This definition of mean particle diameter was chosen for two main reasons. The first is, that the volume of particle size ranges is easily measured and the volume of the bed is continuous throughout the experiment. Surface area is difficult to measure with irregularly shaped particles and is constantly changing and unknown throughout the experiment. The number of particles in each size range is not measured and therefore is also unknown. Secondly, particle weight and thus the particle volume* is responsible for particles defluidizing. When the weight of a single particle becomes too large for the pressure pushing up on them by the fluidizing gas to support, they defluidize. Volume weighted mean particle diameter is affected by the weight of single particles as opposed to number weighted (D_{10}) or area weighted (D_{32}) particle size distributions

Determination of Data Analyzed

Not all samples taken from the bed are used to calculate particle growth rate. As particles grow beyond their maximum fluidizing size they fall onto the distributor eventually forming a layer at the bottom of the bed. This represents a discontinuity in the experiment by changing the conditions at the distributor and by removing material from the bed. The distributor conditions are changed by channeling gas flow through this layer instead of directly into the bed, thus changing the flow of gas into the bed.

The discontinuity created by material leaving the bed affects the overall distribution of particles in the bed by effectively cutting off the large particle end of the distribution. These particles grew but cannot be accounted for because they are no longer represented

* Particle density is assumed to be continuous and evenly distributed

in the bed. The rate of growth in the bed will give a false indication that it has decreased because these particles are not counted.

For these reasons, particle growth rate is determined from data taken before the bed starts to defluidize or fall onto the distributor. This point is determined by the temperature of the thermocouples in the bed. When the bed is completely fluidized, all thermocouples read the same temperature, plus or minus approximately 3°C. As material falls onto the distributor, it covers up the thermocouple at the distributor (T_0), which removes it from contact to the hot fluidized bed, but not with the cool fluidizing gas. The thermocouple begins to cool. The first indication of the cooling is used as the point to stop analyzing particle growth rate. An example of this can be seen in Figure 42.

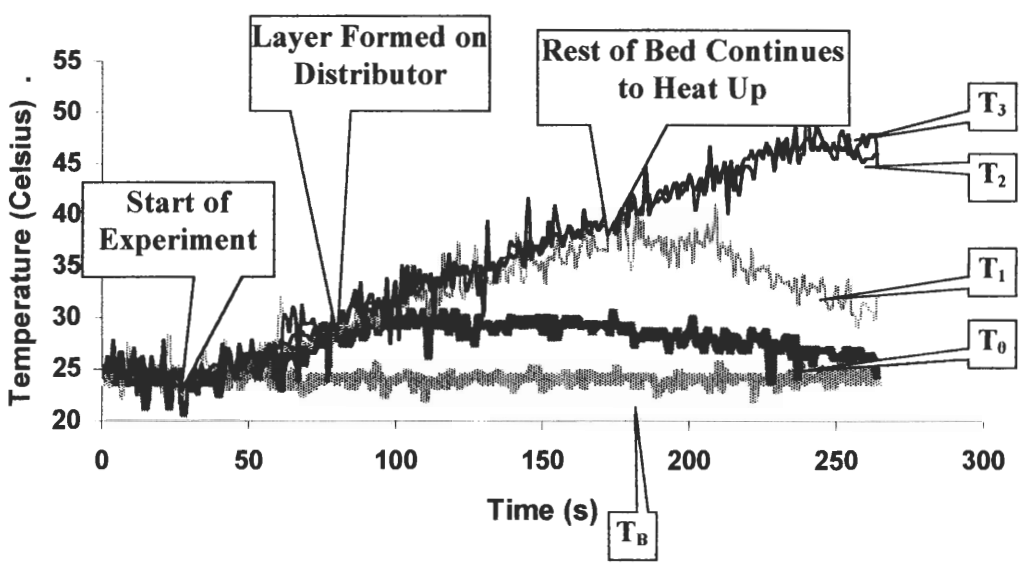

Figure 42. Temperature profile of fluid bed

Design of Experiments

The main focus of this project's experimental design is to determine the effect of fluidization regime on particle growth mechanism and rate. It is also desired to know the impact of other variables and their possible interaction with changes in fluidization regime. Using a factorial design allows the effect of fluidization regime on particle growth rate to be analyzed, along with possible interactions with other operational variables.

Operational Variables Chosen

There are many variables in the fluidized bed that might affect particle growth rate. Four have been chosen for use in this project because of their association with the proposed smelt solidifier. These variables and the explanations of why they have been chosen are discussed in this section.

Superficial Gas Velocity (u_0)

The superficial gas velocity is the primary focus of this project because it directly affects the type of fluidization or the fluidizing regime in the bed. It directly affects the magnitude and type of interactions between, and among, solid, liquid, and gas phases in the bed as well as the overall rate of heat transfer. It is probably the most significant operational variable in the system due to its universal impact.

Molten Salt Feed Rate (F_0)

The molten salt feed rate has been chosen to represent the rate at which the molten salt stream enters the top of the bed. It was chosen because there will most certainly be changes in the flow rate of molten smelt into the proposed molten salt solidifier on which

this project is based. Changes in flow rate from the recovery boiler are part of the reason for the development of this system.

The stream integrity into the top of the bed was determined by injecting a short pulse of molten salt into the fluidized bed reactor with fluidizing gas flow and no bed material. The pattern of solidified molten salt on the distributor plate indicated that the stream had impinged on a single point on the distributor, thus indicating that the molten salt stream did not break up into droplets as a result of fluidizing gas flow. This particular test measures the continuity of the stream over the entire length of the reactor. In an actual experiment, the presence of the bed would limit the travel of the molten smelt. The stream would travel only through the disengaging section where lower gas velocities would have less opportunity to break the stream apart. The results of this test under these exaggerated conditions suggests that the molten salt stream remains continuous into the top of the fluidized bed and thus precludes the use of droplet size as an operational variable.

Molten Salt Feed Temperature (ΔT)

The molten salt feed temperature has also been chosen because changes in the temperature of smelt flow out of the recovery boiler are expected in the proposed system on which this project is based.

Distance from Top of Bed (D)

It was decided to take samples from the upper and lower sections of the bed to determine if any changes in particle growth result from where the molten salt enters the bed.

Factorial Design

The system operational variables have been studied with the use of a 2^4 factorial. The setup of these experiments can be seen in Table 8.

Table 8. Factorial design of experiments

EXPERIMENT	MOLTEN SALT INJECTION RATE (g/s)	GAS VELOCITY (mm/s)	MOLTEN SALT INJECTION TEMPERATURE (°C)	UPPER SAMPLE (mm)	LOWER SAMPLE (mm)
1	1.1	1000	260	-324	-391
2	2.2	1000	260	-324	-391
3	1.1	2000	260	-324	-391
4	2.2	2000	260	-324	-391
5	1.1	1000	300	-324	-391
6	2.2	1000	300	-324	-391
7	1.1	2000	300	-324	-391
8	2.2	2000	300	-324	-391

Values Chosen

Superficial Gas Velocity (u_0)

The high and low values of superficial gas velocity have been chosen to produce either a turbulent or bubbling bed respectively. These values are determined by using established empirical relationships.[2] Equation 23 and Equation 24 are applied to a map of bed fluidizing regimes seen in Figure 43 by using the properties of the bed in Table 9, where d_P^* is a modified form of the mean seedbed particle diameter ($\bar{d}_{Po}$).

$$d_{Po}^* = \bar{d}_{Po}\left[\frac{\rho_g(\rho_S - \rho_g)g}{\mu_g^2}\right]^{1/3} \qquad \textbf{Eqn 23}$$

and u_o^* is a modified form of the superficial gas velocity.

$$u_0^* = u_o\left[\frac{\rho_g^2}{\mu_g(\rho_S - \rho_g)g}\right]^{1/3} \qquad \textbf{Eqn 24}$$

These equations are solved using the initial bed conditions because the properties of the bed change as the experiment progresses as a result of particle growth and increasing fluid bed temperature. Table 9 lists the initial conditions of the experiments.

Table 9. Initial conditions of experiments in this project

PROPERTY	VALUE
Fluidizing Gas Viscosity (μ_g (g/cm s))	**$1.95X10^{-4}$**
Fluidizing Gas Density (ρ_g (kg/m^3))	**$1.12X10^{-3}$**
Turbulent Bed Fluidizing Velocity (u_H (cm/s))	**200**
Bubbling Bed Fluidizing Velocity (u_L (cm/s))	**100**
Mean Seed Bed Particle Diameter ($\bar{d}_{Po}$ (μm))	**570**
T_{bed} (°C)	**35**

Figure 43 maps the various fluidization regimes in a fluid bed as a function of bed particles and gas properties. Also contained on the map are the coordinates of the experiments as determined by Equation 23 and Equation 24 that determine the fluidizing regime resulting from a given particle size and superficial gas velocity. The intersection of the broken lines indicate that the choice of a mean seedbed particle diameter of 570 microns results in a bubbling bed regime when fluidized at 100 cm/s and a turbulent bed regime when fluidized at 200 cm/s.

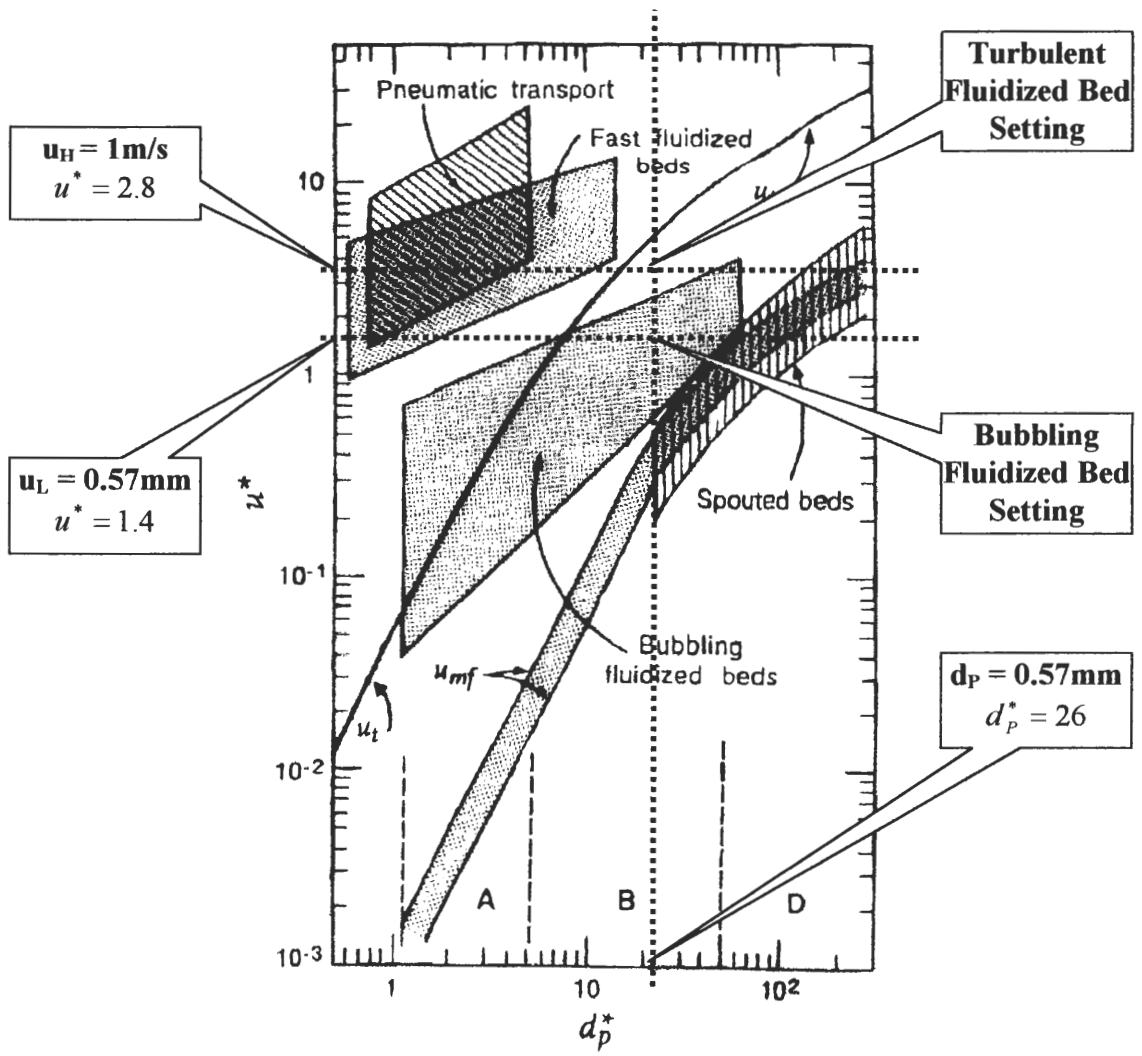

Figure 43. Fluidizing regime in terms of u_0 and $\bar{d}_{Po}$[2]

Molten Salt Feed Rate (F_0)

The lower molten salt feed rate in the factorial design was determined by establishing the lowest possible stable flow obtainable from the molten salt injection system. It was found that a molten salt feed rate below 1.1g/s resulted in either sporadic drops or a flow that could not be accurately directed into the center of the fluidized bed. Using lower flow rates is desirable because it increases the duration of the experiment before excessive particle growth leads to defluidization. This increase in the duration of the experiment allows for more samples to be taken in a single experiment and thus a longer examination of particle growth before the bed defluidizes. This low setting was then doubled to obtain the higher molten salt flow rate in order to determine an effect of molten salt feed rate. The resulting molten salt flow rates are 1.1 and 2.2 grams per second.

Molten Salt Feed Temperature (ΔT)

The two settings for molten salt feed temperature are 260°C and 300°C. These settings are the result of safety considerations. It was decided to operate well below the decomposition temperature of $NaNO_3 - KNO_3$ which is 500°C.[77] Establishing a maximum feed temperature of 300°C set the upper injection temperature. The difference between 300°C and the melting point, 222°C[78], is 78°C. This value of 78°C was divided in half for the sake of the factorial design to establish the lower injection temperature which is 39°C above the melting point or approximately 260°C.

Sampling Distance from the Top of Bed (D)

The upper and lower sampling ports are used to sample the upper and lower sections of the bed. The upper and lower sampling ports are located 324 mm and 391 mm below the surface of the bed respectively.

Seed Bed Particle Size Distribution ($\bar{d}_{Po}$)

The seedbed particle size distribution was determined by the mean particle size produced by sieving the model chemical in the range that would produce results indicated in Figure 43. This nominal diameter was determined to be 570 μm by sieving between 710 and 425 μm sieves.

Results and Discussion

The Results and Discussion section of this dissertation is divided into four sections to address the project objectives. Section 1 verifies the effectiveness of the sampling equipment and the techniques used to analyze the samples. Section 2 determines that there is minimal attrition of the seedbed during fluidization. Both of these sections are necessary to determine the ability of the experimental setup and procedures to effectively fulfill the objectives of this project.

Sections 3 and 4 address Objectives 2 and 3 of this project. Section 3 determines the particle growth rate results of the factorial design and determines the resulting particle size distributions. Section 4 determines the dominant mechanism of growth of particles in the bed.

Section 1 Test of Sampling Method

A test of the sampling method has been performed in this project to verify the accuracy and precision of the sampler as well as the techniques used to collect and analyze data. A known bimodal distribution of particle sizes was fluidized and five samples were taken with the sampler and compared to one another. This was done at both bubbling and turbulent fluid bed conditions.

The bimodal distribution used in this test was composed of 30% large particles and 70% small. The large particles were sieved between 1 mm and 1.4 mm sieves for a nominal diameter of 1.2 mm. This nominal diameter was later calculated as the mean particle diameter through image analysis. The small particles were sieved between 0.425 mm and 0.850 mm sieves for a nominal particle diameter of 0.63 mm. This also was later calculated to be the mean particle diameter of the smaller particle distribution. The small particle size range here was used as the initial particle size distribution in particle growth experiments. The combination of this distribution yielded a base mean particle diameter of 0.88 mm. This mean particle diameter is used in this section for comparison of the sampled distributions as well as direct comparison of the distributions.

1.1 Comparison of Sampling in Both Fluidizing Regimes

Two separate experiments were conducted in order to determine the effectiveness of the sampling method. Two identical batches of the bimodal distribution described previously were fluidized at bubbling (u_o=100 cm/s) and turbulent (u_0=200cm/s) as determined in the Design of Experiments Section. The mean particle diameters for each of these plots can be seen in Figure 44.

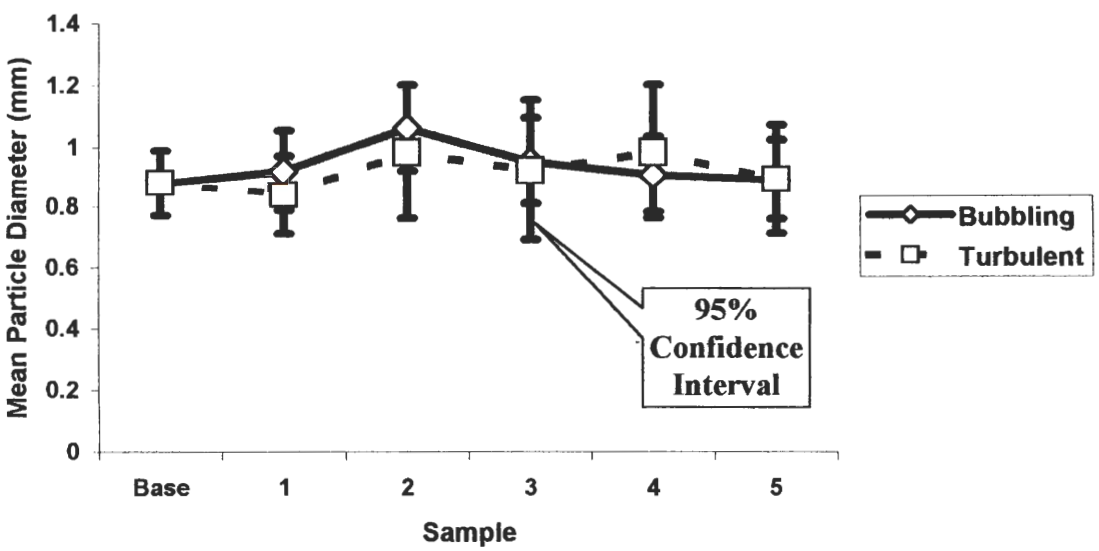

Figure 44. Mean particle size comparison of samples for both bubbling and turbulent distributions

These mean diameters and error bars indicate that there is no significant difference between the particle size distributions sampled but does not show any details concerning the individual distributions. For this reason, normalized cumulative distributions were analyzed.

1.2 Normalized Cumulative Distributions

The five samples represented by the mean particle diameters in Figure 44 for the bubbling bed sampling can be seen in Figure 45. The 70% mark indicates the division between the large and small particle sizes.

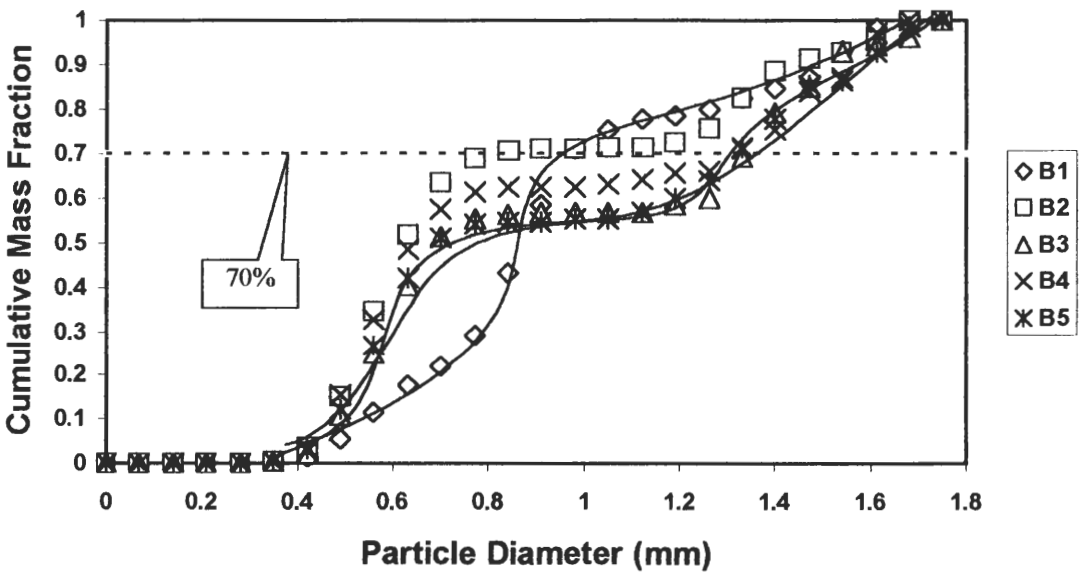

Figure 45. Bubbling bed cumulative mass distribution of both large and small particle sizes for bed samples (B1-B5).

As can be seen in Figure 45, there is a lack of sampling accuracy when comparing the relative masses of the larger and smaller particles. All curves should be horizontal at the 70% mark reflecting the 70% small particles and 30% large particles in the original particle size distribution. A normalized cumulative distribution was also prepared for the five samples taken from the turbulent fluidized bed. These can be seen in Figure 46.

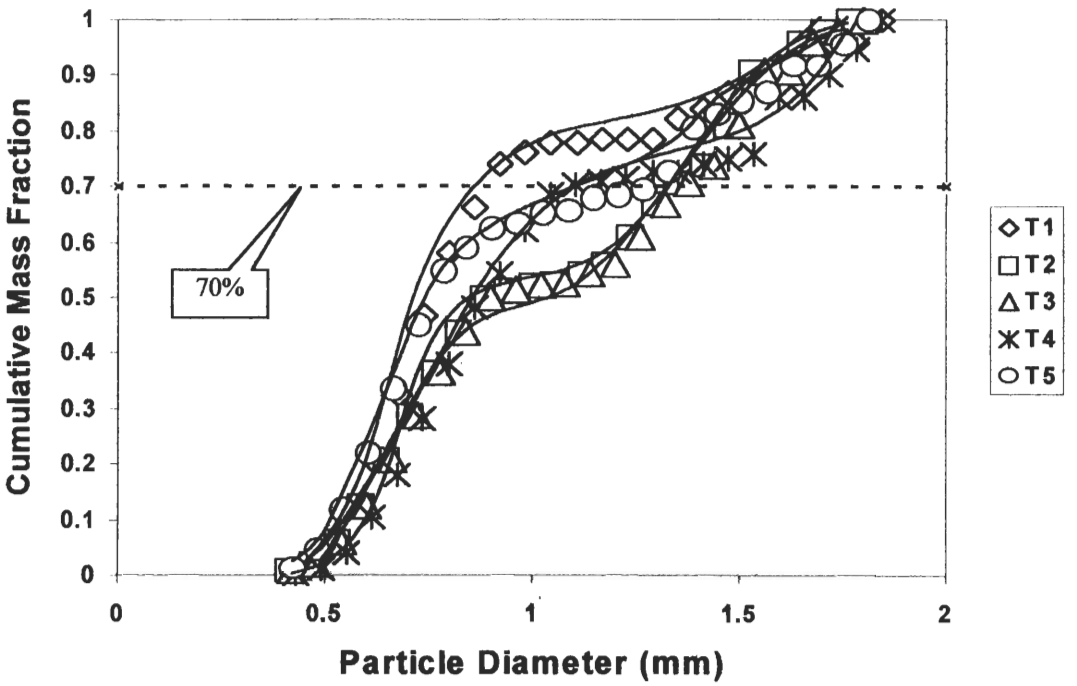

Figure 46. Turbulent bed cumulative mass distribution of both large and small particle sizes for bed samples (T1-T5)

Once again, there is a relatively large difference between the ratio of masses between large and small particles sizes as shown in Figure 46. This lack of accuracy is believed to be the result of errors in microscopy due to the size of the large particles relative to the microscope's field of view. An example of what occurred can be seen in Figure 47.

Frame 1 is able to sample large particle 1 but not large particles 2 and 3 because they overlap with the borders of the frame which means they will not be analyzed. Adjusting the field of view of the microscope to Frame 2 allows for all three particles to be included in the distribution.

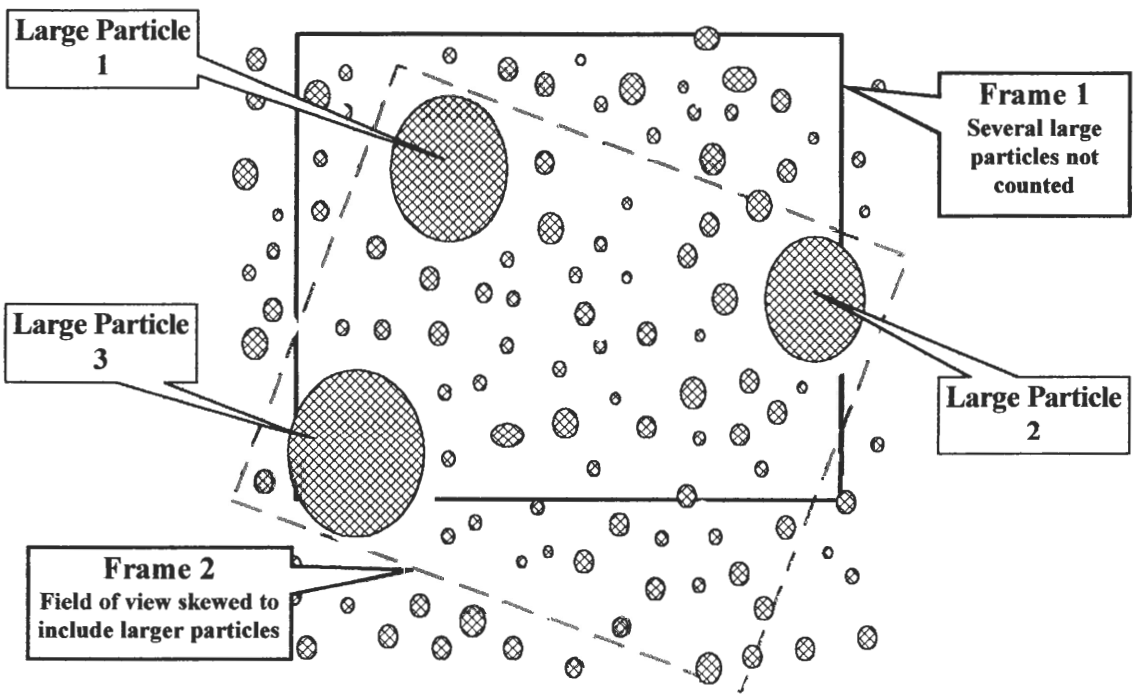

Figure 47. Example of how results are skewed when sampling larger particles

This results in nonrandom sampling of the large particles due to their large size relative to the size of the field of view. The use of Frame 1 results in an under representation of large particles by ignoring the partial effect of large particles 2 and 3, while Frame 2 over represents the large particles by catering the sampling toward them. As can be seen from the cumulative size distributions of both turbulent and bubbling bed samples, the latter was the case. This problem was solved in later experiments by dividing the samples taken from the bed into large and small particles, which are then analyzed separately with each having the appropriate size field of view.

As can also be seen in Figure 47, the small particles are randomly sampled in both Frame 1 and Frame 2. Their small size relative to the field of view allows for many to be sampled (photographed) in one frame so that the impact of particles not sampled because they overlap with the edge of the frame is not significant.

Because the smaller size range represents the initial particle size distribution where the majority of experimental data occurs and was randomly sampled, it was decided to look at only the small particles sampled. The cumulative distributions for the small particle size distributions for bubbling and turbulent bed sampling can be seen in Figure 48 and Figure 49 respectively.

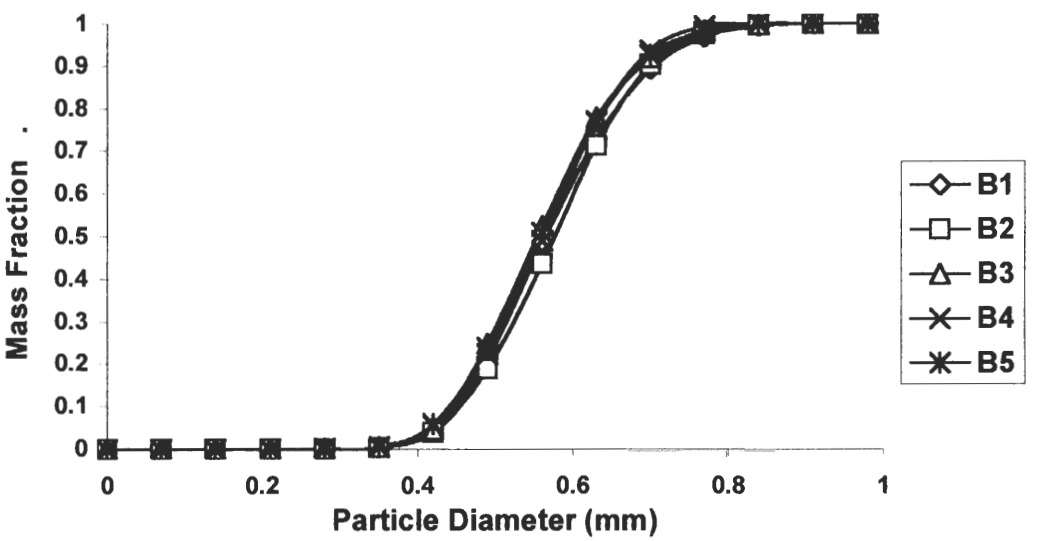

Figure 48. Cumulative distribution of small particle size for bubbling bed

This shows a precise sampling distribution with good repeatability. All of the curves follow the same path. The individual data points vary no more than +/-2% for each size increment (discussed in greater detail in Section 1.3).

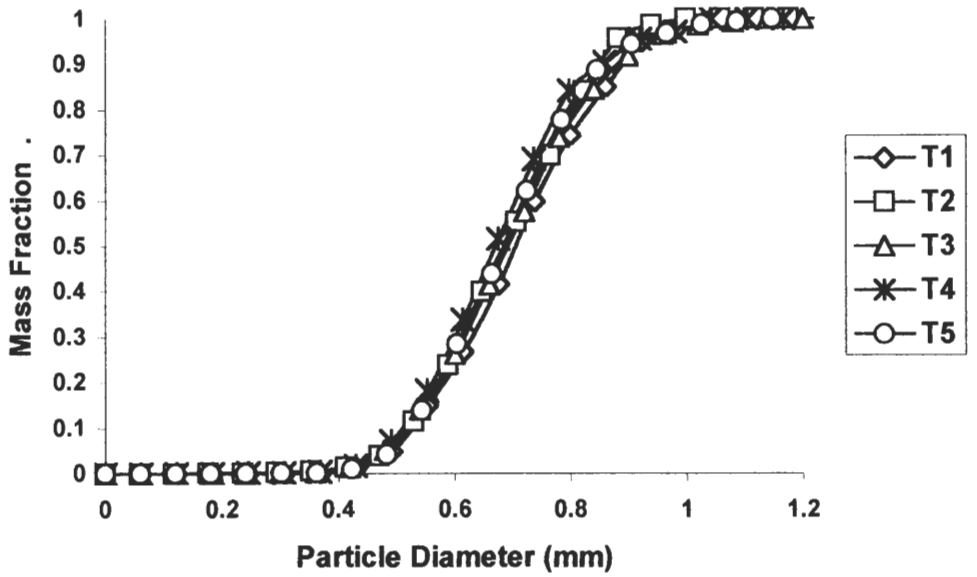

Figure 49. Turbulent samples compare well to one another

The turbulent bed also shows a precise sampling distribution with good repeatability. All of the curves follow the same path while individual data points vary no more than +/-2% for each size increment (discussed in greater detail in Section 1.3).

These two distributions were then compared with one another and with a particle size distribution generated by taking random samples from the small particle material apart from the fluidized bed.

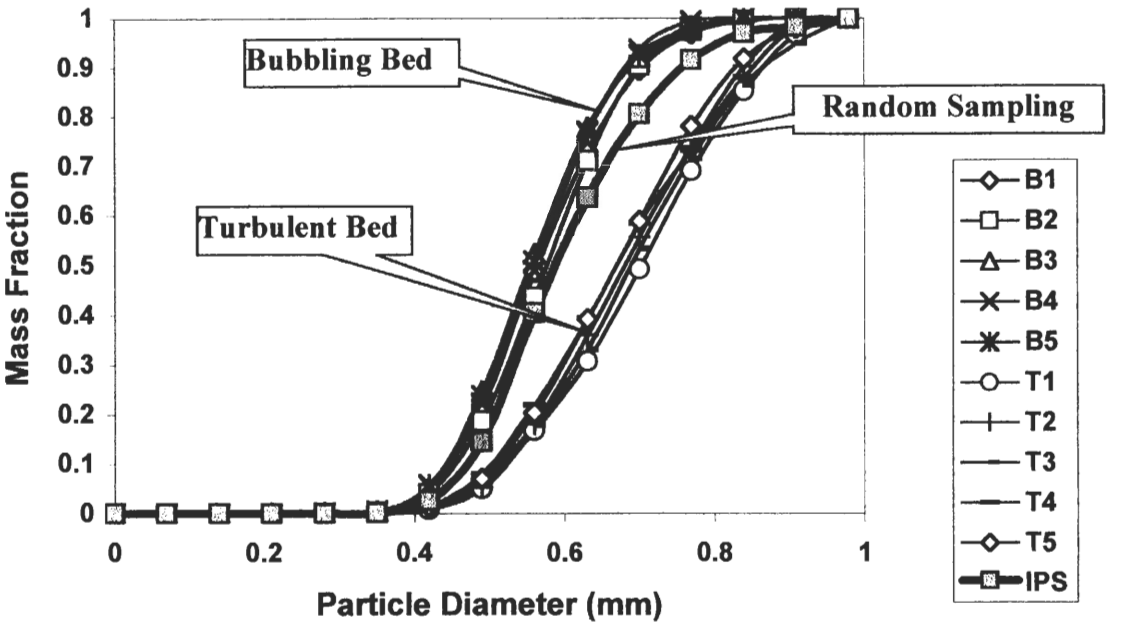

Figure 50. Comparison of normalized cumulative distributions for bubbling, turbulent, and a distribution formed from several random samples taken apart from the fluidized bed. The individual distributions are in chronological order of sampling (1-5) where B –Bubbling and T - Turbulent

The bubbling bed and random samples compare well but the turbulent bed sample is showing a large amount of larger material. This is believed to be the result of the breakup of particles in the large particle distribution under the higher stress environment of the turbulent bed. These larger particles were ball milled unlike the smaller particles, which had been broken down in a blender to achieve their small particle size. These ball milled particles contained void spaces that may have caused them to partially break up and add more material to the smaller particle distribution.

Other possibilities for this difference were considered but rejected such as elutriation of smaller material out of the bed due to higher fluidizing velocities. This was

rejected due to the consistent presence of small particles in the turbulent sampled distribution (A). The size of particles that could be elutriated was calculated to be < 0.2 mm at the bubbling bed velocity (1 m/s) and < 0.36 mm for the turbulent bed velocity (2 m/s) while all particles used in these tests were > 0.425 mm. Also, if elutriation were the cause, then a curve like the broken line marked elutriation in Figure 51 would be expected, where much of the small material has been blown out of the bed.

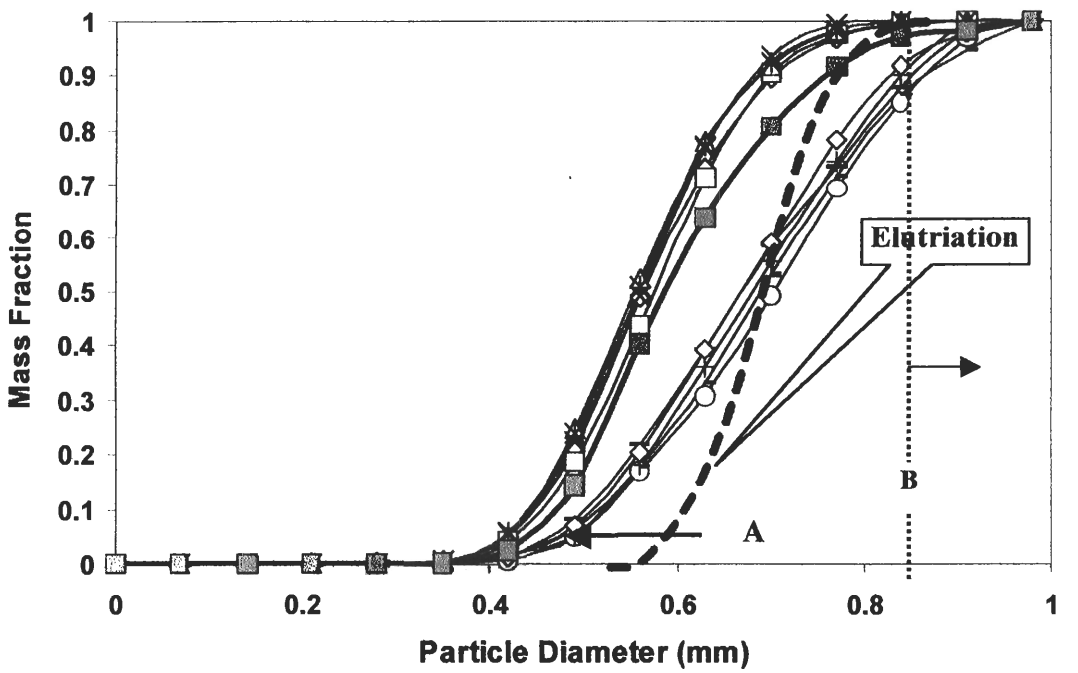

Figure 51. Cumulative distribution argument

The argument that attrited material is responsible for the difference seen between the distributions is further supported by the existence of material to the right of broken line B. No material was added to the bed in this size range as is indicated by the other two distributions. The turbulent distribution however has a noticeable amount of this material, which could have only come from larger particles breaking down, and adding material.

Mean particle diameters were calculated for each of these five distributions and compared to one another and the base mean particle diameter. These mean particles were then plotted together for comparison as can be seen in Figure 52. The error bars represent a 95% confidence interval of each distribution while the solid horizontal line represents the average of each set of these five values.

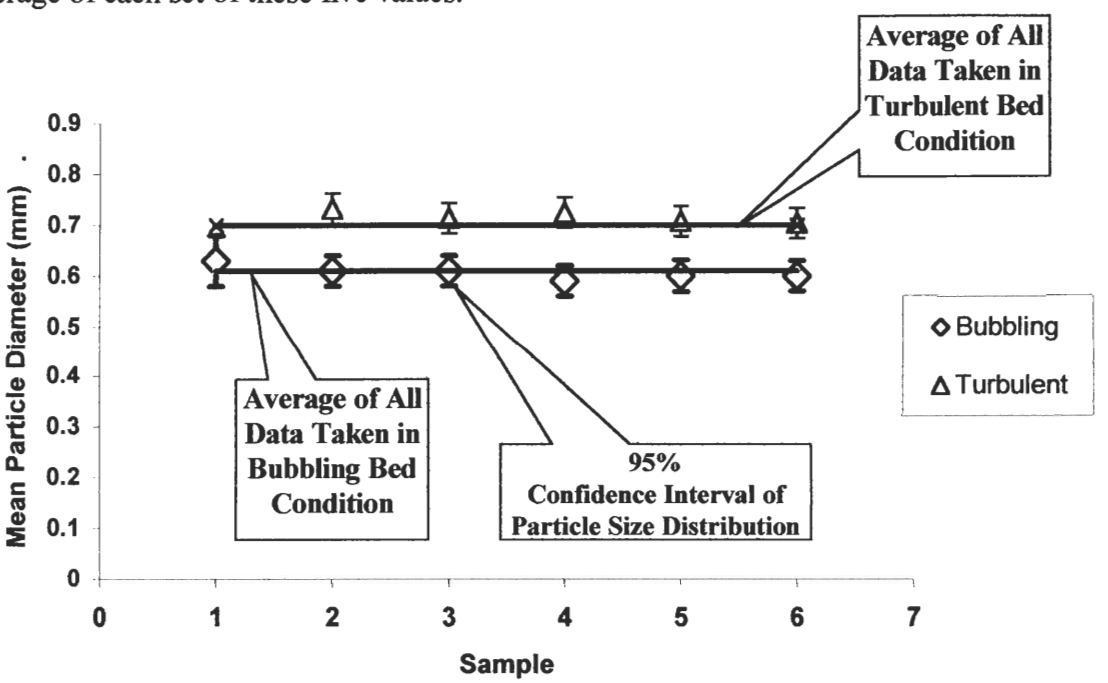

Figure 52. Mean particle diameter of comparison of bubbling and turbulent bed samples

It should be noted that the error bars of all sampled mean diameters and the calculated base mean particle diameters overlap with each other as well as with the average of all particle means (indicated by the straight horizontal line). This indicates an accurate and precise sampling technique under bubbling bed conditions. As stated previously, there is a slight difference between the mean particle diameters of the turbulent sample as compared with those of the bubbling sample.

1.3 Sensitivity of Sampling

Sampling at each fluidization condition was further analyzed to determine the sensitivity of the sampling test to noise or random errors. In order to accomplish this, a plot of the average of the five separate distributions was plotted for each condition with error bars representing one standard deviation of each of the replicated points. The average normalized frequency distribution for the bubbling bed sampling condition can be seen in Figure 53.

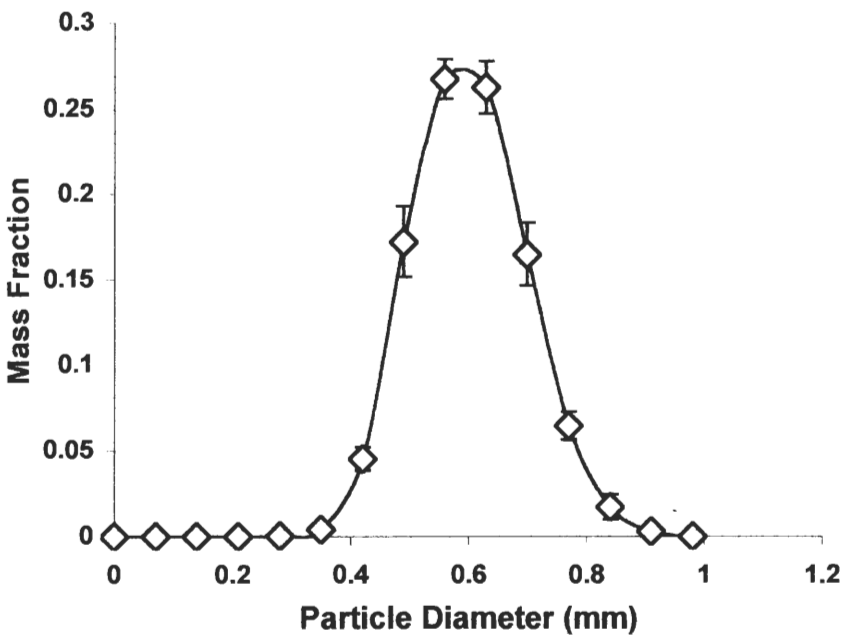

Figure 53. Bubbling bed normalized frequency distributions averaged. Error bars represent +/-1 sigma.

The range of standard deviations varies at most +/-0.02 or +/- 2% of the mass of any one-particle size range. Next, the average normalized frequency distribution for the bubbling bed sampling condition can be seen in Figure 54.

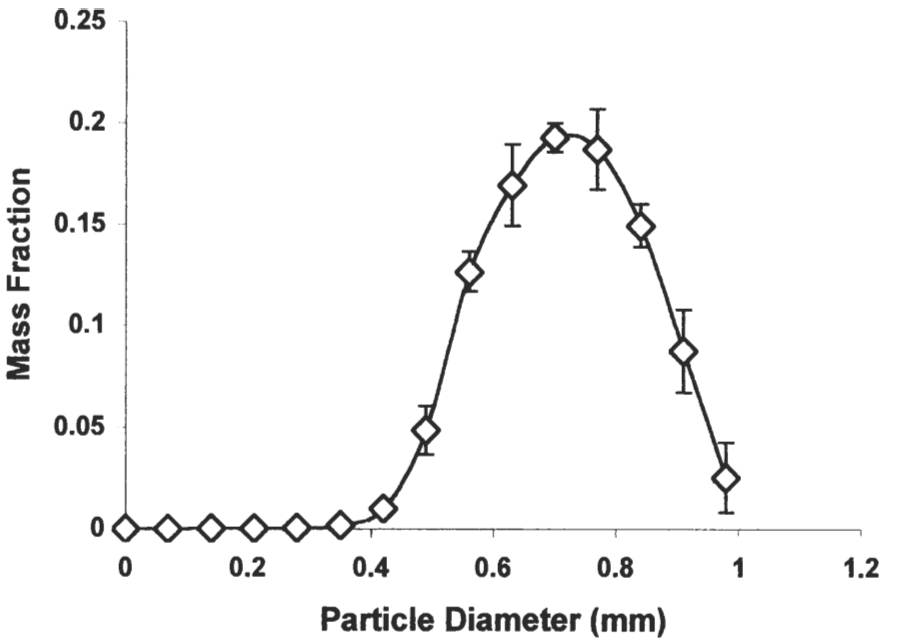

Figure 54. Turbulent bed normalized frequency distributions averaged. Error bars represent +/-1 sigma.

The range of standard deviations varies at most +/-0.02 or +/- 2% of the mass of any one-particle size range.

1.4 Conclusions

Samples taken with the sampler and analyzed with the developed sampling technique are repeatable and representative of the bed sampled. Repeated samples are shown to have a +/- 2% standard deviation associated with them when averaging over five replications, therefore showing that the technique is relatively sensitive.

Section 2 Test of Seedbed Attrition

A test of seedbed attrition was performed to verify that the initial particle size distribution to be used in particle growth experiments would not degrade or breakdown as a result of attrition caused by fluidization conditions. A breakdown in the seedbed distribution due to attrition would make interpretation of results difficult because the initial starting point for particle growth would not be constant and defined. All particle growth analysis in this project is based on the initial particle size distribution, making it very important that it remain constant and definable. It is, therefore, important to determine if the particle size distribution is changing with time under fluidizing conditions with no molten salt feed.

The bimodal distribution used in this test was composed of 30% large particles and 70% small where the small particle size distribution represents the initial particle size distribution used in the particle growth experiments discussed in Section 3. The small particles were sieved between 0.425 mm and 0.850 mm sieves for a nominal particle diameter of 0.63 mm. This also was later calculated to be the mean particle diameter of the small particle size distribution. The large particles were sieved between 1 mm and 1.4 mm sieves for a nominal diameter of 1.2 mm.

Only attrition of the small particle size distribution is analyzed in this section because it is the initial particle size distribution used for all particle growth experiments. As stated earlier, this section determines if the initial particle size distribution will break down under fluidized bed conditions in the absence of molten salt.

2.1 Bubbling Bed

The bimodal distribution of particles was used as a seedbed and fluidized at 100 cm/s to create a bubbling bed. Five samples were removed from the bed at five-minute intervals and compared with one another as can be seen in Figure 55.

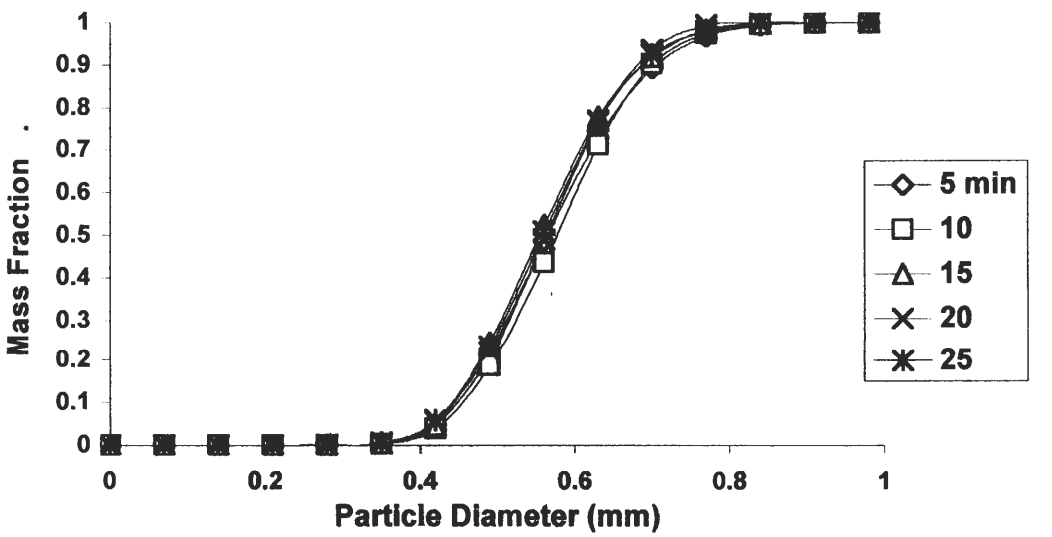

Figure 55. Bubbling bed shows no change in particle size distribution over time and no increase in small particles without molten salt feed

As can be seen in Figure 55, there is no increase in small particle sizes over time. The volume of small particles would be expected to increase during attrition as a result of the fragmentation of seedbed particles. There is also no change in the particle size distribution over time as can be seen from the close fit of all the curves in Figure 55. This indicates that there is no attrition of the initial particle size distribution under bubbling bed conditions.

The mean particle size for each of these distributions was calculated and compared to one another and the base mean particle diameter (Figure 56). The error bars represent a 95% confidence interval of each distribution.

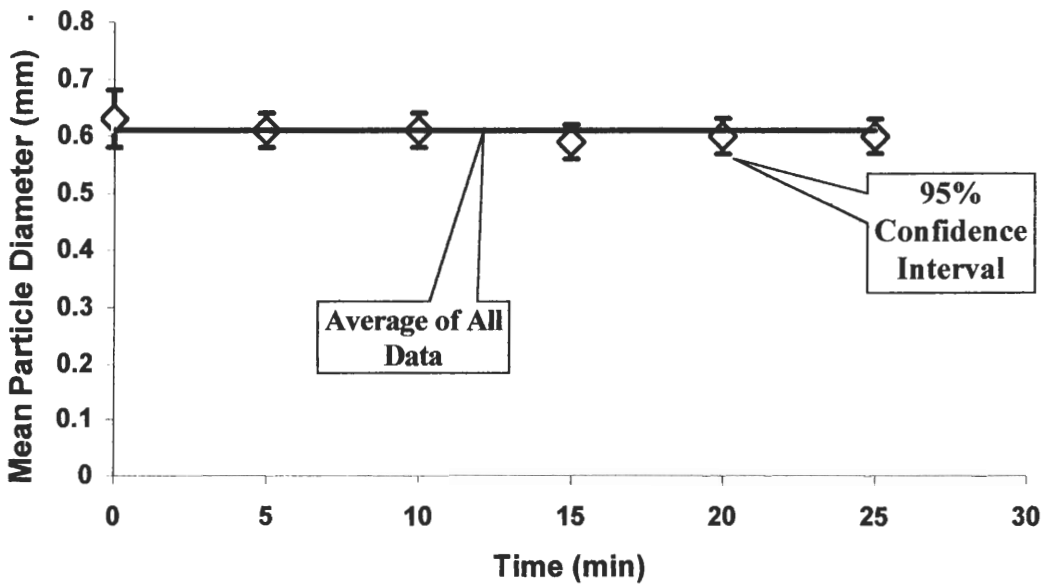

Figure 56. Plot of mean particle diameter over time shows no attrition of the initial particle size distribution

Because there is no molten salt feed, the plot of mean particle size in the bed should either decrease as a result of attrition or remain the same in the absence of attrition. As can be seen from Figure 56, the mean particle size does not decrease over time indicating that there is no attrition of the seedbed during bubbling bed fluidization. This experiment was conducted approximately four times longer than experiments with molten salt feed to insure that the seedbed or initial particle size distribution remained constant.

2.2 Turbulent Bed

The bimodal distribution of particles was used as a seedbed and fluidized at 200 cm/s to create a turbulent bed. Five samples were removed from the bed over a 25-minute period and were compared to one another. This comparison can be seen in Figure 57.

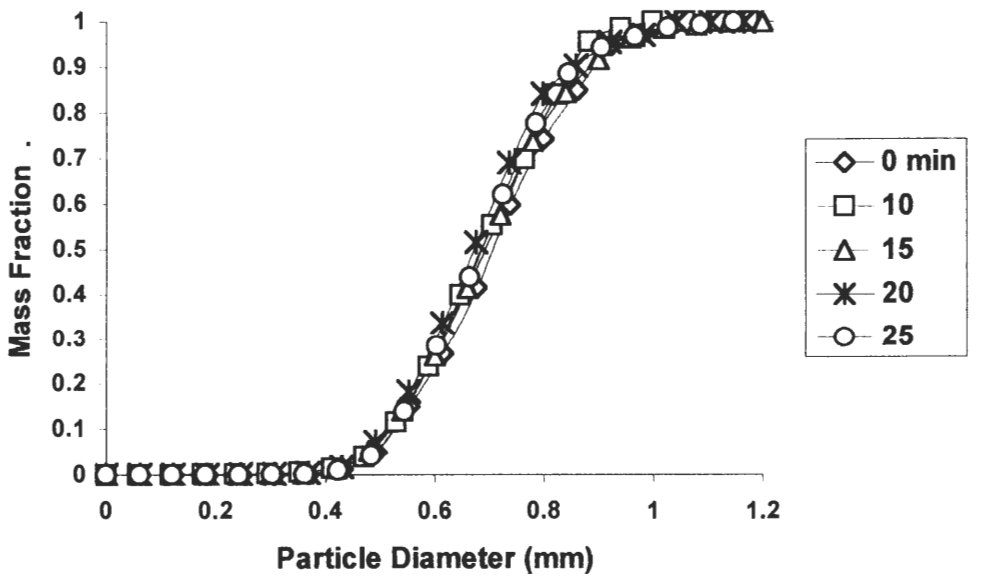

Figure 57. Turbulent bed shows no change in particle size distribution over time and no increase in small particles without molten salt feed

There are no signs of smaller seedbed material being generated through attrition over time, as can be seen in the closeness of fit of the plotted curves in Figure 57. If attrition were a factor there would be a change in these curves relative to one another over time. This indicates that there is no seedbed attrition at turbulent bed conditions.

Mean particle diameters were calculated for each of these particle size distributions and compared to one another over time and with the calculated base mean particle diameter. This comparison can be seen in Figure 58.

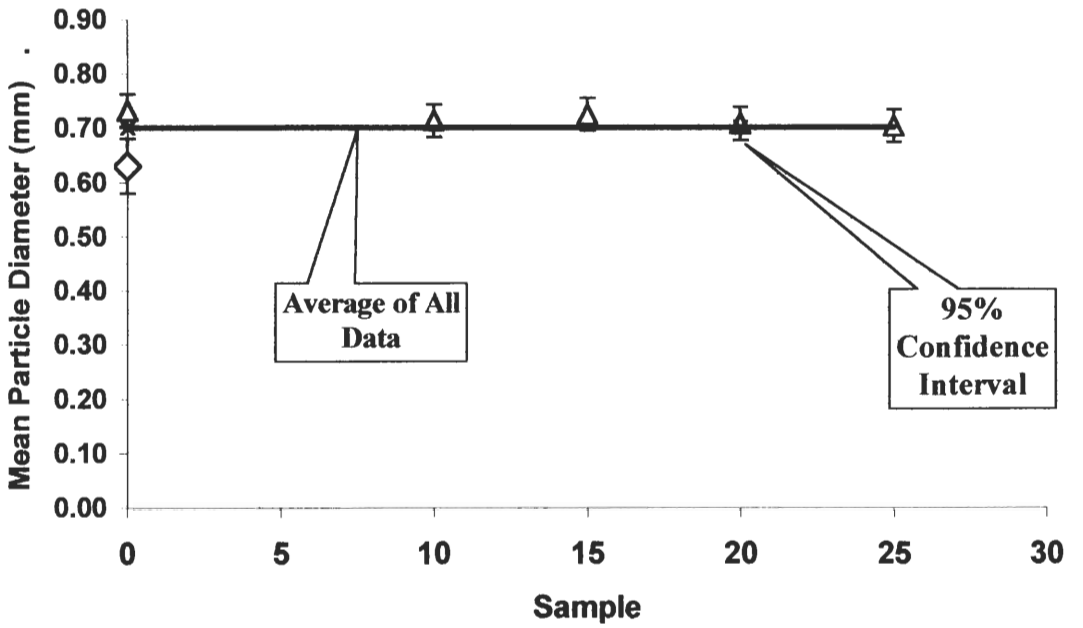

Figure 58. Plot of mean particle diameter over time shows no attrition of the initial particle size distribution

It should be noted that the error bars of all sampled mean diameters overlap with each other and with the overall average of mean diameters as indicated by the straight horizontal line. There is no decrease in mean particle size over time, which shows that there is no seedbed attrition. The mean particle diameters are slightly higher than would be expected, as indicated by the base mean particle diameter (0.63 mm). This difference is discussed in Section 1 concerning the breakdown, not of the initial particle size distribution, but of the larger particle size distribution. These mean particle diameters as well as the normalized cumulative particle size distributions show no attrition of the initial particle size distribution under turbulent fluidizing conditions.

2.3 Conclusions

Particle size distributions indicate no increase in small particles as would be expected if the seedbed were undergoing attrition. The mean particle diameter of the particle size distributions in both bubbling and turbulent fluidizing regimes show no significant decrease over 25 minutes of fluidization which is approximately 4 times longer than any of the experiments run in this project. This indicates that the particle seedbed distribution does not break down under fluidizing conditions and can be used as a base for growth analysis in particle formation experiments.

Section 3 Particle Growth Rate and Size Distribution

Sections 1 and 2 show that samples taken from the bed can be used to represent the particle size distribution in the bed, and that the initial seed bed particle size distribution is constant and can be used as a starting point from which to measure particle growth rate. This section contains the results of particle growth rates for each condition of the factorial design. These particle growth rates were determined from the rate of change of the mean particle diameter as determined by the centroid of the particle size distribution.

These particle growth rates were then analyzed using analysis of variance to determine significant effects to particle growth rate as a result of changes in the values of system variables according the factorial design of experiments (Experimental Design). Significant interactions between variables within the factorial design were also determined in the analysis of variance. An empirical equation was then developed using result from the analysis of variance to calculate particle growth rate.

3.1 Particle Growth Rate

The particle growth rate in the bed has been determined by the change in the fluid bed mean particle diameter with respect to time. The growth rate that is referred to here is the rate of change in mean bed particle diameter until material begins exiting the bed, as discussed earlier in the Experimental section under Procedures. These mean particle diameters were then plotted against time to determine the rate of particle growth, as can be seen in Figure 54.

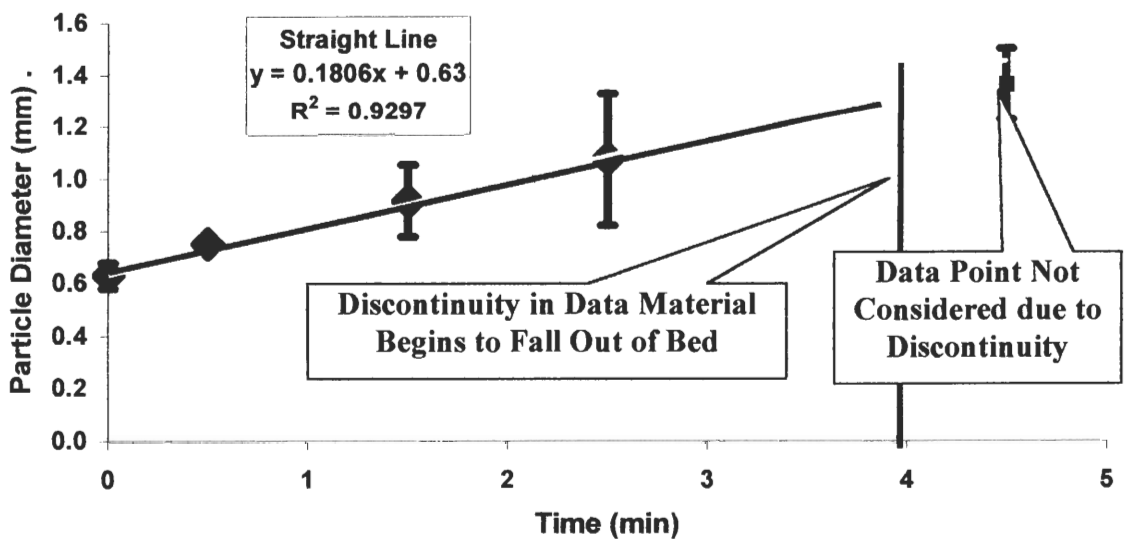

Figure 59. Linear rate of mean particle growth with time. Experiment 3.1

These growth rates can be seen in Table 10 where D_{Lower} and D_{Upper} refer to growth rates measured in the upper and lower sampling positions respectively.

Table 10. Particle growth rate as expressed by rate of change of mean particle diameter (mm) with time (min)

EXPERIMENT	F_0 (g/s)	U_0 (m/s)	T (^oC)	D_{LOWER} (mm/min)	D_{UPPER} (mm/min)
1	1.1	1	260	0.24	0.22
2	2.2	1	260	0.25	0.34
3	1.1	2	260	0.16	0.17
4	2.2	2	260	0.15	0.19
5	1.1	1	300	0.2	0.24
6	2.2	1	300	0.25	0.34
7	1.1	2	300	0.12	0.14
8	2.2	2	300	0.18	0.19

The particle growth data in Table 10 are the result of three experimental replications. These experiments were randomly ordered to insure the integrity of the factorial design. The plots from which these growth rates were derived can be seen in Appendix 3.

3.2 Determining Statistically Significant Effects of System Variables

An analysis of variance has been used to determine the statistical significance of the effects of changes of experimental variables, as well as any significant interactions taking place between experimental variables.

3.2.1 Analysis of Variance [79]

An analysis of variance has been performed in order to determine the significant main effects and interactions that occur in the bed. Three main effects and three interactions between main effects were determined to be significant by this analysis and can be seen in Table 11. The entire analysis results can be seen in Appendix 3.

Table 11. Significant effects resulting from analysis of variance. Effect used here refers to the whether an increase in the source of variation increases (+) or decreases (-) the overall particle growth rate

Main Effects			
SOURCE OF VARIATION	**EFFECT**	**F RATIO**	**CRITICAL F (95% CONFIDENCE)**
Molten Salt Feed Rate (F_o)	+	**23.7**	**4.21**
Superficial Gas Velocity (u_o)	-	**136.6**	**4.21**
Sampling Position (D)	+	**10.1**	**4.21**
Interactions			
SOURCE OF VARIATION	**EFFECT**	**F RATIO**	**CRITICAL F (95% CONFIDENCE)**
F_o x u	-	**10.6**	**4.21**
F_o x ΔT	+	**4.5**	**4.21**
u_o x ΔT	+	**4.6**	**4.21**

3.2.2 Main Effects of Experimental Variables on Particle Growth

Superficial Gas Velocity (u_0)

As stated earlier, the low and high superficial gas velocities in this project have been chosen to produce bubbling and turbulent fluidizing regimes respectively. As seen in Table 11, the effect of changing the fluidizing regime on particle growth rate is extremely negative. This large negative effect (–0.19 mm/min) indicates that there is a significant decrease in the rate of particle growth rate by changing the fluidizing regime from a bubbling bed to turbulent bed.

This decrease in particle growth rate with a change from a bubbling to a turbulent fluidizing regime is believed to be the result of two things: the first is an increase in the amount of mixing in the bed and the second is an increase in the rate of heat transfer. An increase in the amount of mixing in the bed increases the forces that tear apart agglomerated particles bound by molten salt before the salt can solidify and form a solid particle.

An increase in the rate of heat transfer decreases the amount of time that molten salt is available in the system to bind particles together. This increase in heat transfer is a result of the increased flow of cool air through the bed and also an increase in mixing. The same increase in the mixing of gas that creates the forces that tear apart particles also increases the amount of cool gas contacting the surface of the molten salt in the bed through turbulence at the boundary layer of the molten salt. This increases the heat

transfer and thus decreases the amount of time the molten salt is available to bind particles into agglomerates.

Molten Salt Feed Rate (F_0)

An increase in the flow rate of molten salt results in an increase in the growth rate of particles in the bed. This makes sense because an increase in the flow rate of molten salt into the bed increases the amount of binder (molten salt) available to bind or stick particles together as agglomerates.

Level in Bed (D)

The significant decrease determined in particle growth rate between the upper sampling position and the lower sampling position is believed to be the result of attrition at the distributor. Attrition as used in this project refers to the reduction in diameter of solid particles by collisions in the bed. The distributor is a region of high local turbulence, which increases the number and force of particle collisions.[2]

3.2.3 Interactions of Experimental Variables Affecting Particle Growth

Molten Salt Feed Rate - Molten Salt Feed Temperature (F_0 - ΔT)

The higher settings of molten salt feed temperature (T_{ms}) and feed rate (m_{ms}) were determined to have a positive effect on particle growth rate by increasing the dispersion (A_{ms}) and residence time (dt) of the molten salt as can be seen in the relationship expressed by Equation 25.

$$h(T_{MS} - T_{Bed})A_{MS} = m_{MS}C\frac{dT_{MS}}{dt} \qquad \textbf{Eqn 25}$$

The dispersion of the salt is increased by the higher molten salt stream velocity which increases the shear forces that tear the stream apart and decreases the resistance of the stream to be torn apart by lower surface tension and viscosity caused by the higher injection temperature. A two-fold increase in the mass flow rate of molten salt also doubles the molten feed stream velocity into the top of the bed. This 2.2 g/s is being transferred out of the same 3.2mm tube (14.5cm/s) as used for the lower flow rate of 1.1 g/s (7.2cm/s). This increase in velocity increases the penetration of the molten feed stream into the fluidized bed, which further increases the overall dispersion of the salt. The residence time of the molten salt (dt) is increased due to the greater sensible heat in the salt (C dT_{ms}) and the lower heat transfer coefficient (h). The heat transfer coefficient is at a low level due to the lower fluidizing gas velocity (u_o) as can be seen using Equation 26 in conjunction with the calculations of Reynolds number (Re) from Equation 27 and the calculation of Prandtl number from Equation 28.[2]

$$h = \left[2 + 0.6\,\mathrm{Re}_{sph}^{1/2}\,\mathrm{Pr}^{1/3} \right] \frac{k_g}{\bar{d}_p} \qquad \textbf{Eqn 26}$$

$$\mathrm{Re} = \frac{\rho_g \bar{d}_p u_0}{\mu} \qquad \textbf{Eqn 27}$$

$$\mathrm{Pr} = \frac{C_g \mu_g}{k_g} \qquad \textbf{Eqn 28}$$

Molten Salt Feed Rate -Superficial Gas Velocity (F_0 - u_0)

As can be seen in Table 11, the overall rate of growth decreases as result of the interaction between increases in molten salt feed rate and superficial gas velocity. This is

believed to be the result of an increase in heat transfer rate in the bed and an increased dispersion of molten salt. The increased heat transfer in the bed is the result of an increase in the heat transfer coefficient when the higher fluidizing velocity is applied to Equation 26, 27, and 28.

A greater dispersion of molten salt in the bed is the result of increases in the velocity of each of these two experimental variables. The increase in the superficial gas velocity results in more turbulence (turbulent bed), which serves to disperse the molten salt by an increase in overall bed mixing.

An increase in the dispersion of molten salt increases its overall surface area which, in combination with the higher heat transfer rates of the bed due to increased superficial gas velocity, decreases the overall time that molten salt is available in the bed to grow particles. This fact, in combination with the increased mixing forces in the bed due to an increased superficial gas velocity, further decreases the opportunity for particle growth.

Superficial Gas Velocity - Molten Salt Feed Temperature (u_0 - ΔT)

The interaction of the superficial gas velocity and the molten salt feed temperature results in an increase in the particle growth rate. An increase in the molten salt feed temperature increases the ability of the superficial gas velocity to disperse the molten salt by reducing the surface tension and viscosity of the salt as discussed in previous subsections. The effect of the increased heat transfer due to increased superficial gas velocity is believed to be reduced by the increase of sensible heat in the molten salt in accordance with Equation 25 and is discussed in greater detail in previous subsections.

An increase in the residence time of the molten salt increases the opportunity to coat or agglomerate particles.

3.3 Regression Analysis

Two regressions were calculated using the significant experimental variables and interactions as determined in the analysis of variance. The first was calculated allowing a free-floating intercept and the second by force fitting the intercept of the equation to zero. The goodness of fit of the two distributions is then compared to determine whether a linear regression adequately represents particle growth.

Finally, a linear regression is calculated using the dimensionless groups defined in Table 5. The terms of this regression are then analyzed for their overall impact on particle growth in order to identify the more important dimensionless groups.

3.3.1 Free Intercept

Allowing the truest fit of the experimental data results in

Empirical particle growth equation with free intercept ($R^2 = 0.93$)

$$\frac{d\bar{d}_P}{dt} = 0.35 + 0.087(F_o) + 1.8x10^{-5}(u_o) + 5.2x10^{-4}(D) - 4.8x10^{-5}(F_o)(u_o) + 5.9x10^{-4}(F_o)(\Delta T) - 7.4x10^{-7}(u_o)(\Delta T) \quad \left(mm/_{\min}\right) \qquad \textbf{Eqn 29}$$

This is the truest fit of the data but not necessarily the most accurate outside the experimental values used in this project. This can be observed by setting all of the variables in the equation to zero resulting in a particle growth rate of 0.35 mm/min for particles with nothing happening to them.

3.3.2 Zero Intercept

Force fitting the origin of this regression to zero allows a more accurate representation of the entire process as seen in

Empirical particle growth equation with intercept at zero ($R^2 = 0.8$)

$$\frac{d\bar{d}_p}{dt} = 0.18(F_o) + 1.2x10^{-4}(u_o) - 5.2x10^{-6}(D) - 1x10^{-4}(F_o)(u_o) + 5.9x10^{-4}(F_o)(\Delta T) - 7.4x10^{-7}(u_o)(\Delta T) \quad \left(mm/\min\right) \qquad \textbf{Eqn 30}$$

The reduction in accuracy of this forced fit equation is the result of using a linear regression to describe a system that is not linear. This is apparent by the truest linear fit of the data resulting in a 0.35mm/min Y-intercept, which indicates that bed particles will grow with no molten salt feed or fluidizing gas. This is obviously not true and therefore indicates that the best fit of the data points and the Y-intercept should be a curve. A more accurate model will require multiple values of each experimental variable over a broad range to be used in a large and extensive experimental design[2], which is beyond the scope of this project.

3.3.3 Dimensionless Group Regression

A linear regression of the dimensionless terms introduced in Table 5 was calculated using experimental conditions. The overall impact of these terms on particle growth was then determined by multiplying the coefficients of each dimensionless group, as determined by linear regression, by the average value of that group (Table 4). The absolute values of these products were then compared to determine the relative importance that each dimensionless group had on particle growth. This can be seen in Table 12. The meaning of these relationships is discussed later in this subsection.

Table 12. Overall impact of dimensionless terms on particle growth rate ($R^2 = 0.91$) Classic dimensionless terms Re (Reynolds), Nu (Nusselt), Pr (Prandtl), We (Weber)

DIMENSIONLESS GROUP		VALUE OF GROUP	COEFFICIENT	PRODUCT	RANK OF IMPORTANCE
Re	$\frac{\bar{d}_{po} u_0 \rho_g}{\mu_g}$	**59**	**$5.6x10^{-5}$**	**$3.0x10^{-3}$**	**4**
Nu	$\frac{h \bar{d}_{po}}{k_g}$	**6.12**	**$-1.9x10^{-3}$**	**$1.2x10^{-2}$**	**2**
Pr_L	$\frac{C_{P_L} \mu_L}{k_L}$	**16.5**	**$2.5x10^{-2}$**	**$1.8x10^{-1}$**	**1**
Pr_g	$\frac{C_{P_g} \mu_g}{k_g}$	**0.71**	**$8.4x10^{-4}$**	**$8.1x10^{-4}$**	**6**
$\frac{Re_L^2}{We}$	$\frac{\sigma_L \bar{d}_{P_o} \rho_g g_c}{\mu_L^2}$	**6500**	**$-3.9x10^{-7}$**	**$1.0x10^{-2}$**	**3**
A	$\frac{\Delta T \bar{d}_{Po}^2 \rho_L^2 k_L g_c J}{\mu_L^3}$	**$4.1x10^{8}$**	**$-7.7x10^{-14}$**	**$2.5x10^{-4}$**	**7**
B	$\frac{F_0 \Delta H_f \bar{d}_{P_o}^2 \rho_L}{\mu_L J}$	**50**	**$1.2x10^{-5}$**	**$9.3x10^{-4}$**	**5**

Linear regression equation of dimensionless groups (mm/min)

$$\frac{d\bar{d}_P}{dt} = \frac{\left[\begin{array}{l} 5.6x10^{-5}\,\mathrm{Re}_g - 1.9x10^{-3}\,Nu + 2.5x10^{-2}\,\mathrm{Pr}_L + 8.4x10^{-4}\,\mathrm{Pr}_g \\ \qquad - 3.9x10^{-7}\left(\frac{\mathrm{Re}_L^2}{We}\right) - 7.7x10^{-14}\,A + 1.2x10^{-5}\,B - 0.02026 \end{array}\right]}{\left(\frac{\bar{d}_{Po}\rho_L}{\mu_L}\right)} \qquad \textbf{Eqn 31}$$

As can be seen in Table 12, the three dimensionless groups with the greatest impact on particle growth, Pr (Prandtl), Nu (Nusselt) and, Re^2/We (Reynolds^2/Weber), are all indicators of how long the molten salt remains molten in the fluidized bed. The impact of the other four terms is not considered due to their small overall products.

Prandtl number (Equation 32) was shown to have the greatest impact on particle growth and can be used to describe the ratio of the ability of the molten salt to remain molten relative to its ability to spread over the surface of the particle it is coating.

$$\mathrm{Pr} = \frac{C_{P_L}\mu_L}{k_L} = \frac{C_{PL}/k_L}{1/\mu_L} \qquad \textbf{Eqn 32}$$

The ability of the molten salt to remain molten is represented by the ratio of the specific heat capacity of the molten salt (C_{Pl}) or the amount of heat energy held in the molten salt divided by the molten salt's thermal conductivity (k_L) or its ability to get rid of this heat energy. The ability of the molten salt to spread over the surface of the particle is represented by the molten salt viscosity (μ_L) or the resistance of the molten salt to deformation or spreading.

The coefficient representing Prandtl number is positive, which indicates that a higher overall number leads to an increase in particle growth rate. The impact of this number is most likely a decrease in thermal diffusivity and not momentum diffusivity[63], because the viscosity of the molten salt is a second and third order term in other groups with much smaller impacts on particle growth (i.e. A and B).

Nusselt number (Equation 33) is an indicator of the rate of heat transfer at the surface of the particle shown mainly by the convection coefficient (h), which indicated the rate of heat transfer by convection from the surface of the molten salt.

$$Nu = \frac{h\bar{d}_{Po}}{k_g} \qquad \textbf{Eqn 33}$$

The coefficient representing Nusselt number, as determined by regression, is negative which indicates that an increase in this number, and thus an increase in heat transfer from the molten salt, leads to a decrease in overall particle growth. Once again, the heat transfer rate is a strong determinant of particle growth rate. The rate of heat transfer determines the molten salt's residence time and dispersion of molten salt within the system and thus the opportunities for agglomeration.

Dimensionless group Re^2/We (Equation 34) is a representation of the thickness of molten salt coatings on particle surfaces.

$$\frac{\mathrm{Re}_L^2}{We} = \frac{\sigma_L \bar{d}_P \rho_g g_c}{\mu_L^2} \qquad \textbf{Eqn 34}$$

An increase in the quantity of this group leads to a thinner layer forming on the surface of the particle. This results from a decrease in the viscosity in the denominator and thus a decrease in the ability of the particle to resist deformation or an increase in the surface tension, which increases the tendency of the molten material to spread.

The coefficient for this group is negative which indicates that an increase in this number decreases the overall growth rate of particles. This may be the result of an increase in the heat transfer out of the molten salt and thus it's residence time in the bed. By decreasing the thickness of molten salt coating on bed particles, the molten salt surface area increases, which increases the pathway through which heat is transferred, and the effective heat transfer length decreases over which heat must travel. Both of these acting

together increases the heat transfer out of the molten salt and thus decrease the residence time of molten salt in the bed.

The results of this regression equation were plotted against actual growth in order to understand how the dimensionless group regression compared. The results of this comparison can be seen in Figure 60.

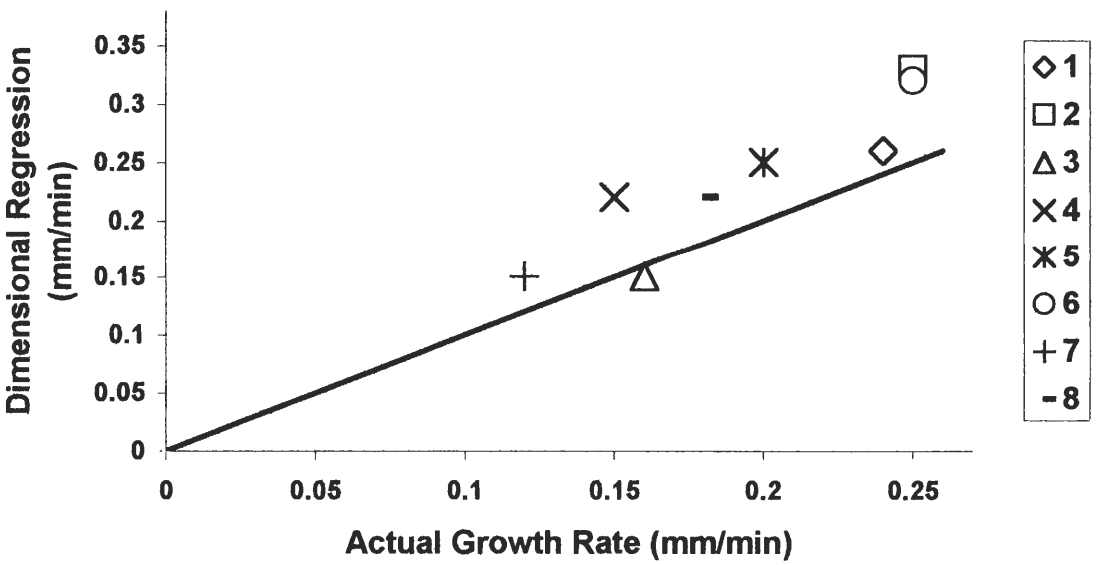

Figure 60. Comparison of predicted and actual growth rates

As can be seen from Figure 60, there does not appear to be any second order trend in the data or, in other words, the error existent in the data appears to be the random error resulting from the first and second regressions.

3.4 Particle Size Distributions

Particle size distributions for all of the experiments can be seen in Appendix 3. Analysis of these distributions is contained in Section 4.2.

3.5 Conclusions

Three of the four main variables used in this project gave significant changes to particle growth rate. It was determined that increasing the fluidizing intensity had a significant impact on particle growth rate. This increase in intensity was accomplished by changing the fluidizing regime from bubbling to turbulent. This was found to significantly decrease the overall particle growth rate. Conversely and to a lesser extent, it was determined that increasing the flow of molten salt into the bed increased the particle growth rate in the bed significantly.

There was a significant decrease in particle growth rate when comparing samples taken at the upper sampling position to the lower. This is believed to be the result of harsher conditions experienced by samples at the lower position due to its proximity to the distributor. The upper sampler was found to take a more representative bed sample.

Three interactions were also determined to be significant. The interaction between the molten salt feed rate and the fluidizing velocity resulted in an overall decrease of the particle growth rate. Interactions between molten feed rate and molten feed temperature decreased overall particle growth rate. Interactions between superficial gas velocity and molten feed temperature also resulted in an overall increase in the particle growth rate.

Section 4 Particle Growth Mechanism

Section 3 shows the particle growth rate resulting from changes to system variables. This section explains which mechanism of growth, agglomeration or coating, is responsible for particle growth by comparison of measured experimental growth rates with theoretical growth rates. These theoretical growth rates are determined by calculating the rate of mean particle diameter increase of particles growing by either coating or agglomeration. This section further describes the type of particles created by analyzing changes in particle size distributions and particle micrographs.

4.1 Comparison of Observed and Theoretical Growth Rates

4.1.1 Coating Model

The coating model assumes that all molten feed is deposited on single particles and that no particles combine by agglomeration. The following assumptions were made in the determination of particle growth rates using the coating model.

1. The probability of particles being coated is independent of particle size.

Particles have been shown to grow and interact randomly as indicated by Table 14 and the analysis thereafter. This also makes sense with a general understanding of bubbling bed fluidization where well-mixed particles are spread homogeneously, both in discrete volumes, and throughout the bulk of the bed.[2] It is therefore assumed that any coating that occurs in a discrete volume will be the result of the number of particles in that volume (probability) and not the type of particles (particle size).

2. Particles grow in proportion to their weight.

As particles are coated, heat from the coating begins to transfer to the particle and the fluidizing gas. As this happens, the coating begins to solidify and thus becomes unavailable to be stripped away by other bed particles colliding with it. The rate at which the coating solidifies is strongly influenced by the mass of the particle it is coating, because larger particles have a greater mass to absorb heat faster in relation to smaller particles. The longer the coating remains molten, the more opportunities there are for molten material to be stripped away by cold particles colliding with the hot molten coating which would serve to limit the amount of coating per particle. It is therefore assumed that particles grow in proportion to their weight.

With these two assumptions, the particle growth rate due to pure coating was determined by calculating the particle growth rate of all of the particles in the bed being coated evenly with the injected molten salt. The calculated number of particles in the bed was determined by dividing the volume of particles in each particle size range by the average volume of a particle in that size range. This calculation can be seen in Equation 35.

$$Number\ of\ Bed\ Particles\ (N_P) = \sum_{1}^{N} \frac{V_i}{\frac{4}{3}\pi\left(\frac{d_{Pi} + d_{Pi+1}}{4}\right)^3} \qquad \textbf{Eqn 35}$$

The calculated number of particles in the bed (N_P) is approximately 1.1×10^7. Assuming that the volume of the molten salt feed is divided equally over all bed particles, the growth rate observed in Figure 61.

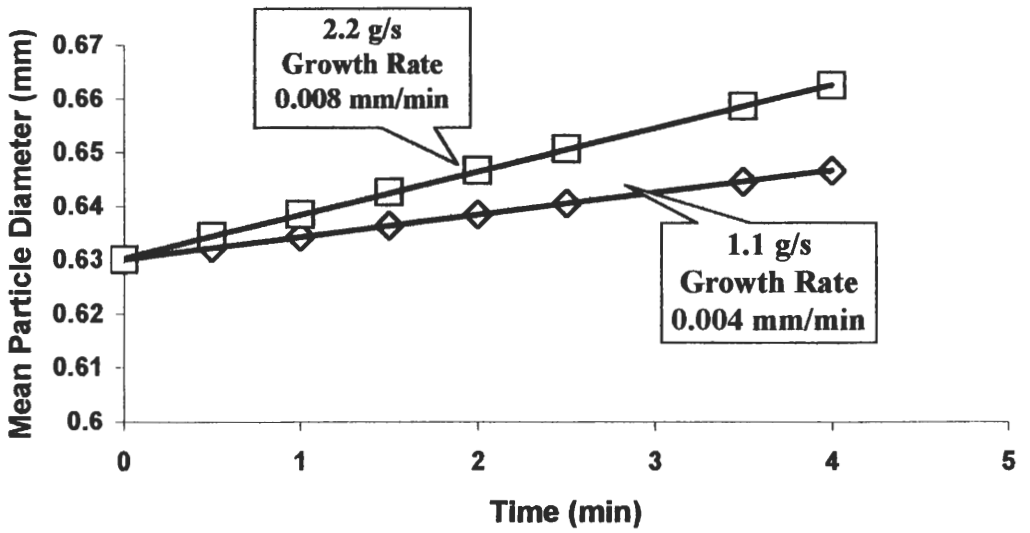

Figure 61. Coating mechanism theoretical particle growth rate for both molten salt feed rates assuming molten feed evenly coated all bed particles. This plot assumes that 100% of bed particles are coated.

The rate of increase in mean particle diameter is 0.004 mm/min for the low molten salt flow rate and 0.008 mm/min for the high molten salt flow rate under the conditions of 100% coating of the particles in the bed.

The range of particles affected by molten feed may not be 100%, however. The amount of the bed affected by molten salt depends strongly on the ability of the molten stream to penetrate through the bed as well as the time that it takes for the bulk of the bed to circulate completely through this affected area. Neither of these values is known so the mean particle growth rates resulting from the assumption of 100% particle coating are only one of many growth rates that might result from pure particle coating. For this reason, the growth rates resulting from different coated bed proportions were determined. These results can be seen in Figure 62.

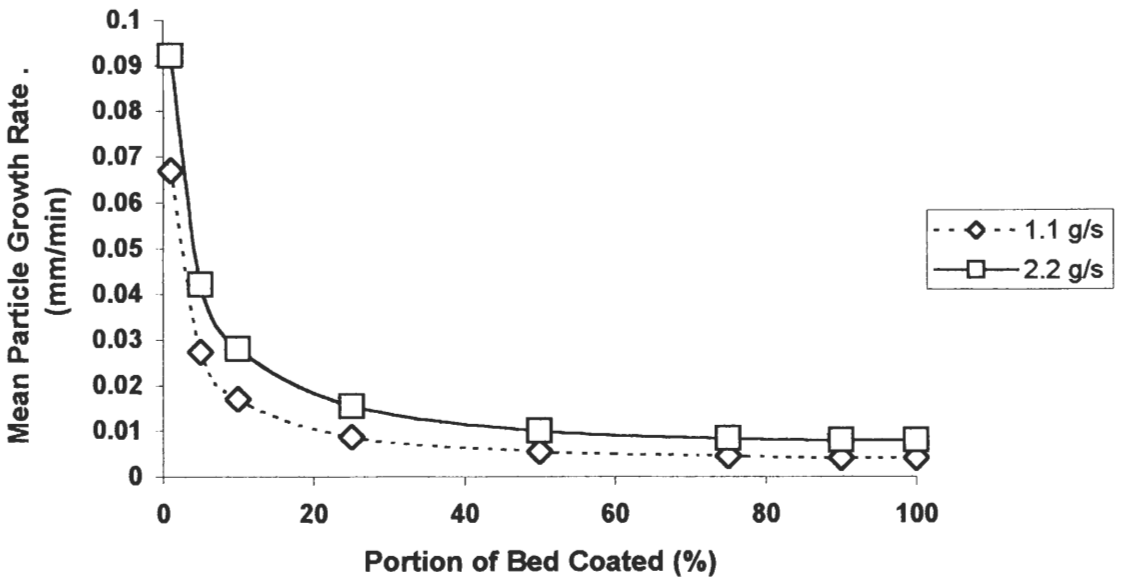

Figure 62. Theoretical mean particle growth rates for coating different percentages of the particle population at high and low molten salt feed rates

As can be seen from Figure 62, the overall mean particle growth rate increases as a smaller portion of the bed is coated. Assuming the most extreme scenario of only one-percent of the bed being coated, results in mean particle growth rates of 0.092 and 0.067 mm/min at 1.1 and 2.2 g/s of molten salt feed respectively. This means that for pure particle coating there is the possibility of a 0.004 to 0.067 mm/min particle growth rate at the low molten salt feed rate and a 0.008 to 0.092 mm/min particle growth rate at the high molten salt feed.

4.1.2 Agglomeration Model

This agglomeration model assumes that particles become bound together by the molten salt feed therefore forming larger particles and increasing the bed mean particle diameter in the process. This mechanism of particle growth can be the result of any

growth rate greater than the growth rate seen in the coating model. This model assumes that bed particles combine at a constant rate for each set of experimental conditions.

To better illustrate this idea with an example, assume that every seed particle in the bed combines with another seed particle at a constant rate that results in a bed composed of 2-particle agglomerates at 1.5 minutes. This resulting increase in the mean particle diameter of the distribution in this scenario can be seen in Figure 63.

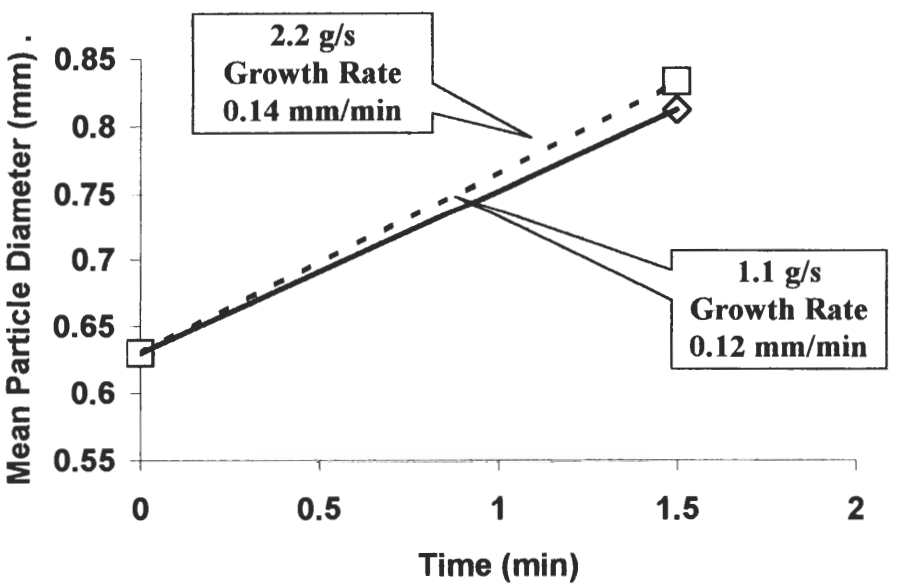

Figure 63. Rate of increase of mean particle diameter much greater than possible for coating mechanism.

The rate of increase in mean particle diameter is 0.12 mm/min for the low molten salt flow rate and 0.14 mm/min for the high molten salt flow rate which are both several times greater than what is possible with the coating mechanism as seen when comparing Figure 63 and Figure 61. The particle growth rate for the low flow condition, 0.12 mm/min, matches the growth rate seen in Experiment 7 which was the lowest particle growth rate observed in all conditions tested in this project. This indicates that all particle growth

rates resulting from the experimental conditions used in this project are the result of agglomeration.

4.1.3 Comparison of Models with Experimental Results

Particle growth rate in the bed is a result of both coating and agglomeration, but as can be seen in comparing the growth rates of both models with those of the experimental data in Table 10, it becomes apparent that agglomeration is the dominant mechanism of particle growth. Both models are ideal representations of particle growth and are not used here to represent what is actually happening in the experiment, but to indicate which mechanism is having the greatest impact on particle growth. A comparison of coating model growth rates and experimental particle growth rates in Table 13 illustrates the impossibility that coating is the dominant mechanism of particle formation. A comparison of initial (seed) particle volume in the bed shows that the mean particle volume has increased by 31-90% after thirty-seconds which is not possible to be the result of the coating mechanism which would have only increased the volume of the bed, and thus the mean bed particle, by 1-3%.

Table 13. Growth rates observed in the bed are much greater than those possible with the coating mechanism and mean size of particles being formed are much larger than the original seed particles. All values measured in (mm/min).

EXPERIMENT	EXPERIMENTAL GROWTH RATE	MAXIMUM POSSIBLE COATING GROWTH RATE	AVERAGE NUMBER OF SEED PARTICLES PER BED PARTICLE AT 30 SECONDS
1	0.23	0.067	1.65
2	0.3	0.092	1.9
3	0.17	0.067	1.46
4	0.17	0.092	1.46
5	0.22	0.067	1.62
6	0.3	0.092	1.90
7	0.12	0.067	1.31
8	0.19	0.092	1.52

Greater detail on the type of particles formed is contained later in section 4.2 and 4.3.

4.2 Difference of Distributions

Particle growth was analyzed in greater detail by determining the differences between the initial particle size distributions and the resulting particle size distributions of each experiment. This method was chosen because it clearly shows particles that grew (d_{PG}) and which particles were formed as a result of that growth (d_{PF}). Then determining the mass average particle diameter of each of these separate distributions allows for a more direct comparison of particles that grew (d_{PG}) and that were formed (d_{PF}). Calculating the mean particle diameter of each entire distribution without first isolating those particles that grew and that were formed, gives results obscured by the large amount of unaffected particles in each distribution. This can be seen in Figure 64 and Figure 65.

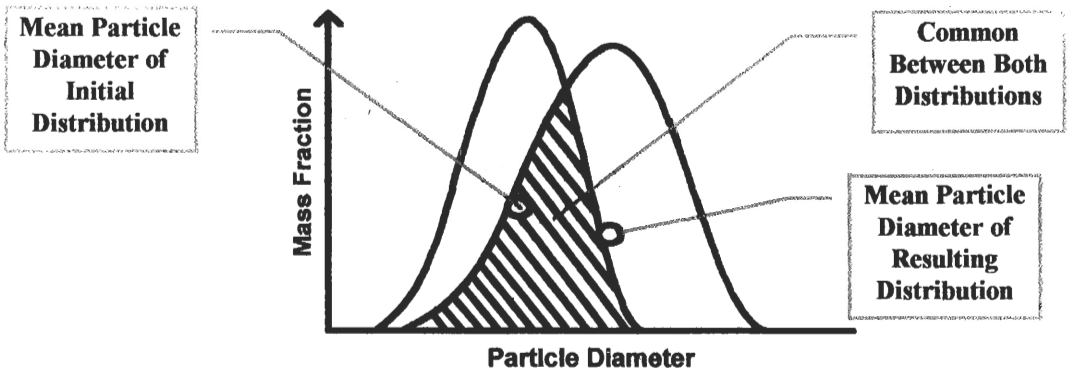

Figure 64. Mean diameters of distributions before affected particles are isolated

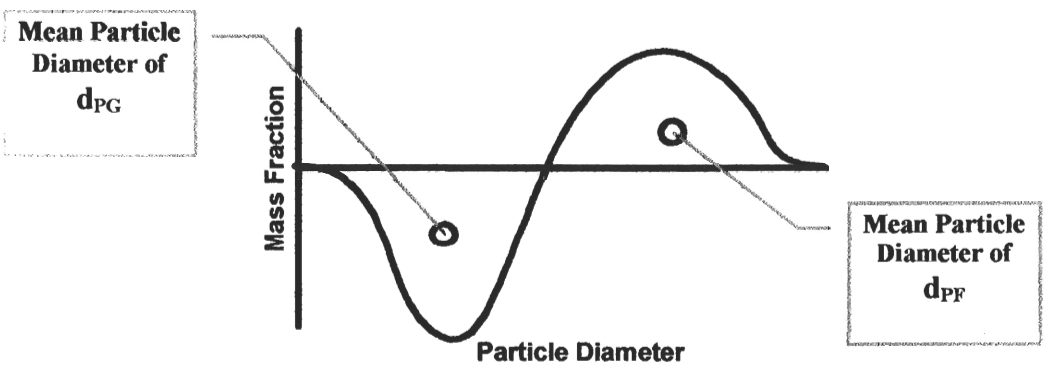

Figure 65. Separating the affected elements of each distribution increases understanding of how particles grew by focusing on what actually happened

4.2.1 Determining the Difference of Distributions

The differences between distributions were calculated by first normalizing the initial and resulting upper and lower distributions on a mass basis. Mass is used to normalize these distributions because it is continuous while variables such as the number of particles and surface area are changing as new particles form. The mass fractions of the upper (U1) and lower (L1) particle size distributions for Experiment 1.1 and, the initial particle size distribution (D_{Po}) can be seen in Figure 66.

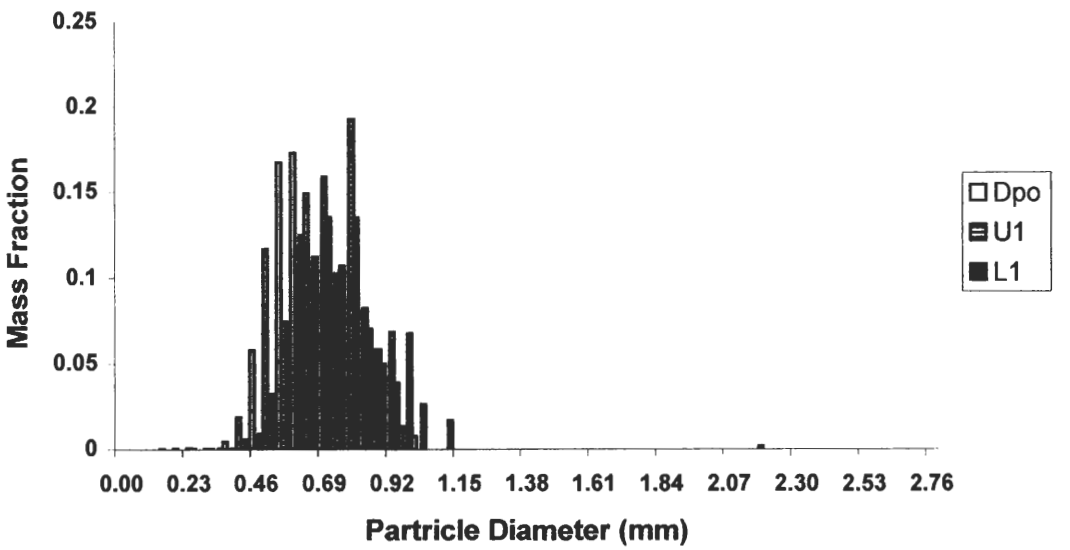

Figure 66. Normalized mass distributions for initial particle size and upper and lower samples at 30s

Individual mass fractions were determined by dividing the volume of particles within a particular size range (V_i) by the volume of the entire distribution ($\sum_1^N V_i$). It should be noted that, because of a homogeneous and uniform density*, volume is used in place of mass. This can be seen in Equation 36.

$$X_i = \frac{V_i}{\sum_1^N V_i} \qquad \textbf{Eqn 36}$$

The overall change from the initial particle distribution was then determined by subtracting individual particle size ranges of the resulting mass fraction distribution at 30 seconds ($X_{i_{30}}$) from the corresponding particle size range in the initial particle size distribution (X_{i_0}) as represented in Equation 37.

* It is assumed that there are no void spaces in these agglomerates

$$X_i = X_{t_{30}} - X_{t_0} \qquad \textbf{Eqn 37}$$

The results of this can be seen in Figure 67.

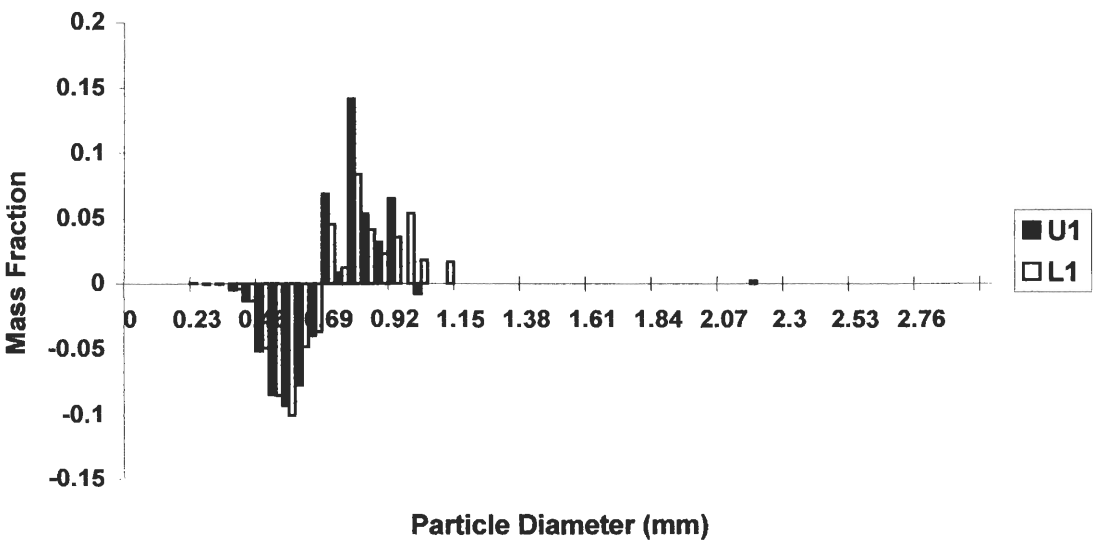

Figure 67. Experiment 1.1 Mass fraction

The possibility that the distributions seen in Figure 67 could be the result of random sampling noise was analyzed and determined to be unlikely. As can be seen from Figure 67, up to 10% of the mass of individual particle size ranges is indicated to have grown into larger particles. This change is well above the 2-3% noise levels seen in bubbling bed samples in Section 1. Coupled with the fact that this difference is repeated three times in replications suggests that this is a true indicator of particle growth.

A number fraction plot was created to reflect the relative numbers of particles in each of the mass fractions in Figure 67. In order to do this, the total number of particles of each sample ($N_{1\ total}$ and $N_{2\ total}$) was first adjusted to be equal to one another. Equation

38 can illustrate this, where the numbers of particles in each individual particle size range were adjusted so that the overall number of particles in each distribution is the same.

$$\left[\frac{N_{1\,total}}{N_{2\,total}}\right]N_{2i} = N_{2i}^{*} \qquad \textbf{Eqn 38}$$

$$N_{total} = N_{1\,total} = N_{2\,total}{}^{*} = \sum_{1}^{N} N_{2i}^{*} = \sum_{1}^{N} N_{1i} \qquad \textbf{Eqn 39}$$

These distributions were then normalized and subtracted from one another by Equation 40.

$$\frac{N_i}{N_{total}} = Y_i \qquad \textbf{Eqn 40}$$

The number fraction distribution for the initial particle size was then subtracted from the resulting number fraction distribution by the same means that the mass fraction distribution was generated. This method can be seen in Equation 41 and its results can be seen in Figure 66.

$$Y_i = Y_{i_{30}} - Y_{i_0} \qquad \textbf{Eqn 41}$$

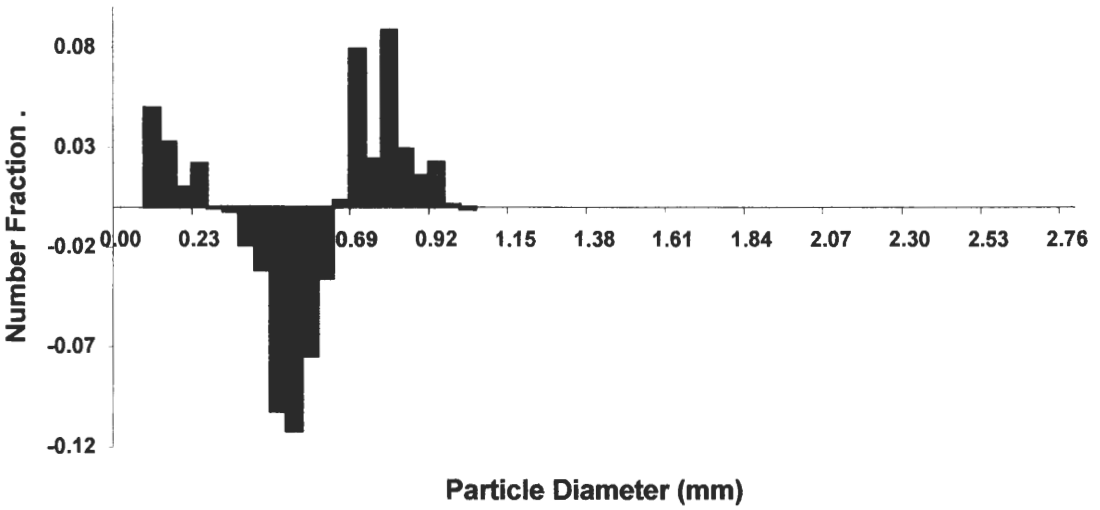

Figure 68. Experiment 1.1 Number fraction plot (initial particle size distribution represents 1,462 particles and the resulting upper sample at 30 s represents 298 particles)

As can be seen from Figure 68, many particles (up to 11%) were shown to grow (d_{PG}) which would indicate that the normalized mass distributions are not based off of just a few particles that may or may not have been counted. The number of small particles created is probably the result of newly formed coated material breaking apart. The overall mass of this material is so small that it does not show up in the plot of mass fraction.

Experiment 1.1 represents a larger change in a particle size distribution, which, if taken to represent all distributions, may give a false indication of the accuracy of the samples taken in experiments with smaller changes. For this reason, Experiment 7.3 was also analyzed in order to determine if a smaller change in a particle size distribution showed in experimental results could be considered more than random noise. Figure 69 contains the results of this calculation for Experiment 7.3.

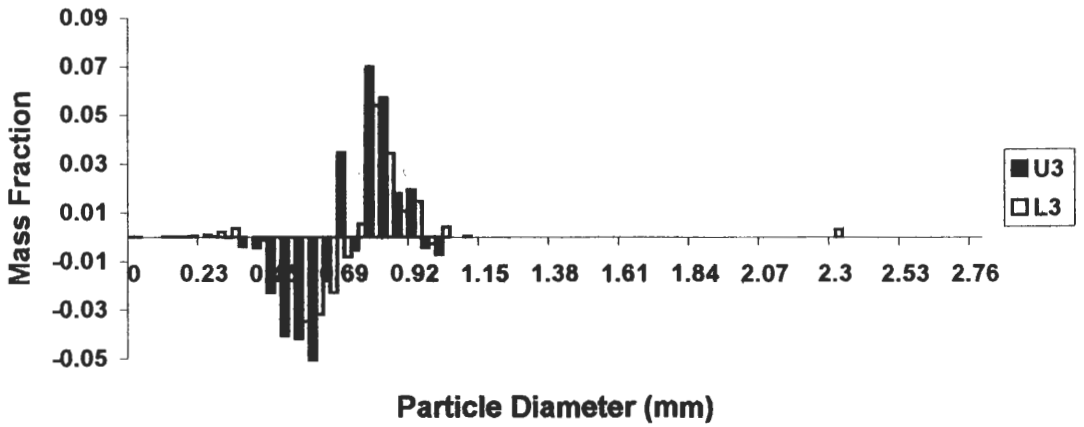

Figure 69. Experiment 7.3 Mass fraction

As can be seen from Figure 69, up to 5% of the total mass distributed over all size categories is shown to have vanished due to the particle growth/agglomeration process from some individual size categories in the initial particle size distribution. This is greater than the range of noise indicated in Section 1 for a turbulent bed (+/- 2%). This difference between the magnitude of noise in sampling and the magnitude of the sample is not tremendous, but is consistent over all three replications of the experiment, which suggests that the difference seen in Figure 4 is real, and not noise.

A number fraction plot was generated to determine the relative number of particles in each particle size range. This can be seen in Figure 70.

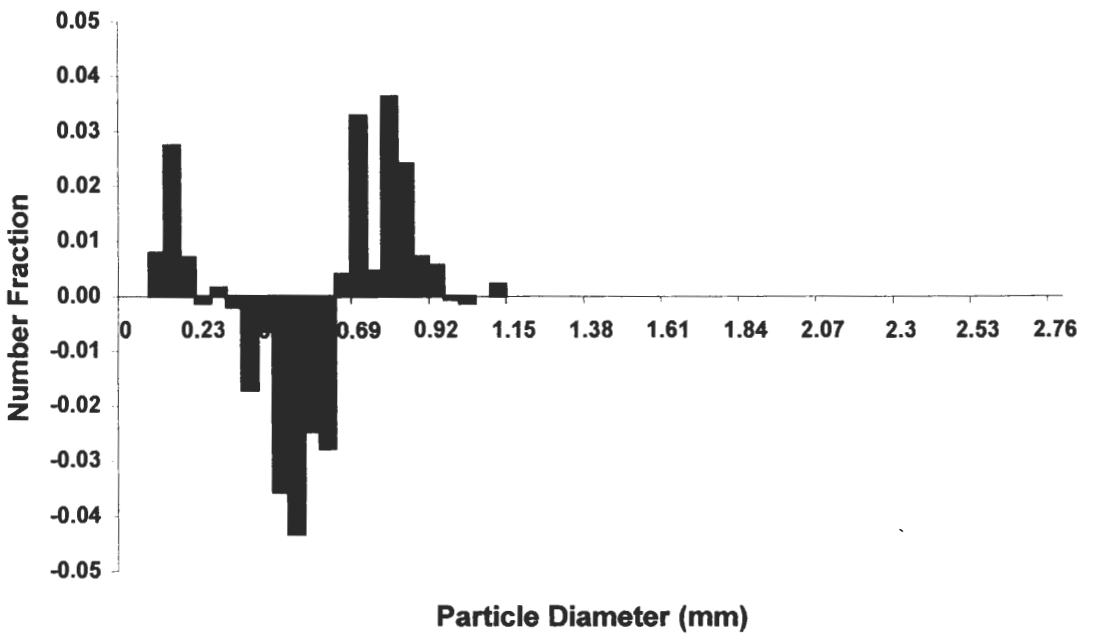

Figure 70. Experiment 7.3 Number fraction (number of particles in the initial particle size is 1,462 and the number of particles in the resulting particle size is 476)

As can be seen from the number fraction plot, the largest weight fraction of the individual particle size ranges seen in Figure 70 is a change of approximately 4.5% or 70 particles. This shows that the change in mass fraction is not merely the result of not counting a few particles.

4.2.2 Analysis of Difference of Distributions

The mass fraction difference of distributions was analyzed by determining the mean particle diameter of the negative (particles that grew) and positive (particles formed) separately in order to quantify each. This was shown earlier in Figure 65 and was accomplished by determining the volume moment of the absolute value of the negative distribution to determine the mean diameter of the particles that grew ($\overline{d}_{P_G}$) and the

moment about the positive distribution to determine the mean diameter of the particles formed ($\bar{d}_{P_F}$).

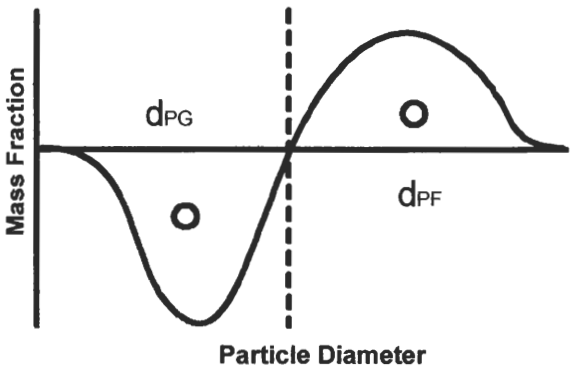

Figure 71. Difference of distributions

Equation 42 and 43 were used to determine the mean diameters of the particles that grew (d_{PG}) and the particles formed (d_{PF}) respectively. Each of these distributions can be seen in Appendix 3.

$$\bar{d}_{P_G} = \sum_{G} |X_i| \left(\frac{d_{P_i} + d_{P_{i+1}}}{2} \right) \qquad \textbf{Eqn 42}$$

$$\bar{d}_{P_F} = \sum_{F} X_i \left(\frac{d_{P_i} + d_{P_{i+1}}}{2} \right) \qquad \textbf{Eqn 43}$$

The results of these calculations can be seen in Table 14. Each is the average of the replicates under that condition. The standard deviation in Table 14 refers to the standard deviation of the average distribution and the standard deviation of the means of those distributions.

Table 14. Characteristics of particles formed and grown in experiments

EXPERIMENT	SAMPLE POSITION	PARTICLES THAT GREW		PARTICLES FORMED	
		$\bar{d}_{P_G}$ (mm)	σ (mm)	$\bar{d}_{P_F}$ (mm)	σ (mm)
1	U	0.55	0.06	0.85	0.1
	L	0.56	0.06	0.88	0.1
2	U	0.54	0.06	0.86	0.08
	L	0.57	0.07	0.83	0.06
3	U	0.55	0.06	0.86	0.04
	L	0.56	0.07	0.9	0.07
4	U	0.57	0.06	0.9	0.11
	L	0.59	0.06	0.87	0.06
5	U	0.55	0.06	0.86	0.09
	L	0.56	0.06	0.91	0.07
6	U	0.55	0.07	0.91	0.09
	L	0.56	0.06	0.82	0.09
7	U	0.69	0.05	0.89	0.08
	L	0.58	0.1	0.89	0.14
8	U	0.59	0.1	0.83	0.06
	L	0.58	0.1	0.88	0.15

The average value of all absorbed mean diameters from Table 14 is 0.57mm for both upper and lower samples with a confidence interval 0.03mm for the upper sample and 0.01mm for the lower sample. These confidence intervals show that there is no significant difference between the mean diameters of the particles that grew in either the upper or the lower sample. These values compare well with the number average mean particle diameter of 0.58mm. This indicates that particle formation in the bed is the result of random particle collisions with the molten feed and with other bed particles.

One notable exception is the mean diameter that grew of 0.69mm shown in the upper sample of Experiment 7. An observation of the difference in distribution plots for Experiment 7 in Appendix 3 show a large amount of smaller material being produced. Because the seedbed material has already been shown not to break down, this must be the result of the attrition of the molten salt that has solidified onto seed particles. This large amount of attrited material has effectively skewed the calculation of the mean diameter falsely towards a larger value.

There is less consistency among the experiments in the average size of the particles formed during particle growth. For instance, the average of the mean particle diameters for Experiment 7, which experienced the lowest particle growth rate, is 0.89mm while for Experiment 6, which experienced the highest growth rate, the average mean diameter is 0.87mm. This would seem to indicate that particle growth is a function of the rate of agglomeration and not just the size of the agglomerates formed.

The respective volumes of each of these mean sized particles formed and that grew in Table 14 were calculated and compared to determine how many mean particles that grew it would take to create a mean sized formed particle. This calculation can be seen in Equation 44.

$$\#\ Particles = \frac{\frac{4}{3}\pi\left(\frac{\bar{d}_{P_F}}{2}\right)^3}{\frac{4}{3}\pi\left(\frac{d_{P_G}}{2}\right)^3} \qquad \textbf{Eqn 44}$$

The number of times in size that a particle formed is greater than a particle that grew gives an indication of whether or not there is agglomeration and if so, what size agglomerates are formed. The results of these calculations can be seen in Table 15 along with the respective particle growth rate of each experimental condition.

Table 15. Average number of seed particles per agglomerate at 30 seconds.

EXPERIMENT	D_{UPPER}		D_{LOWER}	
	# Particles	$\frac{d\bar{d}_P}{dt}$ (mm/min)	# Particles	$\frac{d\bar{d}_P}{dt}$ (mm/min)
1	3.7	0.22	3.9	0.24
2	4.0	0.34	3.1	0.25
3	3.8	0.17	3.6	0.16
4	3.9	0.19	3.5	0.15
5	4.0	0.24	3.6	0.2
6	4.5	0.34	4.3	0.25
7	2.8	0.14	3.6	0.12
8	2.8	0.19	3.5	0.18

As can be seen from Table 15, all of the resulting mean particles formed are several times (2.8 - 4.5) the size of the particles that grew, which shows that agglomeration predominates as a particle growth mechanism in all experiments.

There are two ways that mean particle growth rate can increase by agglomeration, an increase in the rate of agglomerates formed or an increase in the size of agglomerates. The number of particles per agglomerate was plotted against particle growth rate to determine what correlation, if any, existed between the two. This plot can be seen in Figure 72, where the upper and lower samples are plotted against particle growth rates.

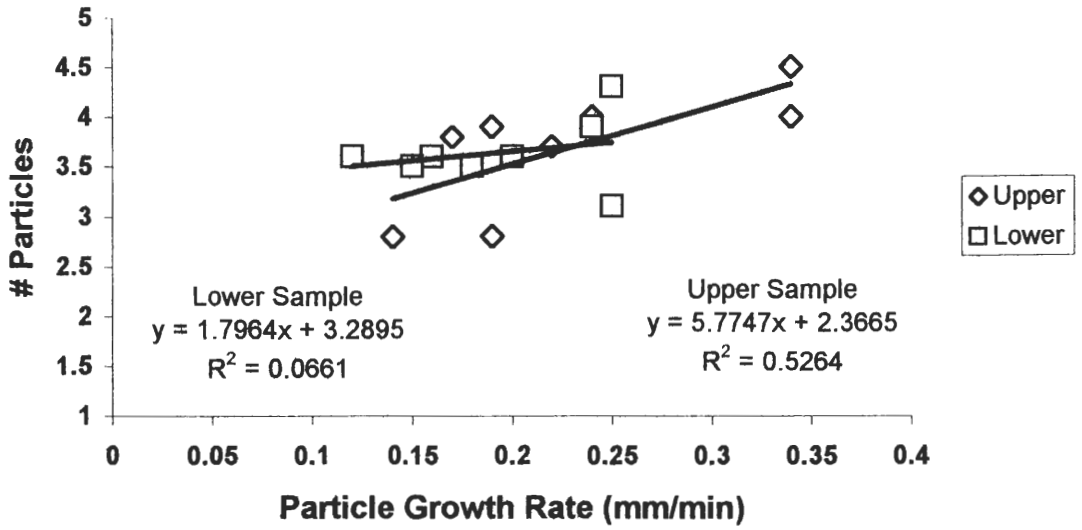

Figure 72. Correlation of formed particle size with growth rate

As can be seen from Figure 72, there is a slight correlation (R^2=0.53) between the particles per agglomerate or size of agglomerates formed and particle growth rate taken from the upper sampler but little or no correlation in the lower sample (R^2=0.07). This may be the result of larger particles being broken up at the distributor where the lower samples are taken. These results indicate that particle growth is the result of both the rate of agglomerate formation and the size of agglomerates formed.*

* Because there is no significant difference between the size of particles that grew, the number of particles per agglomerate also indicated the relative size of the agglomerates formed

4.3 Micrographs of Selected Particles

4.3.1 Seed Bed Particles

Figure 73 is a micrograph of seedbed particles used in this project as a starting material for the particle growth. All of the particles seen later in this section were formed by a combination of these particles and the molten salt feed.

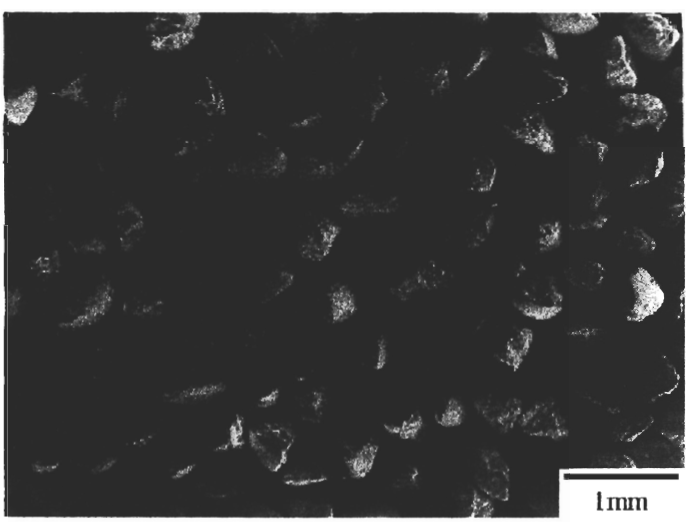

Figure 73. Seed bed particles mean particle diameter = 0.63 mm

Below is a closer example of a particle used in the seedbed

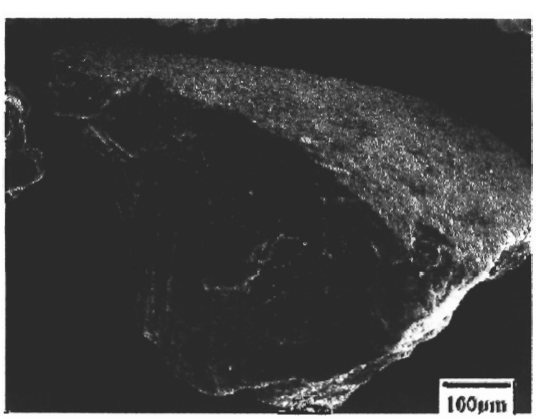

Figure 74. Seedbed particle

4.3.2 Particle Agglomerates

Very few particles produced from experiments grew to the size of the agglomerate seen in Figure 75. It is used here because it was easily identified as an agglomerate during sample analysis and contains many seedbed particles on its surface interfacing with a once-molten salt coating. There appears to be several layers of seedbed particles and coating that make up this agglomerate.

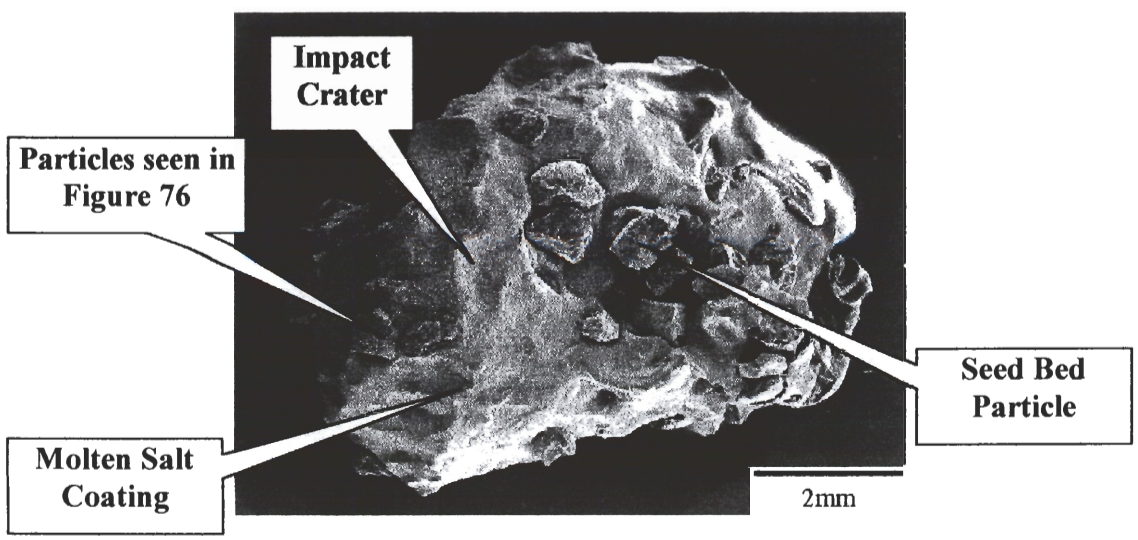

Figure 75. Particle agglomerate

The surface of this agglomerate shows signs of solidified molten salt and bound seedbed particles. The surface of the solidified molten salt is covered with bound seedbed particles and impact craters. These impact craters are believed to be the result of unsuccessful collisions of seedbed particles with the semi molten surface of the particle. As the molten salt was very close to solidifying and therefore very viscous, the results suggest that the viscosity of the melt for these unsuccessful collisions was too high and the energy of impact too low to deform the surface of the semi-molten salt enough to allow

for the intimate contact necessary for the particles to bind together. Two successful particle collisions indicated in Figure 75 can be seen closer up in Figure 76.

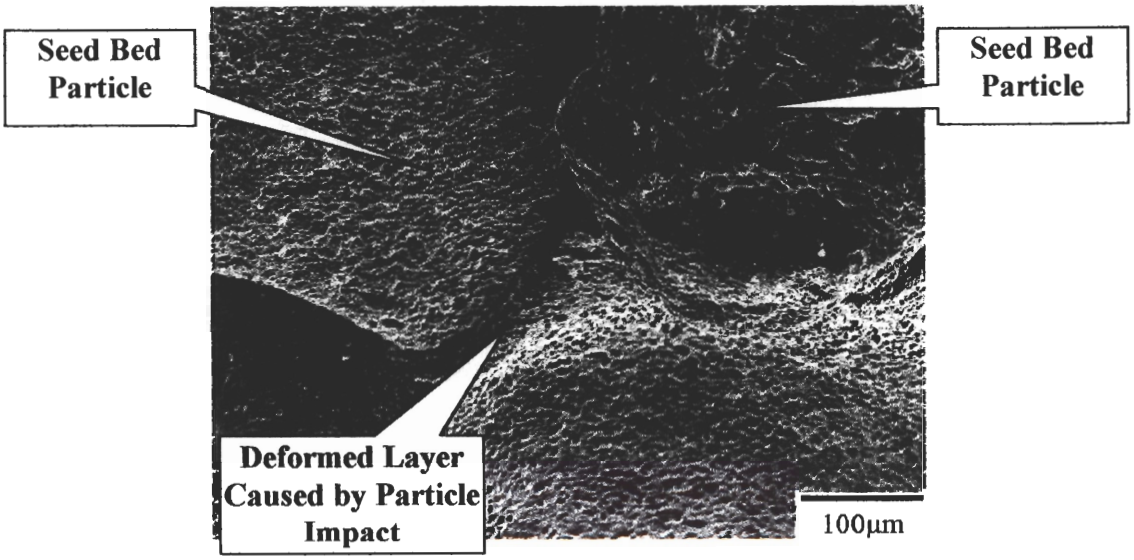

Figure 76. Seed bed particle impacts and deforms molten salt layer

The colliding particle was able to deform the layer of molten salt, allowing it to stick to the surface of the agglomerate. A close-up shot of another seedbed particle salt coating interface can be seen in Figure 77. The seed particle appears to have penetrated through the semi-molten surface layer to interface with a molten layer underneath.

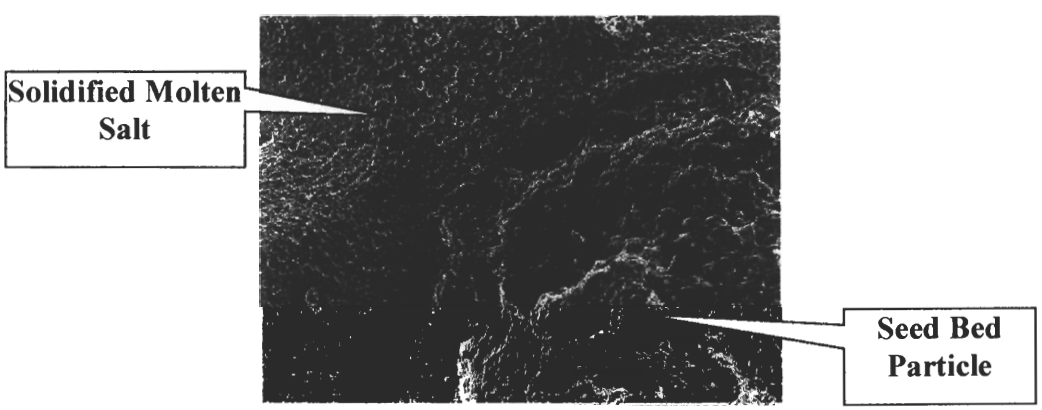

Figure 77. Seed particle embedded in molten salt coating. Frame is approximately 600μm wide

Another example of an observed agglomerate can be seen in Figure 78. In this case it appears that several seedbed particles are bound to the outside of a clump of solidified molten salt feed.

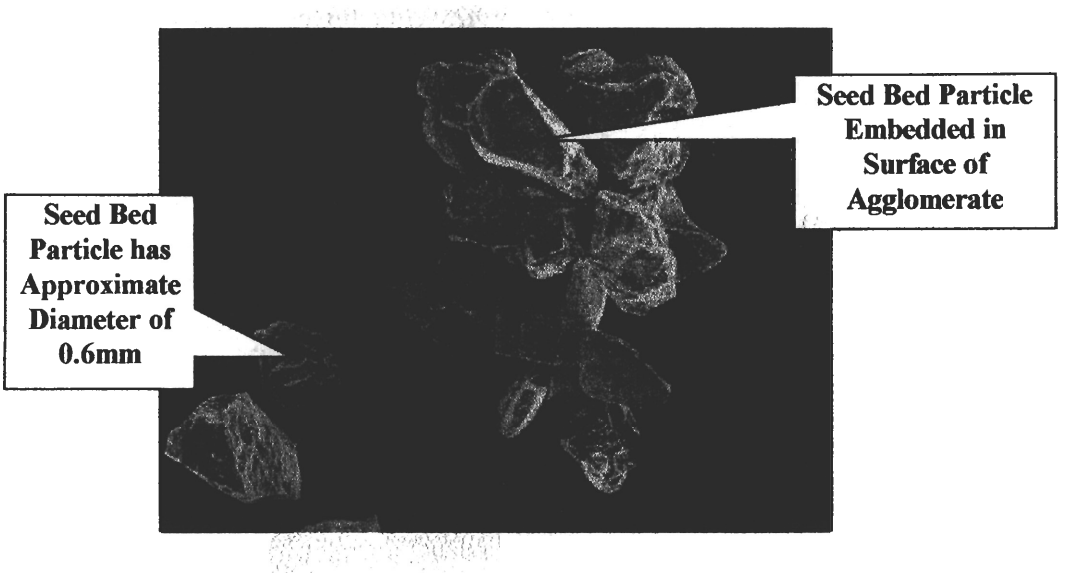

Figure 78. Agglomerate formed of many bound seed particles. Frame is approximately 5mm wide

Some examples of coating were seen using SEM. In Figure 79 can be seen a seedbed particle with two large solidified drops of formerly molten salt on its surface. A closer observation (Figure 80) of the lower coating shows signs of the molten salt having flowed over the surface of the particle for a short distance.

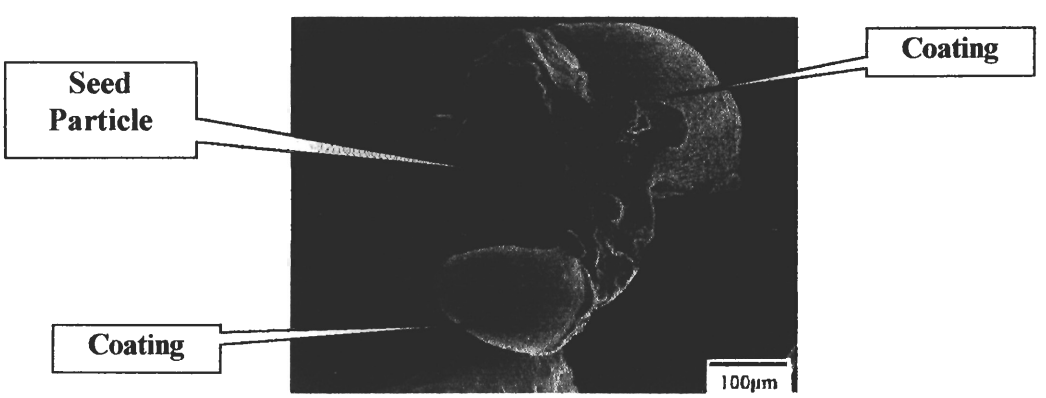

Figure 79. Coated particle

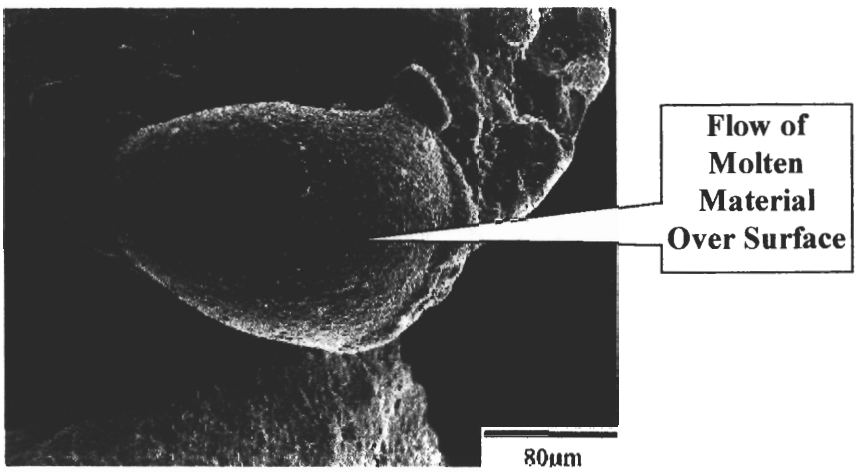

Figure 80. Drop of coating on surface of seed particle

This coating seems to be the result of a molten drop that had formed a solid or a semi-solid surface collided with a seed bed particle and ruptured onto the particle which can be seen from what appears to be the flow of molten material over the seed particle surface. This would have allowed the molten particle to solidify to the surface of the seed particle.

4.4 Conclusions

The dominant mechanism for particle growth was determined to be agglomeration under all experimental conditions. This was strongly suggested by a comparison of growth rates observed during experiments with those calculated using the definitions of coating and agglomeration. The particle growth rates calculated using the agglomeration model were much closer to the experimental data than those of the coating model which at the maximum possible theoretical growth rate was on average approximately fifty percent of the growth rates actually observed.

Analysis of particle size distribution histograms revealed that the mean diameter of particles produced during experiments were composed of a range of approximately 2.8 to 4.5 seed bed particles over all of the experiments, which shows agglomeration to be the dominant particle growth mechanism.

Micrographs of particle agglomerates show that molten salt binds particles together leading to particle growth by agglomeration. These micrographs also seem to indicate that the surface of a molten salt becomes a barrier to agglomeration while semi-molten due to the higher viscosity.

Conclusions

1. No significant change in mean particle diameter was observed as a result of fluidization under bubbling or turbulent bed conditions without molten salt feed.

2. Bed particles grew in the presence of injected molten salt.

3. This growth rate significantly decreased as a result of increased mixing caused by a change from bubbling to turbulent fluidization conditions.

4. Theoretical growth rates were calculated by separately applying the definition of coating and agglomeration to the growth of the particle seedbed used in these experiments. These rates were then compared to the actual experimental growth rates under those experimental conditions. It was determined by this comparison that the greatest impact to particle growth resulted from particle agglomeration.

5. The difference between the initial and final particle size distributions was calculated in order to determine the size of particles that grew and the size of particles formed from that growth. This analysis also showed that the dominant form of particle growth was agglomeration in all experimental conditions.

6. The use of scanning electron microscopy to examine particles formed in the fluid bed under experimental conditions revealed signs of both coating and agglomeration. Though both particle growth mechanisms exist in the final particle size distribution, the extreme rate increase due to the agglomeration mechanism as compared to coating and the overall rate of agglomerate formation caused the agglomeration mechanism to dominate.

Recommendations for Future Work

A better understanding of particle formation by the injection and solidification of a molten salt into a fluidized bed has been established by this dissertation, but much more work is needed before a pilot scale operation can be run. A continuous bed was attempted in this project, but particle growth and formation were not conducive to material removal from the bottom of the bed. It is believed that smaller more uniformly coated particles will solve this problem of materials handling, and therefore, several of the recommendations for future work are an effort to accomplish this. The recommendations for future research are as follows:

1. The effect of gas jets created by the distributor should be incorporated into this project. These jets were minimized in the design of the fluidized bed used in this project but still showed signs of decreasing the overall rate of particle growth. It is believed that a sparger, which is basically a gas jet dominated bed, will cause the coating mechanism to become more important.[80]

2. The value of $\Delta T_{ms} / T_B$ should be increased to more closely match the same ratio for smelt and steam and increase space-time or residence-time of molten salt in bed.

3. Create a continuously operating bed.

4. Determine the effect of other operational variables on particle growth in the bed not considered in this project. Some of these variables include, but are not limited to, composition of the binary salt in relation to the eutectic point and initial seedbed particle size.

5. The internal dynamics of the bed are unknown and would be of great help in understanding the initial internal interaction between molten salt injection and the bed. This could lead to a model of bed particle growth.

6. Increase the number of values tested in this project in order to create a surface response diagram.[81]

7. Develop real-time in-bed particle size analyzer for data collection and use glass beads for bed material to increase capabilities of fluid bed reactor.

Acknowledgments

There are many people who have been of great support to me in my life and in this dissertation. I would like to first thank Jesus Christ to whom I am eternally thankful and without whom, I would not be who I am today. I want to thank my wife, Kristina, whom I cherish and adore. Her support has made such a difference. I want to thank my father and mother, who worked very hard so that I could have opportunities that they never knew or, perhaps, never dreamed possible. My little sister, Holly, who helped me cut insulation for my reactor when she was miserable with the flu which is only one of the many times that she has sacrificed for me. I would like to thank my advisor, Dr. Empie, whose door was always open for a second or an hour or however long it took.

I want also to thank Maribeth Amundsen, who saved me so much time, money and frustration by locating a bulk supplier of my model chemical. I thank the guys in the shop, Blu, Perry and T, who helped me get what I needed to get done over and above the call of duty. And last, I would like to thank IPST for this program that has given me the opportunity to get a Ph.D.

LITERATURE CITED

[1] Empie, H. U.S. Patent 5,545,292 (8/13/96).

[2] Kunii, D.; Levenspiel, O. Fluidization Engineering: Second Edition *Butterworth-Heinmann Series in Chemical Engineering* (1991).

[3] Howard, J.R. Fluidized Bed Technology. Principals and Applications *Adam Hilger Publishing* (1989).

[4] Davidson; Clift; Harrison. "Gas-Solid Fluidization" Fluidization. Second Edition *Academic Press* 30-42 (1985).

[5] Grace, J. "Agricola Aground: Characterization and Interpretation of Fluidization Phenomena" FLUIDIZED PROCESSES: Theory and Practice *AIChe Symposium Series Vol. 88* 1-16 (1992).

[6] Trivedi, R.C.; Rice, W.J. "Effect of Bed Depth, Air Velocity, and Distributor on Pressure Drop in an Air Fluidized Bed" Fluidized Bed Technology 57-63 (1966).

[7] Chesonis, D.C.; Klinzing, G.E. ; Shah, Y.T. ; Dassori, C.G. "Hydrodynamics and Mixing of Solids in a Recirculating Fluidized Bed" Ind. Eng. Chem.Vol. 29 (1990).

[8] Van Demeter, J. "Mixing" Ch 9 Fluidization Second Edition (1985)

[9] Hough, G.W. "Principles of Chemical Recovery" Chemical Recovery in Alkaline Pulping Processes. 9-13 (1991).

[10] Kassem, M.E. "Sintering of Powder Compacts in Fluidized Bed Furnaces" *Metallergia* Jan 29-30 (1985)

[11] Chang; Wen. "Fluid-to-Particle Heat Transfer in Air-Fluidized Beds" Fluidized Bed Technology 111-117 (1966).

[12] Geldart, D. "Elutriation" Ch 11 Fluidization Second Edition (1985).

[13] Sung, J.S.;Burgess, J.M. "Bubble Properties in Two-Dimensional Segregating Gas Fluidized Beds" CHEMECA 85 407-412.

[14] Davidson, J.F., and Harrison, D., *Fluidization*. London: Academic Press (1971).

[15] Fitzgerald, T. "Coarse Particle Systems" Ch 12 Fluidization Second Edition (1985).

[16] Kocatilum; Basesme; Levy; Kozanoglu. "Particle Motion in the Wake of a Bubble in a Gas Fluidized Bed" Fluidized Processes: Theory and Practice 40-50 (1992).

[17] Chiba; Chiba; Nienow. "Prediction of the Steady State Segregation Pattern in Gas Fluidized Beds with Particles in Throughflow" Fluidization 185-192 (1986).

[18] Geldart, D. "Challenges in Fluid Bed Technology" Fluidization and Fluid Particle Systems: Fundamentals and Applications 111-121 (1989).

[19] Rhodes, M.J. ;Geldart, D. "Transition to Turbulence?" Fluidization V 281-288 (1988).

[20] Yong, J. ; Zhiqing, Y. ; Zhaneng, Wang ; Ping, C. "A Criterion for Transition from Bubbling to Turbulent Fluidization" Fluidization V (289-296).

[21] Chesonis; Klinzing; Shah; Dassori. "Hydrodynamics and Mixing of Solids in a Recirculating Fluidized Bed" Ind. Eng. Res.1785-1792 (1990).

[22] Van Deemter. J. "Mixing" Ch 9 Fluidization Second Edition (1985)

[23] Grimmet, E. "Particle Growth and Size Distribution in Fluidized-Bed Processes: A Mathematical Model With Computer Solutions" Fluidized Bed Technology 93-100 (1966).

[24] Beddow, J.K. "The Single Particle" Particulate Science and Technology Ch 2 Chemical Publ. Co.(1980).
[25] Sherrington, P.J. ; Oliver, R. 'Fundamentals of Particle Size Enlargement by Agglomeration' Granulation Heyden (1981).
[26] Turton, R. ; Tardos, G. ; Ennis, B. "Fluidized Bed Coating and Granulation" Fluidization, Solids Handling and Processing (368-383) Noyes Publ. (1999).
[27] Magnusson ; Warqvist "Properties of Sodium Sulfide – Sodium Carbonate Melts" Svensk Papperstidning (1975)
[28] Hills, D.A. ; Sackfield, A., and Truman, C.E. "Elastic contact in the presence of cohesive fluids" *Phys.* 31(1998).
[29] Kono, H. "Granulation and Fluidized Beds" Powder Technology 625p (1984).
[30] Tardos; G.; Mazzone; Pfeffer. "Destabilization of Fluidized Beds Due to Agglomeration Part II: Experimental Verification" The Canadian Journal of Chemical Engineering Vol 63 June 384-389 (1985).
[31] Hoffman; Kamphuis; Janssen. "Avoiding Demixing and Defluidization in Gas Fluidized Bed Reactors" Fluidization and Fluid Particle Systems (1996).
[32] Marinov; Lazarov; Stefanova. " Ash Agglomeration During Fluidized Bed Gasification of High Sulfur Content Lignites" Fuel Processing Technology, 31 181-191 (1992).
[33] Manzoori; Agarwal. "Agglomeration and defluidization under simulated circulating fluidized-bed combustion conditions" 563-568 (1992).
[34] Pietsch, W. "Fundamentals of Agglomeration" Ch2 Size Enlargement by Agglomeration (1991).
[35] Dubois; S.G.; German, R.M. . "Simulation for Sintering Real Powders" Proceedings of the 1995 International Conference & Exhibition on Powder Metallergy & Particulate Materials p4/3-4/17.
[36] Rumpf, H. "Sintering" Ch 4.3.3 Particle Technology 167-169 (1990).
[37] Ashby; Jones. "Production, Forming, and Joining of Ceramics" Ch 19 ENGINEERING MATERIALS 2 An Introduction to Microstructures, Processing and Design *Pergamon Pr* (1986).
[38] Kalpakjian. "Sintering" Manufacturing Processes for Engineering Materials Second Edition Ch 11.4 (1991).
[39] Callister, W. "Powder Pressing" MATERIALS SCIENCE AND ENGINEERING An Introduction 447 (1991).
[40] Nienow; Rowe. "Particle Growth and Coating in Fluidized Beds" Fluidization Second Edition 563-591 (1985).
[41] Werther, J. and Reppenhagen, J. "Attrition in Fluidized Beds and Pneumatic Conveying Lines" Fluidization Solids Handling and Processing: Industrial Applications Ch 7 (1999).
[42] Terence, A. "Particle Size, shape and distribution" Particle Size Measurement p.102-164 (1981).
[43] Sowa, W.A. "Interpreting Mean Drop Diameters Using Distribution Moments" Atomization of Sprays, vol. 2 p. 1-15 (1992).
[44] Stockham, J.D. "What is particle size: The relationship among statistical diameters" Particle Size Analysis (1977).

[45] Boniface, A. "Introduction and Principals of Chemical Recovery" Chemical Recovery in the Alkaline Pulping Process. Third Edition pg.2 (1992).
[46] Empie, H. U.S. Patent 5,545,292 (8/13/96).
[47] Reeves, R. "Analysis of Gaseous Emissions During Dissolution of Hot, Solidified Smelt in Water" A190 Thesis *Institute of Paper Science and Technology* (1995).
[48] Venkoba, R. "Direct Alkali Recovery System (Dars) – The new 'State-of-The-Art' System – A Review" IPPTA Vol. 24, (20-29) Sept (1987).
[49] DiNovo, S. ; Ballantyne, W. "Process and Apparatus for Recovery of Spent Pulping Liquors" US Patent 4,303,469 Dec 1 (1981).
[50] Shick, P. ; Flood, W. "Fluidized Process for Regeneration of Chemicals from Sulfite Pulping Process" US Patent 3,711,593 Jan 16 (1973).
[51] Empie, H. "Recovery of Heat and Chemical Values from Spent Pulping Liquors" US Patent 4,441,959 Apr 10 (1984).
[52] Feldman, H.F. "Method for Operating a Spent Pulping Liquor Apparatus" US Patent 4,522,685 Dec 1 (1981).
[53] Copeland, G.G. "Fluidized Bed Oxidation of Waste Liquors Resulting in the Digestion of Cellulosic Materials for Paper Making" US Patent 3,309,262 Aug1 (1966).
[54] Rockvam; L.N., and Tenore, F. "Spent Liquor Steam Reforming and Recovery" (269-273) Engineering Conference Proceedings (1996).
[55] Liem, A.J ; Sheridan, T.G. "Incremental Kraft Recovery w/ a Fluidized Bed" (79-84) Pulp and Paper Canada Aug 2 (1982).
[56] Magnusson ; Warqvist "Properties of Sodium Sulfide – Sodium Carbonate Melts" Svensk Papperstidning (1975)
[57] Janz, G. ;Allen ; Bansal ; Murphy and, Tomkins Physical Properties Data Compilations Relevant to Energy Storage II. Molten Salts: Data on Single and Multicomponent Systems *National Standard Reference Data System* (April 79)
[58] Janz G.; Allen; Bansal; Murphy and, Tomkins Eutectic Data: Safety, Hazards, Corrosion, Melting Points, Composition and Bibliography *Renssalaer Polytechnic Inst.* (July 76).
[59] Janz, G. ;Allen; Bansal ; Murphy and, Tomkins Physical Properties Data Compilations Relevant to Energy Storage I. Molten Salts: Eutectic Data *National Standard Reference Data System* (March 78)
[60] Janz, G. Thermodynamic and Transport Properties for Molten Salts: Correlation Equations for Critically Evaluated Density, Surface Tension, Electrical Conductance and Viscosity Data *Journal of Chemical and Physical Reference Data Vol. 17* (1988).
[61] Cerisier; Pantaloni; Santini; Occelli; Tadrist; Finiels. "Thermal Energy Storage Using Latent Heat Storage of Molten Salts: Study and Realization of a dynamical Exchange with a Very High Efficiency" Proc. of the Joint Int. Symp. on Molten Salts Vol 87-7 (1987).
[62] Carling. "Heat Capacities of $NaNO_3$, KNO_3 and $(Na,K)NO_3$" Proc. of the Joint Int. Symp. on Molten Salts Vol 87-7 (1987).
[63] Incorpera, F. and, Dewitt, D. Fundamentals of Heat and Mass Transfer *Wiley Publ* (1990).
[64] Kramer; Munir "Thermal Decomposition of $NaNO_3$ and KNO_3" Proc of the 3rd Int. Symp. on Molten Salts p494 (1980).

[65] MSDS Nitrogen Dioxide *BOC Gases* June 7 (1996).
[66] MSDS S4442 *Mallinckrodt Baker, Inc* Nov. 17 (1999)
[67] MSDS P5950 *Mallinckrodt Baker, Inc* Nov. 17 (1999)
[68] *Potassium Nitrate: Chemical 7634* Merck Index (1998)
[69] *Sodium Nitrate: Chemical 8598* Merck Index (1998)
[70] Bradshaw; Carling "A Review of the Chemical and Physical Properties of Molten Alkali Nitrate Salts and Their Effect on Materials Used in Solar Receivers" Proc. of the Joint Int. Symp. on Molten Salts Vol. 87-7 (1987).
[71] Eutectic $NaNO_3$-KNO_3 Drawtemp 430 *Houghton International Corp* (2000).
[72] Amptek Industries 8' heating tape (1999).
[73] Teledyne Instruments *Hastings* Mass Flow Controller HFC-203 (1999).
[74] Empie, H.; Lien, S.; Yang, N.; Samuels and, Adams, "Kraft Black Liquor Delivery Systems" Project 3657-2 Report 3 (December) 1991.
[75] Hawkins, A.E. The Shape of Particle Outlines: Chapter 4 *Wiley and Sons* (1993).
[76] Sowa, W.A. "Interpreting Mean Drop Diameters Using Distribution Moments" Atomization of Sprays, vol. 2 *Beggel House Inc* (1991).
[77] Kramer, C.M. "Thermal Decomposition of $NaNO_3$" *Proc. of the Inter. Symp on Molten Salts* 494p (1980)
[78] Bradshaw, R.W. ; Carling, R.W. (A Review of the Chemical and Physical Properties of Molten Alkali Nitrate Salts and Their Effect on Materials Used for Solar Receivers" *Proc. of the Joint Int. Symp. on Molten Salts* Vol 87 959p (1987).
[79] Walpole, R.; Myers R. "2^k Factorial Experiments and Fractions" Probability and Statistics for Engineers and Scientists 5th Edition Chapter 15 *Macmillan Publ* (1993).
[80] Debayeux, C.; Lacroix, H. Apparatus for Granulating and/or Coating Particles in a Spouted Bed US Patent 4,337,722 July 6 (1982).
[81] Montgomery, D.C. Design and Analysis of Experiments 4th Ed., Wiley, New York (1997).

Appendix 1 Equipment

A1.1 Dimensional Analysis

The experimental design for this project was developed using dimensional analysis. Key variables were identified according to the experimental objectives and were then subjected to dimensional analysis. The use of dimensional analysis guides the selection of a model chemical, thus avoiding the high temperatures of kraft smelt, as well as identifying important relationships among system variables.

Using a semi-batch system (continuous feeds, no bed solids withdrawal), the following relationship states that the rate of change in the mean particle diameter of the bed, and thus the size of the particles, is a function or a result of the following properties of the system and the materials that make up the system. An explanation of the variables and why each was chosen is contained later in this section.

$$\frac{d\bar{d}_P}{dt} = f\left(C_{Pg}, C_{Pms}, \mu_g, \mu_{ms}, k_g, k_{ms} d_{Po}, u_0, \rho_g, \rho_{ms}, \rho_P, \Delta T, F_o, \sigma, \Delta H_f, h\right) \quad \textbf{Eqn A1.1-1}$$

The values of g_c and J are used as dimensional constants because heat (H) and force (F) are used as units in the analysis, which may be expressed in terms of other units.

Explanation of variables chosen

$\bar{d}_{Po}$ The particle diameter affects the fluidization characteristics, growth rate of particles and the amount of surface available in the bed per unit mass

F_0 Mass feed rate of salt to bed.

g_c Dimensional constant necessary for dimensionless analysis due to the fact that force (F) may be expressed in terms of the other variables

h The heat transfer coefficient and determines the rate at which heat is removed from particle surfaces by convection.

ΔH_f The latent heat of fusion determines the amount heat given up by the particle as it solidifies

J Dimensional constant necessary for dimensionless analysis due to the fact that heat (H) may be expressed in terms of the other variables

k Thermal conductivity of material determines the rate of heat lost by conduction

ΔT Temperature difference between injected molten salt and injected fluidizing gas.

u_0 The superficial velocity determines the fluidizing regime of the bed, which in turn has an effect on attrition of particles and heat transfer

Greek

μ The viscosity of incoming fluid will have a strong impact on droplet size as well as the ability of the droplet to spread over the face of the particle surface. Viscosity of the gas will have a strong impact on the flow of the bed.

ρ Relative densities of gas, liquid and solid will determine lift characteristics of the bed, which will in turn affect maximum particle sizes

σ Surface tension of the liquid inserted into the bed will determine the ability of the liquid to spread over the surface of the particles

Mechanics of dimensional analysis

Dimensional analysis was performed by using these key system variables listed in Equation 1 to create dimensionless relationships that describe the system. Use of the Buckingham pi theorem allows for the creation of pi terms, which will be solved for the dimensionless groups. The number of Pi terms is determined by subtracting the number of reference dimensions from the number of variables in Equation 1.

The reference dimensions are as follows:

1) Length (L)
2) Mass (M)
3) Time (θ)
4) Temperature (T)
5) Force (F)
6) Heat (H)

These are the building blocks for all of the variables in Equation 1. The Buckingham pi theorem states that the number of pi terms, and thus the number of dimensionless groups, is determined by the number of variables(14) minus the number of reference dimensions(6). There are therefore eight dimensionless terms needed to describe the system. Next, a number of variables are chosen from Equation 1 equal to the number of reference dimensions. These are known as repeating variables and will be used as group comparisons to each of the remaining variables in Equation 1

The repeating variables used in this analysis can be seen in Equation A.

$$\Pi_1 = (X)\,\bar{d}_P^{\,a}\rho^b\mu^c k^d g_c^e J^f \qquad \textbf{Eqn A1.1-2}$$

These variables were chosen so that dimensional analysis would yield certain well-defined dimensionless groups such as Reynold's, Prandtl and, Nusselt numbers. This does not affect the validity of the analysis but makes the understanding of the results easier.

The dimensionless terms were solved for by substituting each of the remaining variables in place of (X) in Equation A to solve for each dimensionless term. An example can be seen below.

Substituting convection coefficient (h) into Equation A

$$h\,\bar{d}_{Po}^{\,a}\rho^{b}\mu^{c}k^{d}g_{c}^{e}J^{f} \qquad \text{Group 1}$$

These variables are next broken down into their reference dimensions.

$$(H\theta^{-1}T^{-1}L^{-2})(L)^{a}(ML^{-3})^{b}(ML^{-1}\theta^{-1})^{c}(HL^{-1}\theta^{-1}T^{-1})^{d}(MLF^{-1}\theta^{-2})^{e}(FLH^{-1})^{f} = H^{0}F^{0}L^{0}T^{0}\theta^{0}M^{0} \qquad \textbf{Eqn A1.1-3}$$

Solving for the exponents of Equation A1-3 yields

a=1, b=0, c=0, d=-1, f=0, e=0

Substituting these values into the exponents in Group 1 yields the following dimensionless group.

$$\frac{h\bar{d}_{Po}}{k}$$

This is also known as the Nusselt number. This was performed the same way for the remaining variables to obtain the other dimensionless groups.

A1.2

Proof of the Insignificance of Wall Heat Transfer for a Large Scale Fluidized Bed Operating at High Temperatures

(All formulas in this section are taken from Kunii, Levenspiel. Fluidization Engineering: 2nd Edition *Butterworth-Heinemann* (1991))

Introduction

It was a concern during the design phase of this reactor that the use of a lower temperature molten salt system would ignore radiation to the wall of the reactor as a mode of heat transfer from the bed. These relative paths of heat transfer from the bed (convection from particles to the fluidizing gas, convection to the wall, and radiation to the wall) are quantified and compared here to determine if radiation to the wall is significant and therefore precludes the use of a low temperature model chemical.

Assumptions:

d_p = Average particle diameter = 2mm
Reactor size = 3 m diameter X 6m tall (H)
Volume of particle bed = 3m diameter X 3m tall
ε = Void space = 0.6
ϕ = Sphericity = 1
Emissivity = 0.85 $T_{surr} = 150^0 C$ $T_{bed} = 700^0 C$ $\sigma = 5.67x10^{-8}$

Convective Heat Transfer in Bed

The minimum fluidizing velocity was used to determine the fluidizing conditions in the bed. this velocity was calculated using Equation A1.1-2

$$U_{mf}^2 \frac{1.75}{\varepsilon^3 \phi}\left(\frac{d_p \rho_g}{\mu}\right)^2 + U_{mf} \frac{150(1-\varepsilon)}{\varepsilon^3 \phi^2}\left(\frac{d_p \rho_g}{\mu_g}\right) = \frac{d_p \rho (\rho_s - \rho_s) g}{\mu_g^2} \quad \textbf{Eqn A1.2-1}$$

Which resulted in a velocity of U_{mf} = 0.049 m/s

This velocity was used to calculate the heat transfer coefficient of the bed in order to determine the amount of heat transfer taking place due to convection at the surface of the particles. The heat transfer coefficient is determined from the following equation.[1]

$$\frac{h_{bed} d_p}{k_g} = 2 + 0.6 \mathrm{Re}^{1/2} \mathrm{Pr}^{1/3} \qquad \textbf{Eqn A1.2-2}$$

Where Re and Pr are Reynolds number and Prandtl number.

This results in a bed heat transfer coefficient of $h_{bed} = 41\, W/m^2K$

Multiplying this number by the area and the temperature difference between the bed and fluidizing gas gives the overall expected amount of heat transfer due to convection in the bed.

The area of the bed is the area of all of the particles in the bed as calculated in Equation A1.2-3.

$$Area_{bed} = number\ of\ particles\ in\ bed\ x\ area/particle \qquad \textbf{Eqn A1.2-3}$$

Where Equation A1.2-4 can determine the area of a single particle.

$$area/particle = 4\pi\left(\frac{d_p}{2}\right)^2 \qquad \textbf{Eqn A1.2-4}$$

And Equation A1.2-5 determines the number of particles in the bed.

$$number\ of\ particles\ in\ bed = volume\ of\ bed(1-\varepsilon_{mf})/volume/particle \qquad \textbf{Eqn A1.2-5}$$

Resulting in a bed with $Area = 13300 m^2$.

This results in 300 kW transferred from the bed to the fluidizing gas.

Convective Heat Transfer at the Wall

The heat transfer to the wall by convection is determined similarly as within the bed. The following equation is used to determine the wall heat transfer coefficient.[1]

$$\frac{h_w d_p}{k_g} \Big/ (1-\delta) = 5 + 0.05 \,\mathrm{Pr}\,\mathrm{Re} \qquad \textbf{Eqn A1.2-6}$$

Which results in a wall heat transfer coefficient of 65W/m^{2}K.

The area of the wall is determined using the following equation.

$$Area_{wal} = \pi r^2 + 2\pi r H \qquad \textbf{Eqn A1.2-7}$$

Resulting in a total wall area of 36.5 m^2.

The total energy transferred from the bed due to convection is determined by the following equation.

$$TotalEnergy = h_w Area_{wall} \Delta T \qquad \textbf{Eqn A1.2-8}$$

Where the total energy removed from the bed due to convection to the wall equals 1304kW.

Heat Transfer Due to Radiation

The following equation was used to calculate the heat transferred to the wall due to radiation.

$$q = Area\ emissivity\ \sigma\left(T_{bed}^4 - T_{surr}^4\right) \qquad \textbf{Eqn A1.2-9}$$

Radiation between the wall and the bed only takes place at the edge surface of the bed. This analysis therefore treats the bed as one large agglomeration with an outside surface equal to that of the bottom part of the vessel that the particles occupy. The heat transfer coefficient has been calculated for comparison.

Using the previous equation, the heat lost to the wall due to radiation was determined to be 13.6kW.

Using the amount of heat transferred out of the bed through the wall divided by the area of the bed gives a representative heat transfer coefficient for radiation heat transfer to the wall.

$$h_r = q/Area \qquad \textbf{Eqn A1.2-10}$$

$$Area_{radiation} = 2x\pi r^2 + 2\pi rH = 43.8m^2 \qquad \textbf{Eqn A1.2-11}$$

$$h_r = 21 {}^{W}/_{m^2K} \qquad \textbf{Eqn A1.2-12}$$

Conclusions:

A comparison of the relative amounts of heat transferred and the respective heat transfer coefficients can be seen in Table A1.2-1.

Table A1.2-1. Comparison of heat transfer coefficients and magnitudes from hypothetical industrial sized bed

	COEFFICIENT (W/M^2K)	MAGNITUDE (KW)
Bed Convection	41	29,300
Wall Convection	65	1,300
Wall Radiation	21	13.6

It can be seen from the table that heat transfer to the wall due to radiation under these conditions is relatively small. This indicates that the use of a low temperature chemical is acceptable.

Appendix 2 Procedures

A2.1 Bed Operation Instructions

Pre-Check

1) Sufficient chemical is in the melting pot.
2) Everything is plugged in.
3) Air pressure in main bottles is above 500psi
4) Correct distributor plate is being used
5) All thermocouples are attached
6) Overflow catch bucket is in place and secure
7) Inside of vessel is clear from last run
8) Sample bottles prepared and time sheet ready

Startup

1) Set preheat conditions (260 °C)
2) Check that main heaters are working properly
3) Allow to preheat (preheat to internal temp near 200 °C)
4) Once preheat is done go to second phase and set main reservoir temp
5) Once main reservoir temp reached set LT2 to 250 °C
6) Wait until LT1 is approximately 300 °C
7) Turn on LT4 at POT (300 – 350°C)
8) Check fittings to insure that they are tight before calibration

Calibration (Melting Pot)

1) Remove bottom section of bed if attached
2) Place stainless steel bucket under vessel
3) Place curtain across fluid bed to block any spattering of molten salt
4) Put on face shield
5) Turn on molten salt flow

6) With long heat protecting glove, hold a preweighed stainless steel pan under the flow of molten salt and hold under stream for 15 seconds
7) Weigh pan and determine flow rate of chemical
8) Adjust pressure to get desired flow rate
9) Double check desired flow rate once achieved and turn off molten flow
10) Attach bottom of bed with proper distributor plate and insure that it is securely fastened
11) Recheck seals and thermocouples
12) Recheck heating tape and temperatures

Calibration (House Air)

1) Adjust house air to approximately 78psi
2) Pipe house air through main flow meter and record flow
3) Pipe house air into bed
4) Pipe bottle air through flow controller at difference between house air and desired flow

A2.2 Image analysis Instructions

1) Sieve sample in a 10-mesh sieve (2mm). This will separate particle sizes in order to analyze them under the appropriate conditions.
2) Weigh size ranges and record.
3) Mount Samples

   Smaller Size Range: Mount enough of the sample to get good coverage of the contact paper but also don't crowd the surface. Spread sample evenly over an 8.5 X 11 inch sheet of contact paper and then place a labeled transparency over the top of this and tape the edges down.

   Larger Size Range: Mount the entire sample onto contact paper and spread for good coverage. Place another piece of labeled contact paper on top of this. The sticky sides of the contact will help to hold the particles in place.
4) Record Smaller Size Range **(Contrast 255, Brightness 160)**

Segment the surface of the sample using a piece of transparency that forms a 4 X 5 grid of squares measured 2X2 inch so that regions that can be randomly sub sampled. Use optical microscope to photograph particles at a 6,5 magnification. The microscope will have to be calibrated if one does not already exist for that particular microscope.

Save image under the following designation.

EBCDT-H

Table A2.2-1. File designation for image analysis

LETTER	DESCRIPTION
E	Designates an experiment
B	Condition of the experiment (1-8)
C	Where sample was taken from ("U",upper section of bed or "L" from the lower)
D	What replicate is this (1-3)
T	What is the approximate time in minutes that this was taken as measured from the beginning of injection
H	Section of the grid that the picture was taken

Example:
E1U1T5-1

The "E1" represents experiment 1. The "U" represents an upper sample and an "L" would represent a lower sample. The following number represents which replication of this experimental condition is. This will be a 1, 2 or 3. The T represents the approximate time at which the sample was taken. The "-1" represents section of the grid covering the contact paper that the image was taken in.

5) Record Larger Size Range

Table A2.2. Large Particle Camera Setup

OBJECT	SETTING
Camera Height	28.75 inches
Lighting	Top lighting
Shutter Speed	100ms
Gain	0
Bias	0

6) Analyze Smaller Particles

Run images through OPTIMAS 5.2 image analysis software. The following calibration was used to characterize all pictures taken under this condition.

Calibration 1 (Frame Width 15.46 mm, Pixel Width 0.02419mm)

The field of view for the smaller particle size is approximately 15.5 mm by 15mm in size. The largest size that can be seen in this frame is a 2 mm particle. This is more than a seven-fold increase. I would have liked 10 but was limited by time and equipment.

Determine the threshold of the group of pictures that were taken to make sure that 0:150 will be adequate. If this is not the range then the correct range must be placed into the macro.

Run *1.mac* after checking OPTIMAS settings. This will employ some filtering methods to separate any touching particles and will target predetermined characteristics of the particles such as;

Area, Perimeter, Circularity, Major Axis Length, Area Equivalent Diameter, Perimeter Equivalent Diameter

Check all initial settings.

After the macro has run perform a quick visual inspection to determine if there are any visible mistakes. If so, delete or modify the mistake. After all visible mistakes are taken care of, extract and export data to **C:\a490temp\test.asc**.

7) Analyze Larger Particle Sizes

Run images through OPTIMAS 5.2 image analysis software. The following calibration was used to characterize all pictures taken under this condition.

Calibration 2 (Frame Width 70.83 mm, Pixel Width 0.1109 mm)

The field of view for the larger particle size is approximately 71 mm by 71mm in size. This field is more than 10 times the size of the largest expected particle that I expect to see. This is good to ensure that the sampling does not affected by the particle size. Particle measuring 2mm in diameter and higher will be measured. Extract and export data to **C:\a490temp\test.asc**.

Appendix 3 Data

This appendix contains data from the experiments in this project. This data is broken down into four sections. These four sections are as follows:

A3.1 Temperature Profiles of Fluidized Bed During Experiment – This section contains temperature profile of the bed during experiments. This information was used to determine the data that would be used in particle growth rate analysis. There is a point in the experiment (as discussed in the Experimental Procedures – Determination of Data Analyzed) after which, data collected is not used in the determination of the particle growth rate. This is referred to here as the point of discontinuity.

A3.2 Particle Growth Rate Plots – This section contains plots of the increase in the mean particle diameter in the bed with time. Two regressions were performed on the data. A linear regression was performed on all of the data collected before the point of discontinuity and a second order regression was performed on all of the data. The slope of the linear regression is the particle growth rate. Each of these plots represents the average of three replicates.

A3.3 Particle Size Distribution Plots - The difference in distribution plots uses the difference between the particle size distributions of the initial particle size and those of the experiment at 30 seconds to determine which size particles grew and into what size they grew.

A3.4 Analysis of Variance Performed on Particle Growth Rates – Complete results of ANOVA in Section 3.

A3.1 Experiment

Figure A3.1-1 Experiment 1 F_o=1.1g/s, u_o=100cm/s, ΔT=260°C Temperature Profile of Bed for replications 1, 2, and 3 respectively. (Figure 43 has format info)

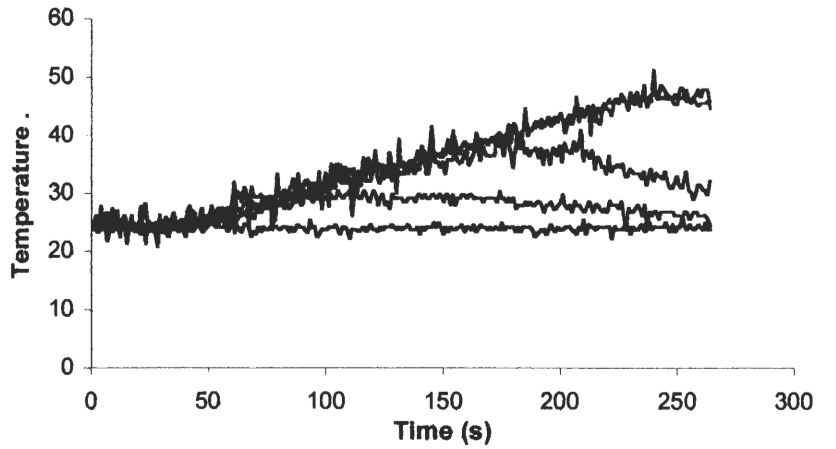

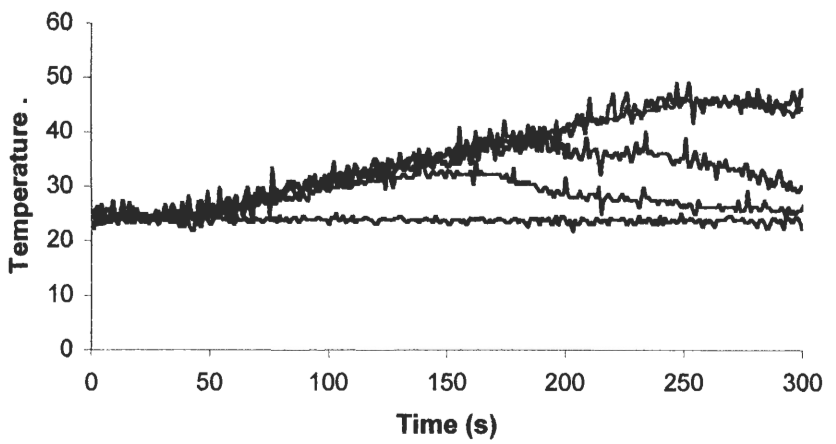

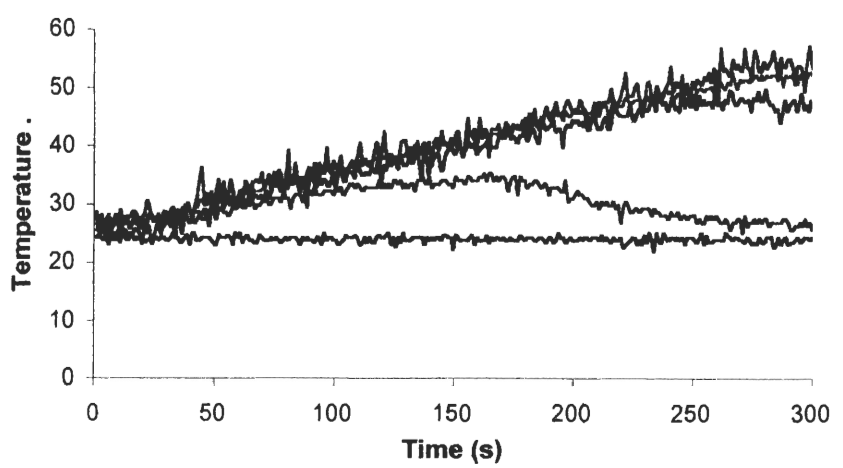

A3.1 Experiment 2

Figure A3.1-2 Experiment 2 F_o=2.2g/s, u_o=100cm/s, ΔT=260°C Temperature Profile of Bed for replications 1, 2, and 3 respectively. (Figure 43 has format info)

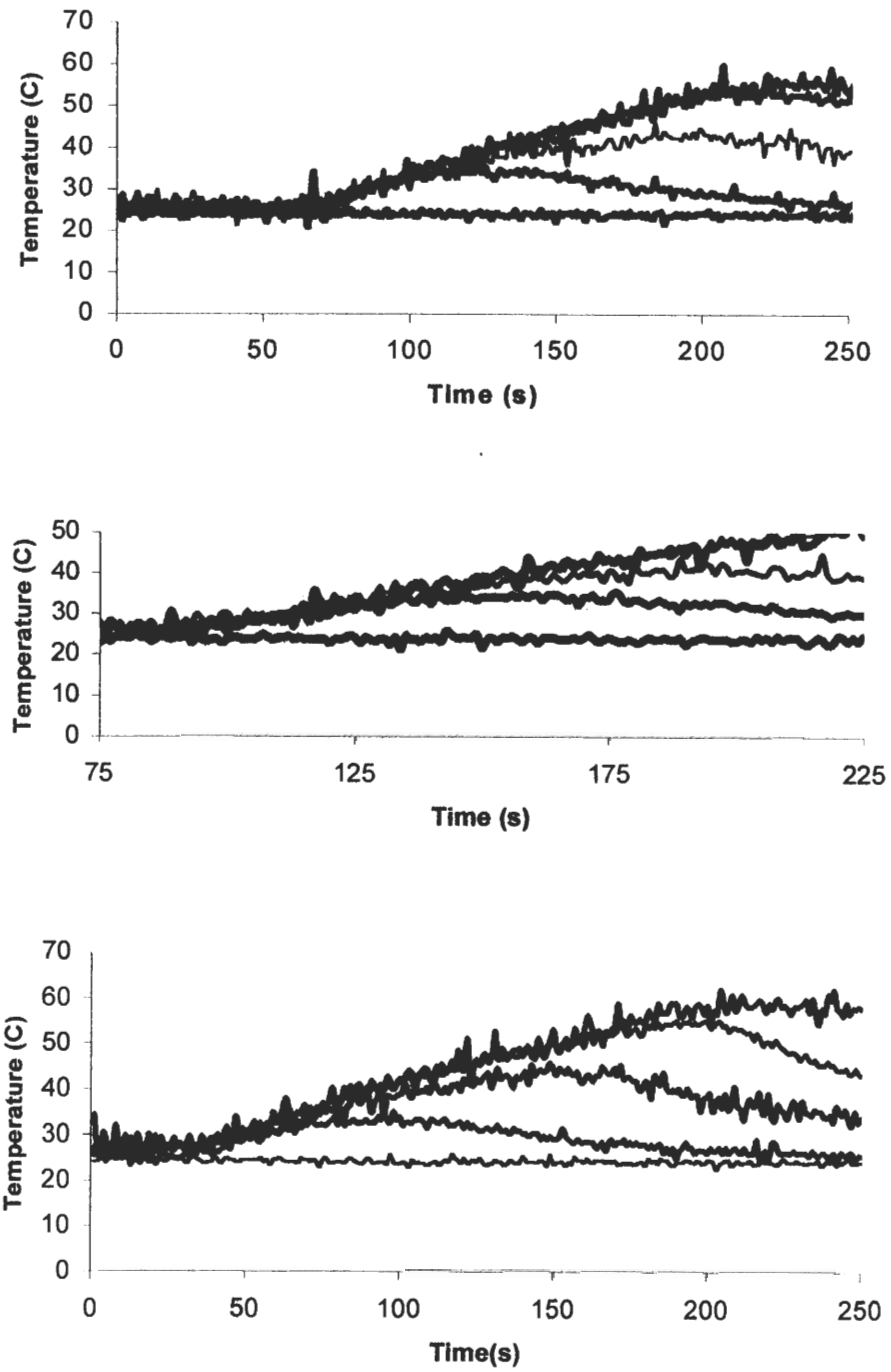

A3.1 Experiment 3

Figure A3.1-3 Experiment 3 F_o=1.1g/s, u_o=200cm/s, ΔT=260°C Temperature Profile of Bed for Replication 3. Problems with thermocouples and data collection prevented temperature profiles from the first replications from being obtained. (Figure 43 has format info)

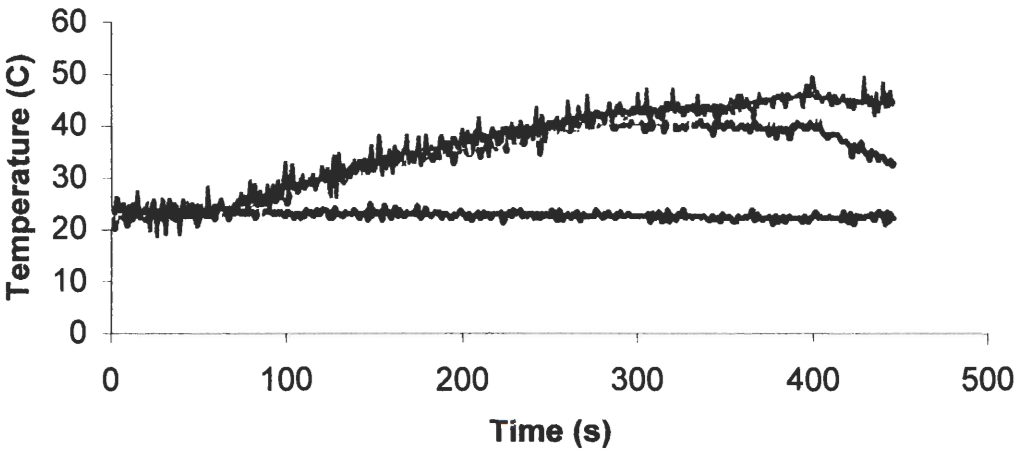

A3.1 Experiment 4

Figure A3.1-4 Experiment 4 F_0=2.2g/s, u_0=200cm/s, ΔT=260°C Temperature Profile of Bed for replications 1, 2, and 3 respectively. (Figure 43 has format info)

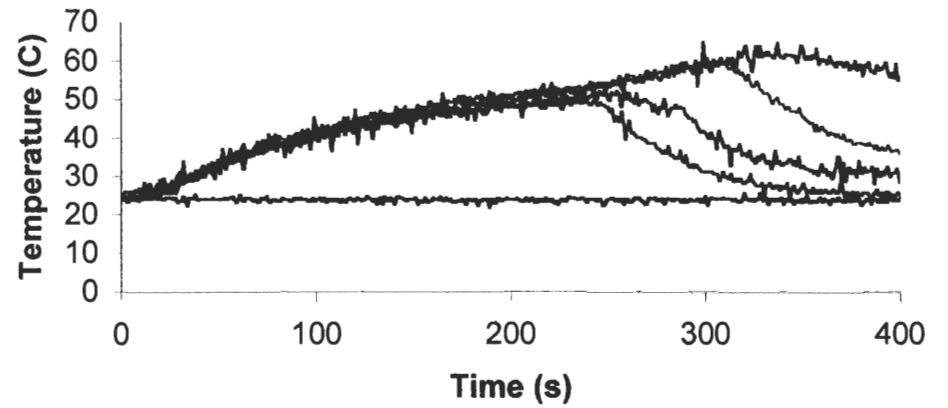

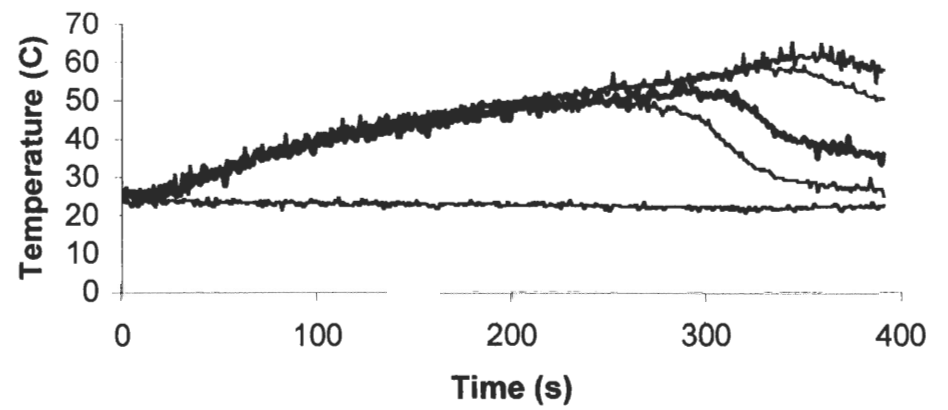

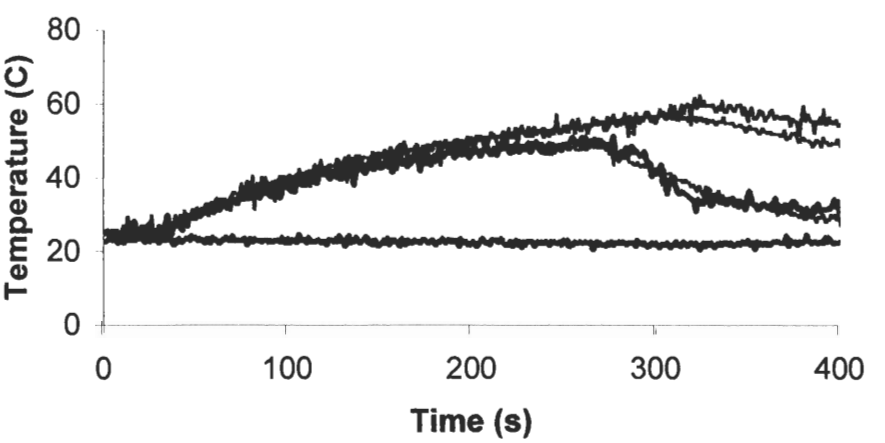

A3.1 Experiment 5

Figure A3.1-5 Experiment 5 F_o=1.1g/s, u_o=100cm/s, ΔT=300°C Temperature Profile of Bed for replications 1, 2, and 3 respectively. (Figure 43 has format info)

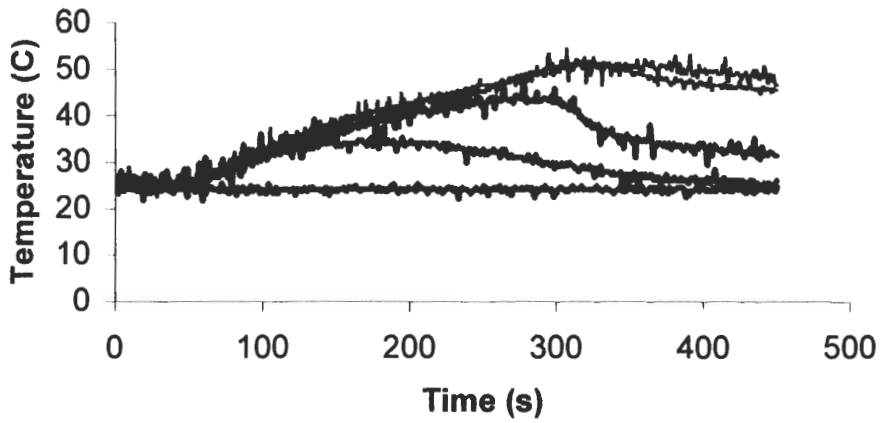

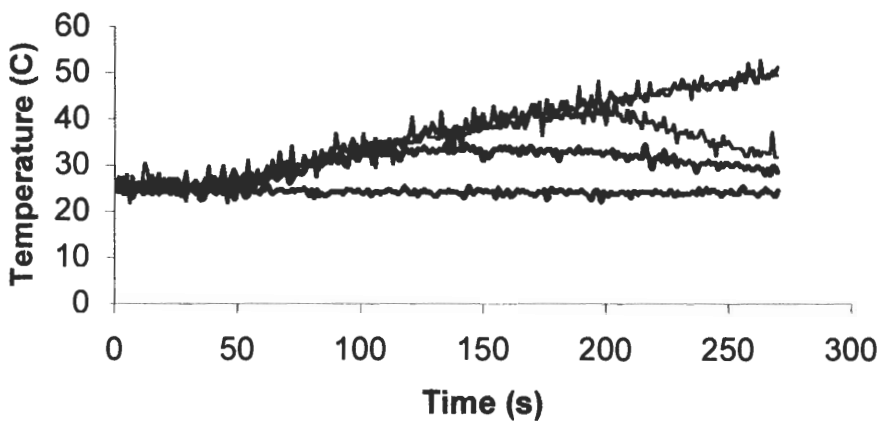

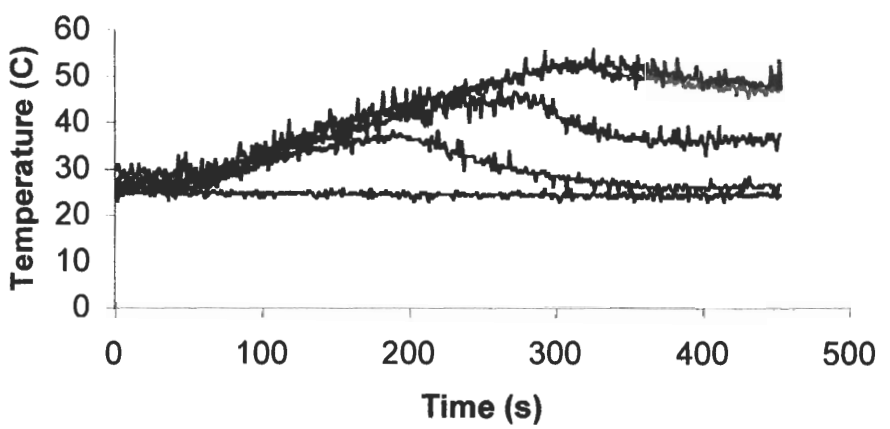

A3.1 Experiment 6

Figure A3.1-6 Experiment 6 F_o=2.2g/s, u_o=100cm/s, ΔT=300°C Temperature Profile of Bed for replications 1, 2, and 3 respectively. (Figure 43 has format info)

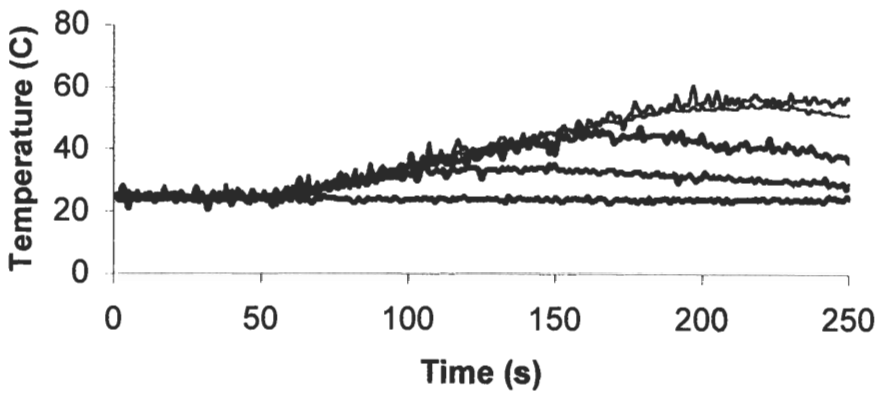

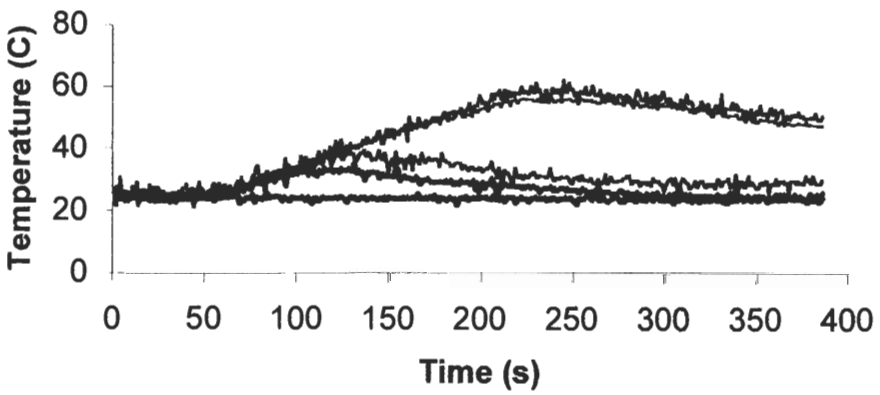

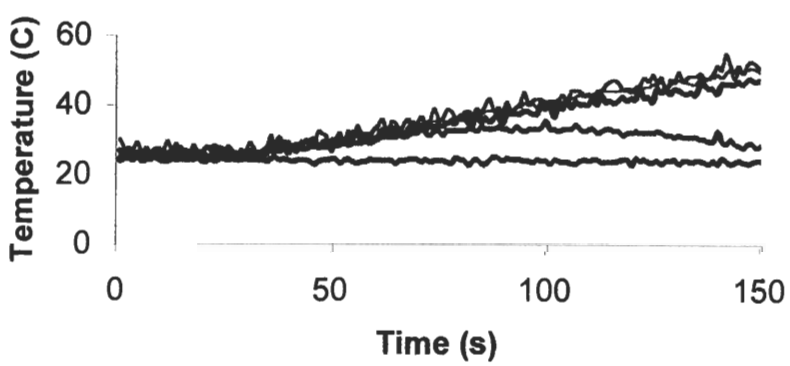

A3.1 Experiment 7

Figure A3.1-7 Experiment 7 F_o=1.1g/s, u_o=200cm/s, ΔT=300°C Temperature Profile of Bed for replications 1, 2, and 3 respectively. (Figure 43 has format info)

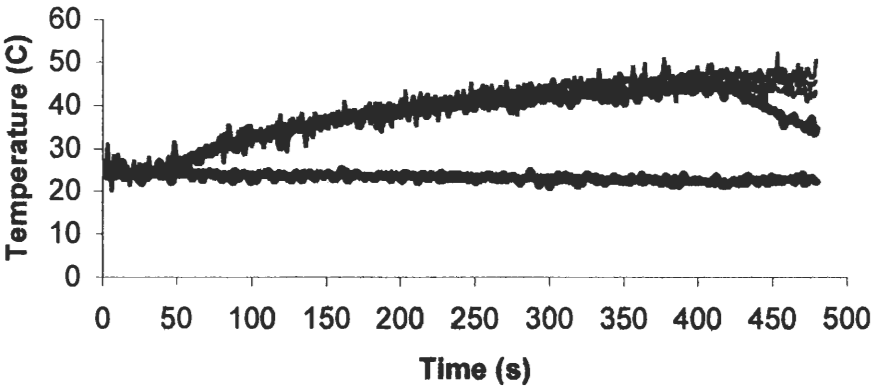

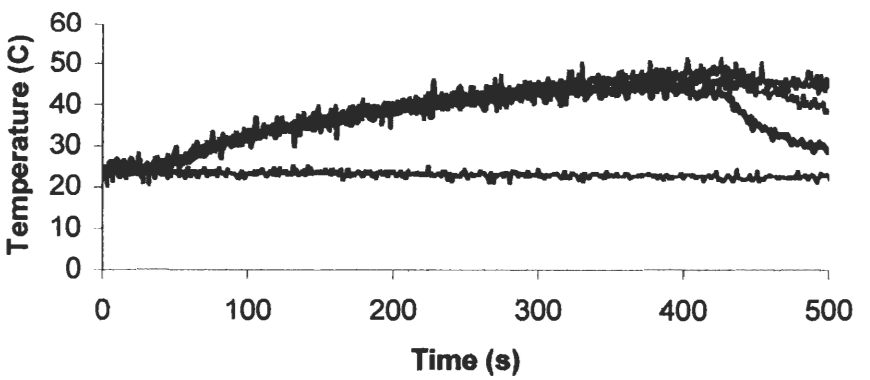

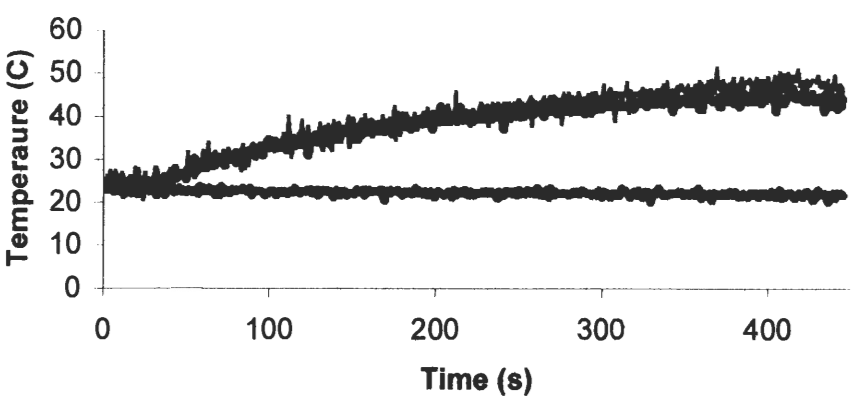

A3.1 Experiment 8

Figure A3.1-8 Experiment 8 F_o=2.2g/s, u_o=200cm/s, ΔT=300°C Temperature Profile of Bed for replications 1, 2, and 3 respectively. (Figure 43 has format info)

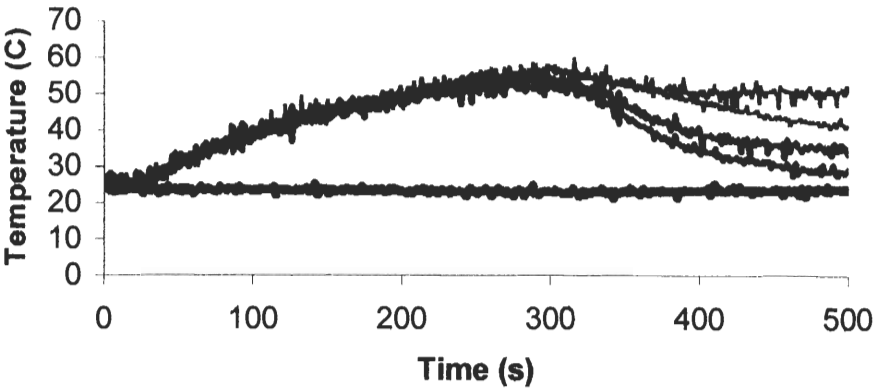

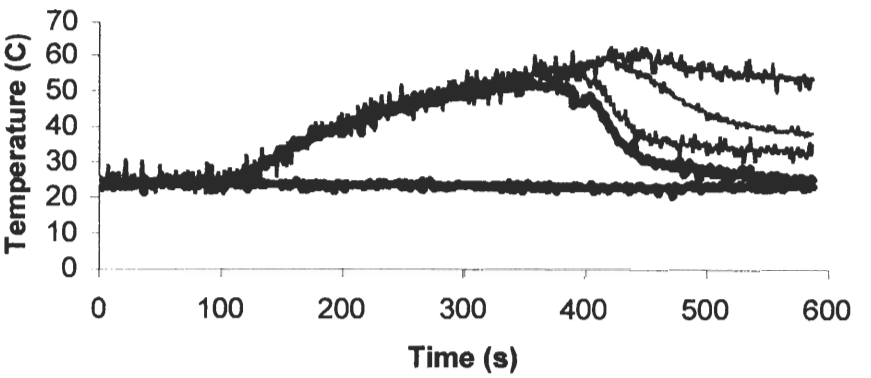

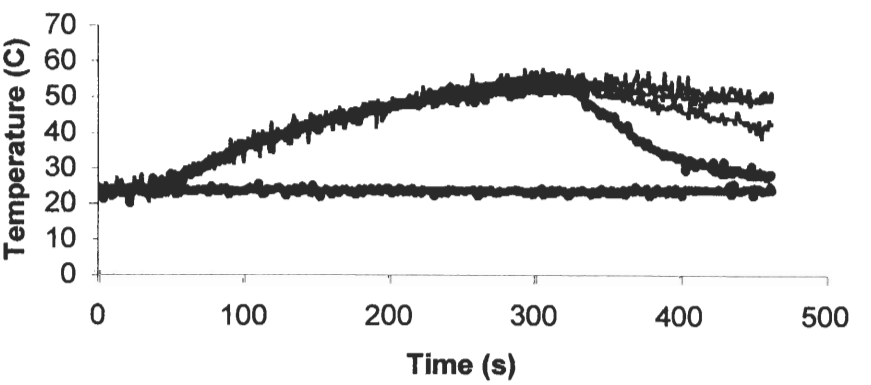

A3.2 Particle Growth Rate Plots

The following plots represent the rate of change of the mean particle diameter with time in the upper and lower sections of the bed. These plots have three points but only the first two points are used in the determination of the particle growth rate. The third point in these plots occurs after a discontinuity in particle growth, which is discussed in greater detail in the Experimental Procedures Section. The slope in the 1st order plot represents the particle growth rate used in this project. Each of these numbers is the result of three replications

A3.2 Experiment 1

Figure A3.2-1 Experiment 1 Upper F_0=2.2g/s, u_0=100cm/s, ΔT=260°C Mean particle diameter growth rate = 0.22mm/min

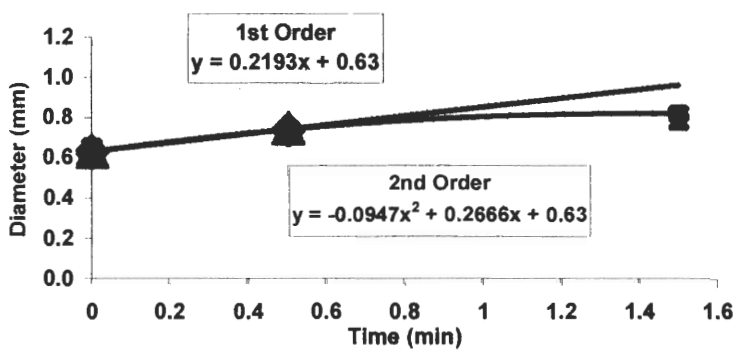

Figure A3.2-2 Experiment 1 Lower F_0=2.2g/s, u_0=100cm/s, ΔT=260°C Mean particle diameter growth rate = 0.24mm/min

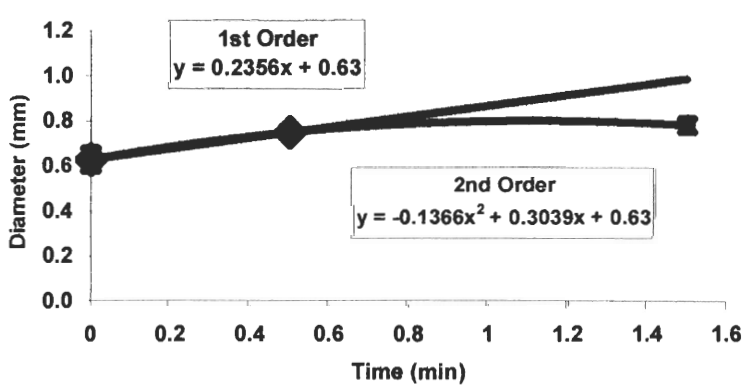

A3.2 Experiment 2

Figure A3.2-3 Experiment 2 Upper F_0=2.2g/s, u_0=100cm/s, ΔT=260°C Mean particle diameter growth rate=0.34mm/min

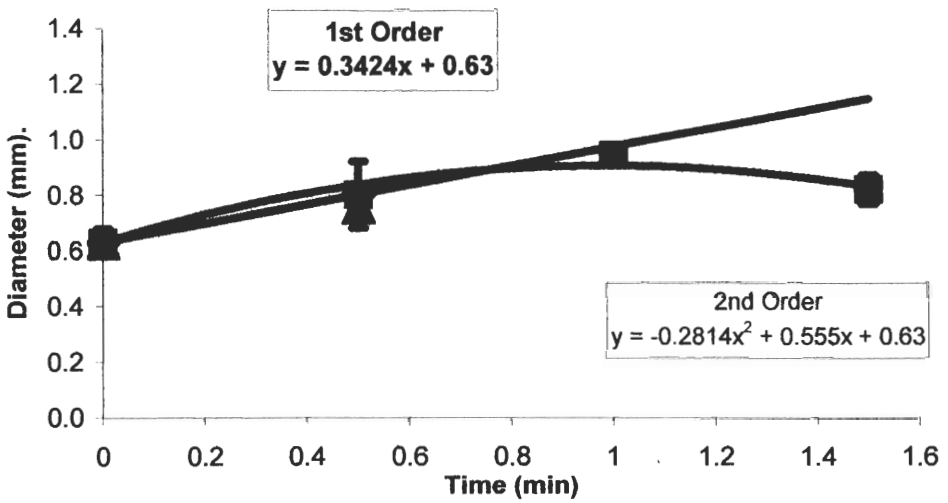

Figure A3.2-4 Experiment 2 Lower F_0=2.2g/s, u_0=100cm/s, ΔT=260°C Mean particle diameter growth rate=0.255mm/min

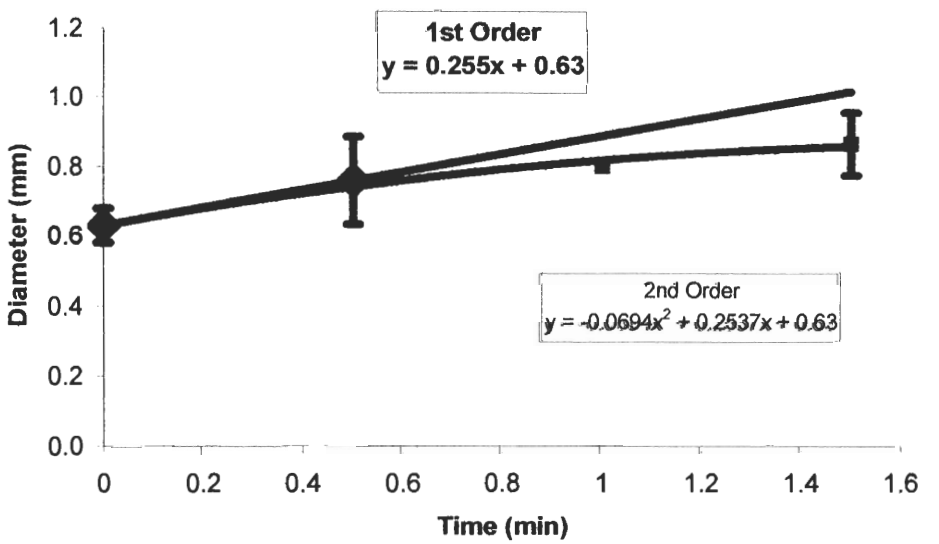

A3.2 Experiment 3

Figure A3.2-5 Experiment 3 Upper F_o=1.1g/s, u_o=200cm/s, ΔT=260°C Mean particle diameter growth rate=0..185mm/min

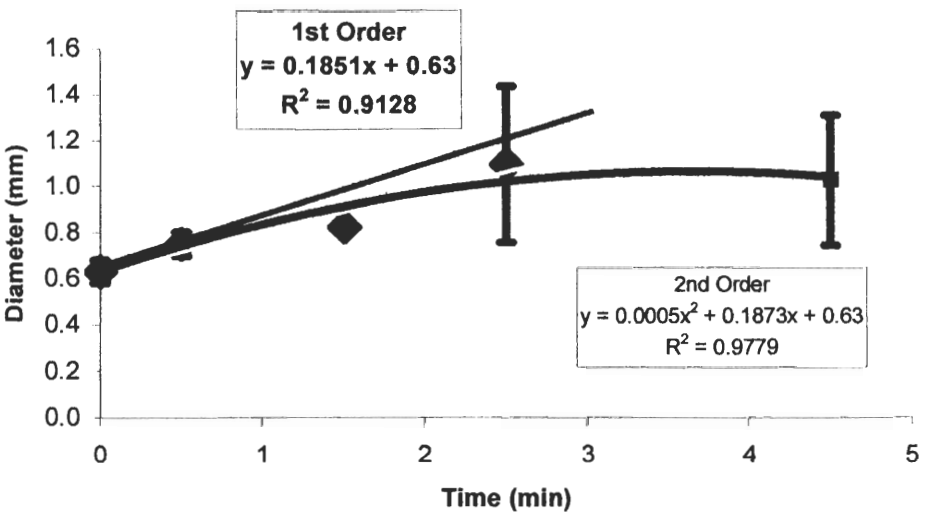

Figure A3.2-6 Experiment 3 Lower F_o=1.1g/s, u_o=200cm/s, ΔT=260°C Mean particle diameter growth rate=0.113mm/min

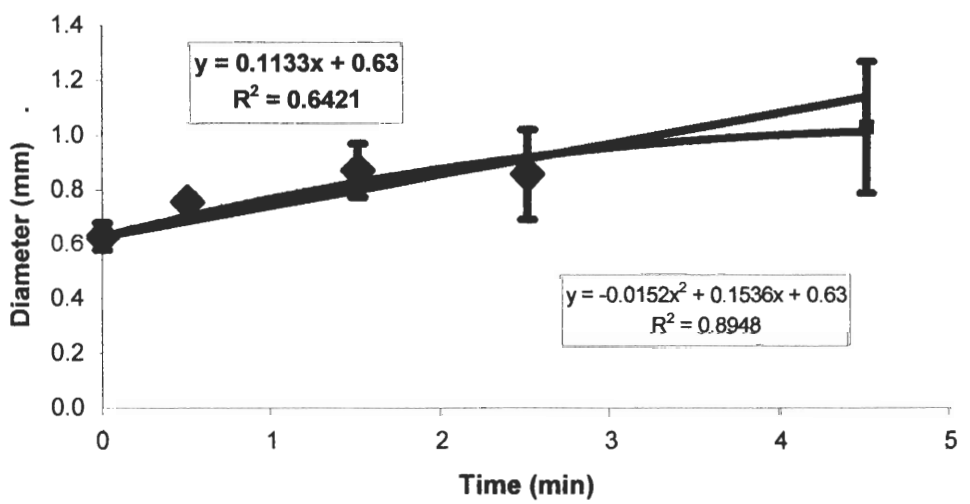

A3.2 Experiment 4

Figure A3.2-7 Experiment 4 Upper F_o=2.2g/s, u_o=200cm/s, ΔT=260°C Mean particle diameter growth rate=0.17mm/min

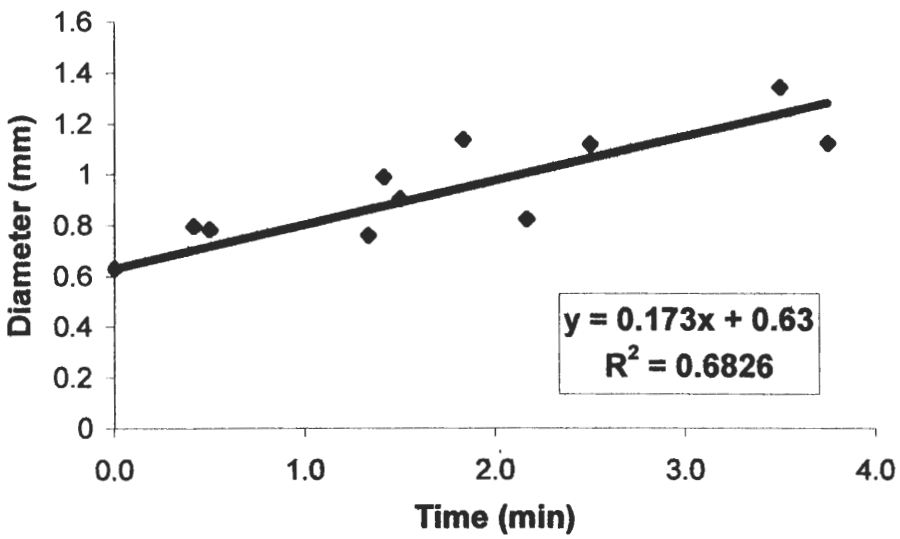

Figure A3.2-8 Experiment 4 Lower F_o=2.2g/s, u_o=200cm/s, ΔT=260°C Mean particle diameter growth rate=0.14mm/min

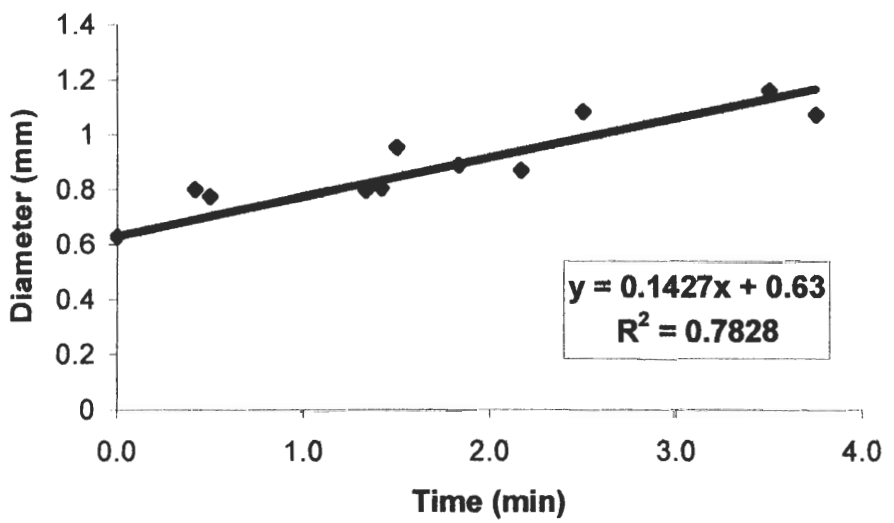

A3.2 Experiment 5

Figure A3.2-9 Experiment 5 Upper F_0=1.1g/s, u_0=100cm/s, ΔT=300°C Mean particle diameter growth rate=0.24mm/min

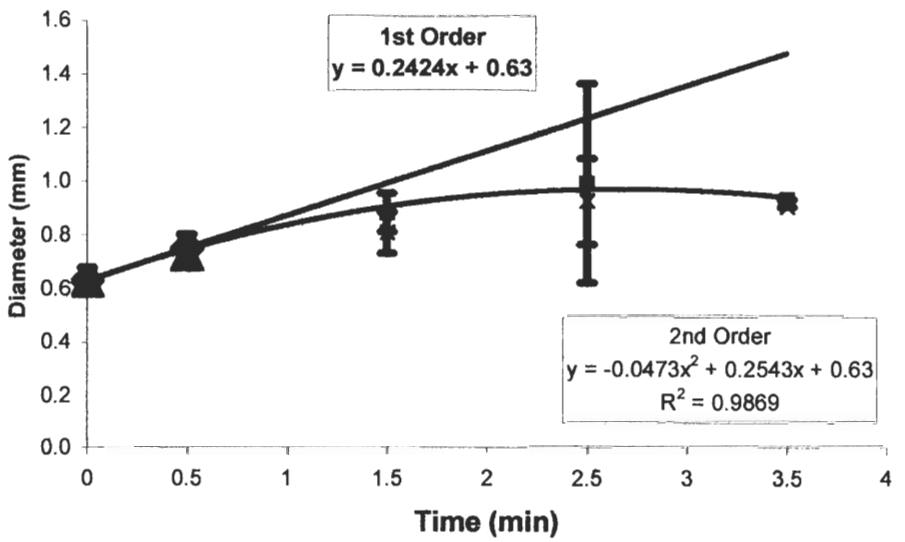

Figure A3.2-10 Experiment 5 Lower F_0=1.1g/s, u_0=100cm/s, ΔT=300°C Mean particle diameter growth rate=0.20mm/min

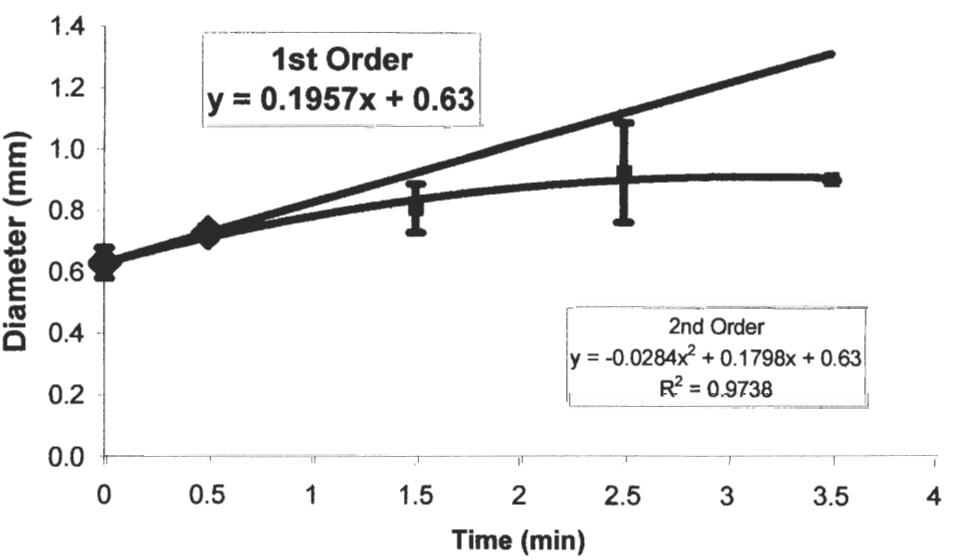

A3.2 Experiment 6

Figure A3.2-11 Experiment 6 Upper F_o=2.2g/s, u_o=100cm/s, ΔT=300°C Mean particle diameter growth rate=0.34mm/min

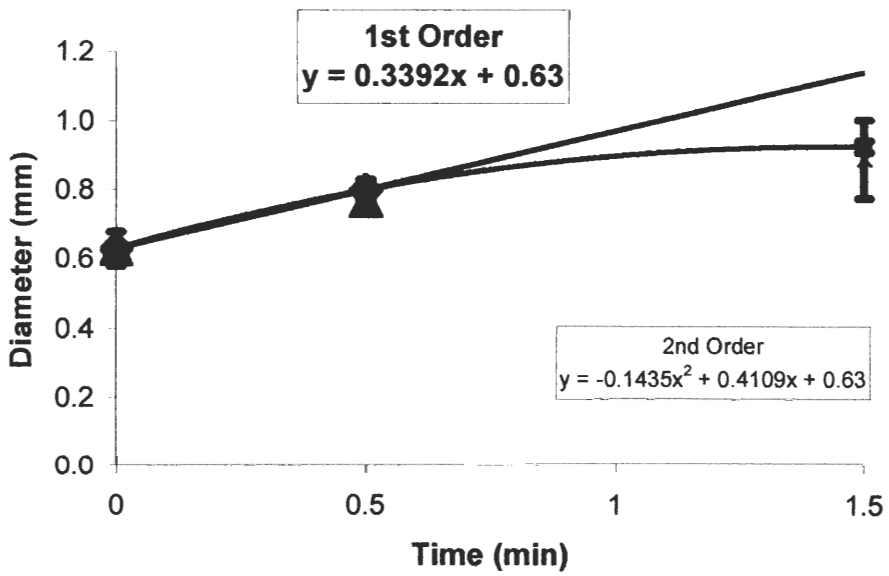

Figure A3.2-12 Experiment 6 Upper F_o=2.2g/s, u_o=100cm/s, ΔT=300°C Mean particle diameter growth rate=0.29mm/min

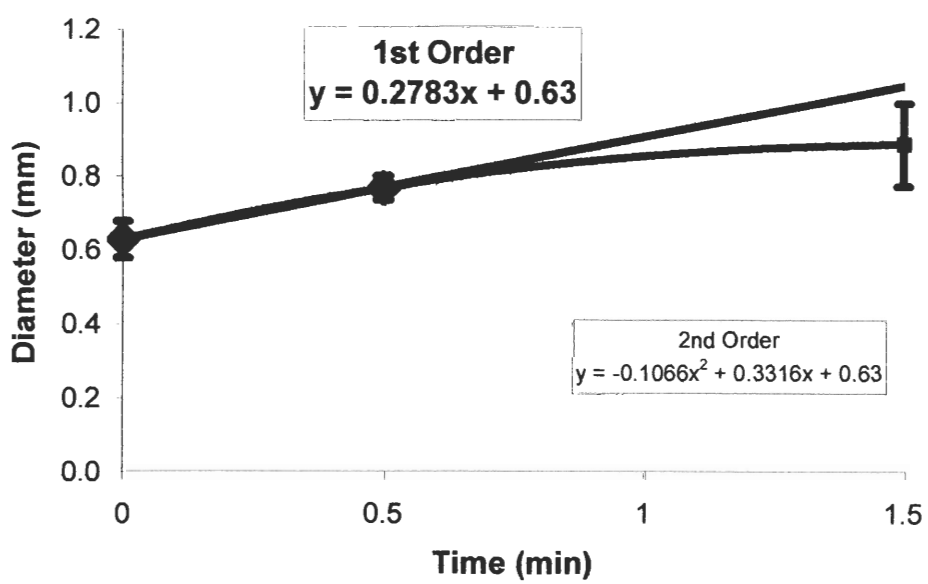

A3.2 Experiment 7

Figure A3.2-13 Experiment 7 Upper F_0=1.1g/s, u_0=200cm/s, ΔT=300°C Mean particle diameter growth rate=0.14mm/min

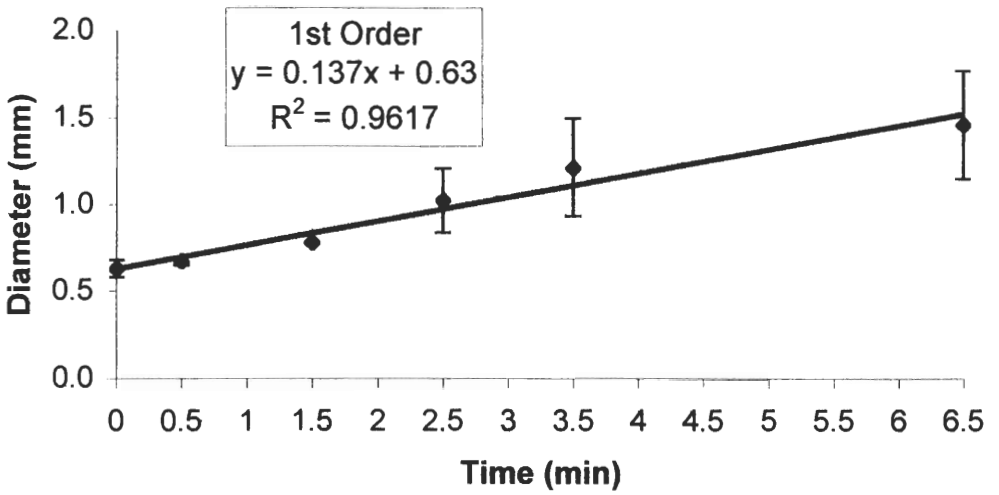

Figure A3.2-14 Experiment 7 Lower F_0=1.1g/s, u_0=200cm/s, ΔT=300°C Mean particle diameter growth rate=0.123mm/min

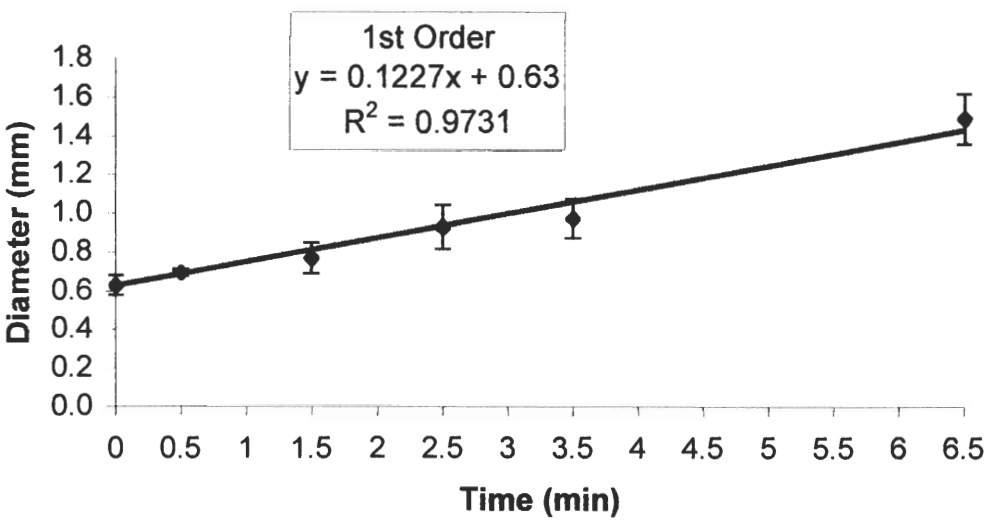

A3.2 Experiment 8

Figure A3.2-15 Experiment 8 Lower F_0=2.2g/s, u_0=200cm/s, ΔT=300°C Mean particle diameter growth rate=0.185mm/min

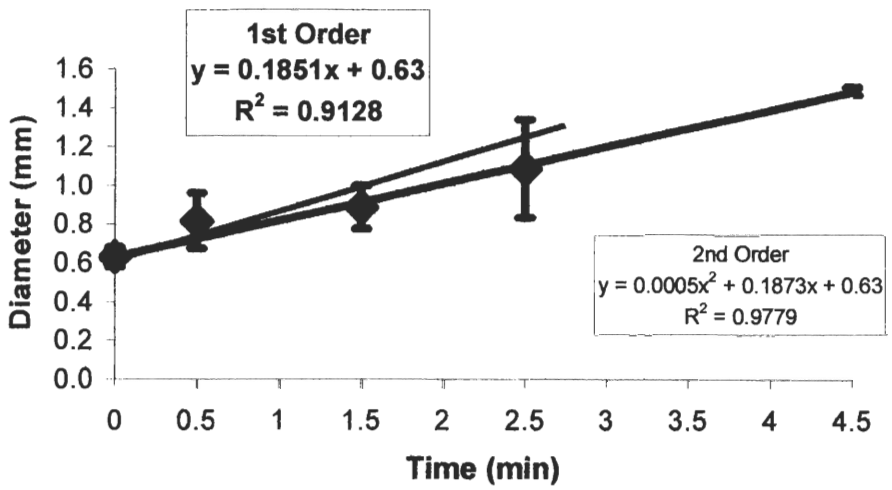

Figure A3.2-16 Experiment 8 Lower F_0=2.2g/s, u_0=200cm/s, ΔT=300°C Mean particle diameter growth rate=0.18mm/min

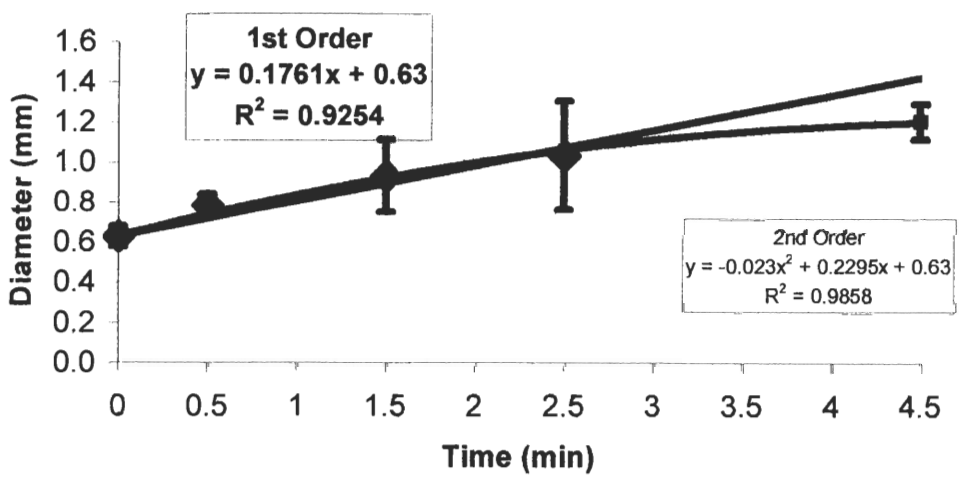

A3.3 Particle Size Distribution Plots

This section gives the results of the differences in distributions between the seedbed particle distribution and the particle size distribution of an experiment at 30 seconds. The distributions used for this analysis combine both the upper and lower sample distributions taken at 30 seconds for those experimental conditions. Below, in Figure A3.3-1, both distributions are plotted together.

Figure A3.3-1 Experiment 1 Combination of seed bed particle distribution and distribution created after 30s

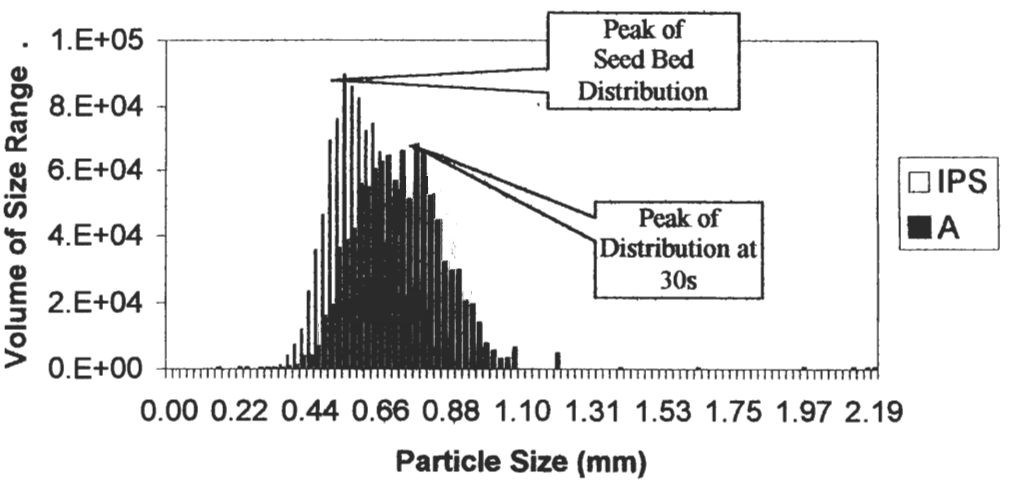

When the difference between the individual bin volumes for particular ranges is determined, the size ranges where particles were absorbed during those 30s are negative and the volume of particles created are positive. An example of this can be seen in Figure A3.3-2 where the initial seedbed is compared to the particle size distribution of experiment one at 30s.

Figure A3.3-2 Difference in distributions between initial particle size distribution and particle size distribution at 30 seconds.

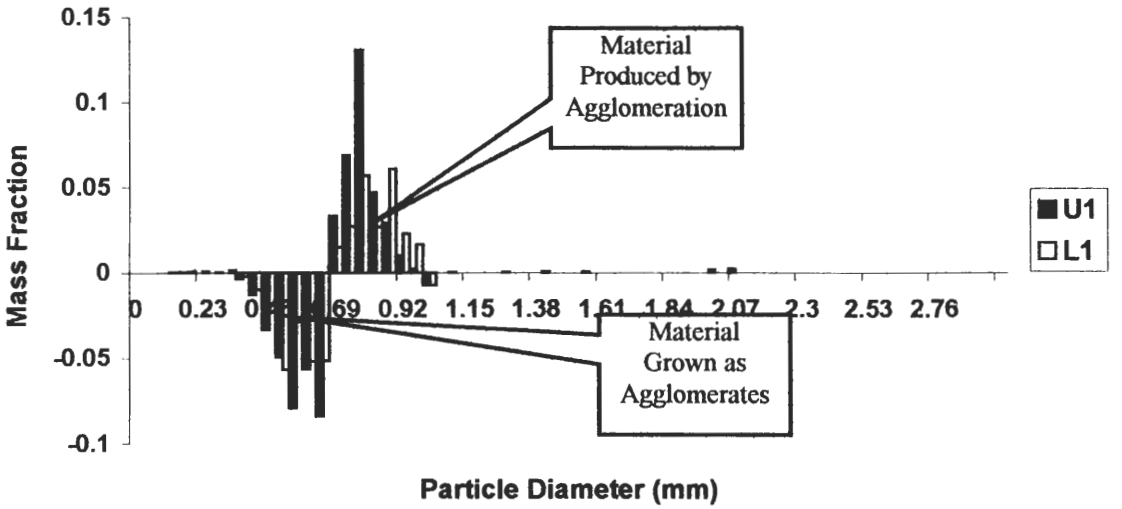

The mean particle size was determined separately for the negative and positive distribution to indicate the type of particle absorbed and the type of particle formed during the 30s of the experiment. The results of this analysis for the various experiments can be seen in Table A3.3-1.

3.4.1 Experiment 1

Experimental Conditions: F_o=1.1g/s, u_o=100cm/s, ΔT=260°C

1.1

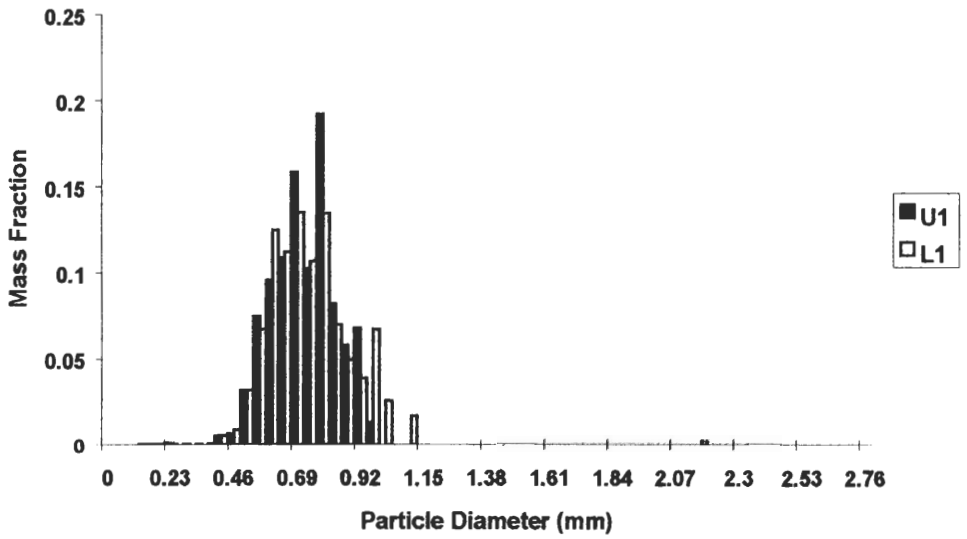

Figure A3.3-3. Experiment 1.1 Upper and lower particle size distribution at 30s

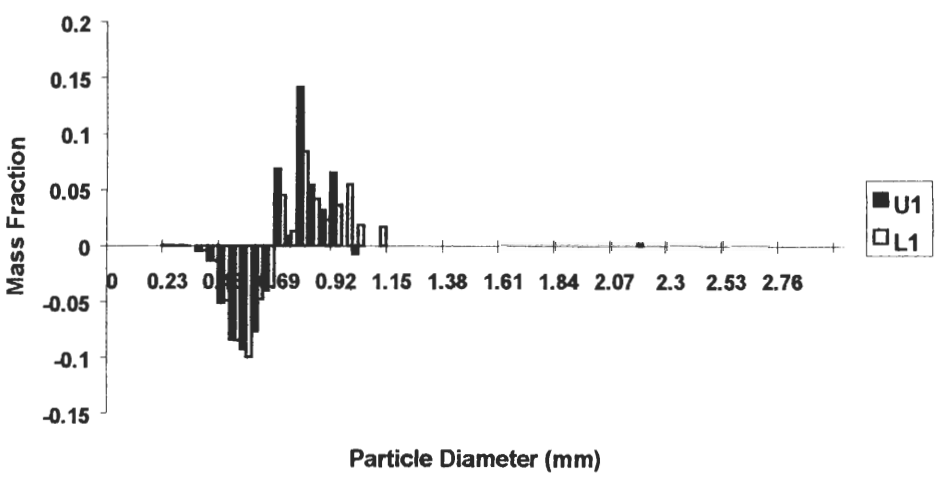

Figure A3.3-4. Experiment 1.1 Several seedbed particles (negative) grew to form larger particles (positive)

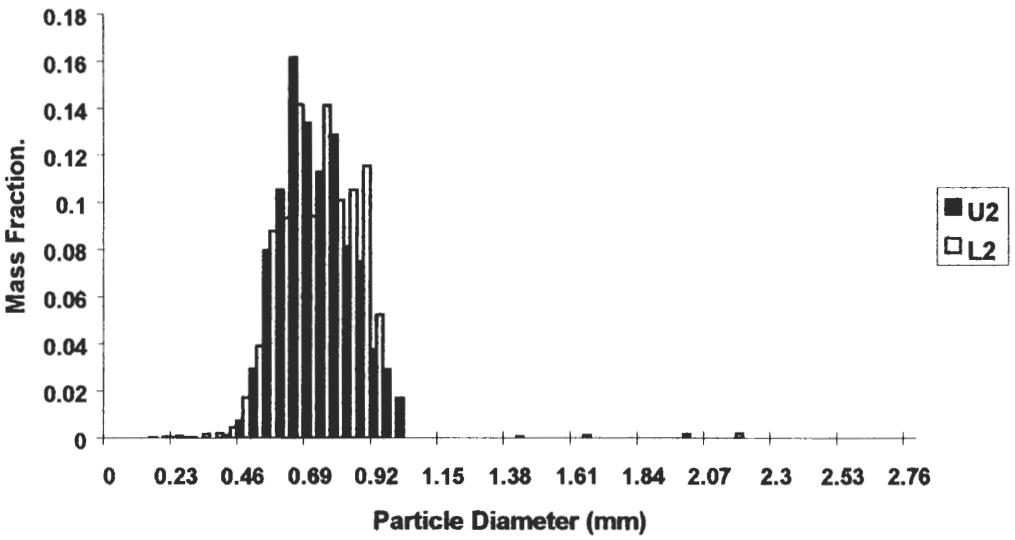

Figure A3.3-5. Experiment 1.2 Upper and lower particle size distribution at 30s

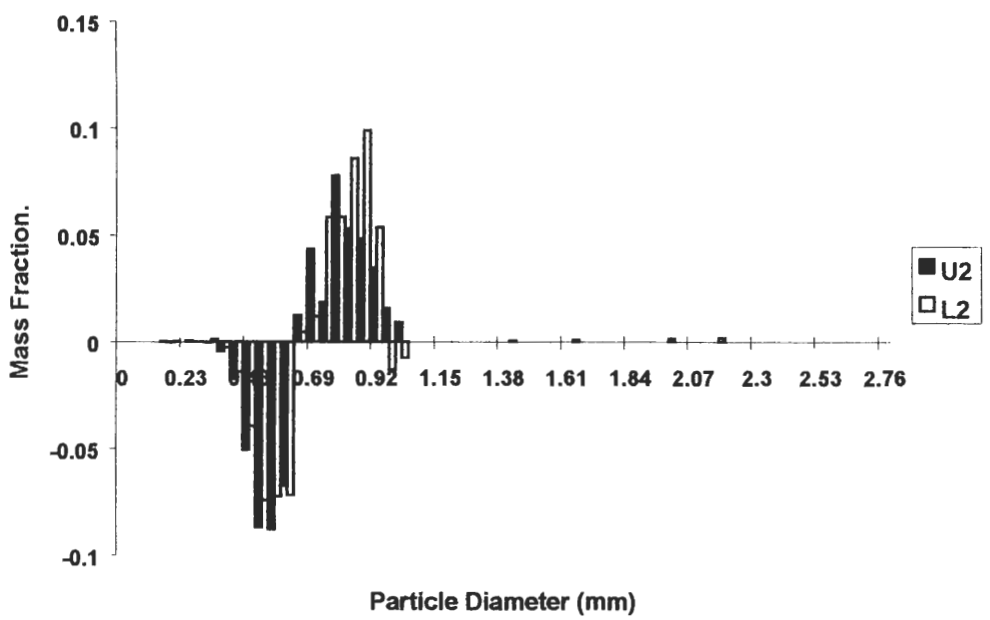

Figure A3.3-6 Experiment 1.2 Several seedbed particles (negative) grew to form larger particles (positive)

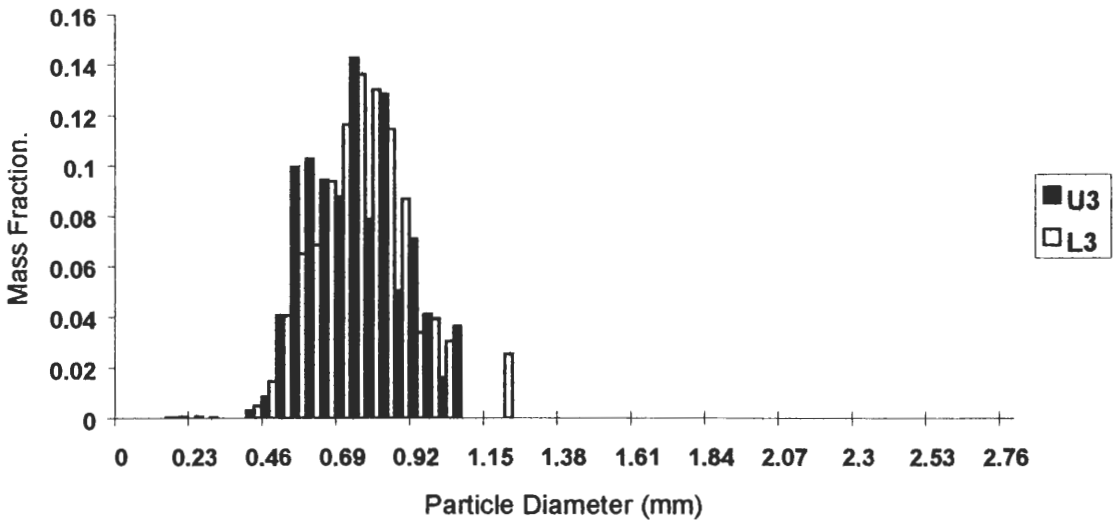

Figure A3.3-7 Experiment 1.3 Upper and lower particle size distribution at 30s

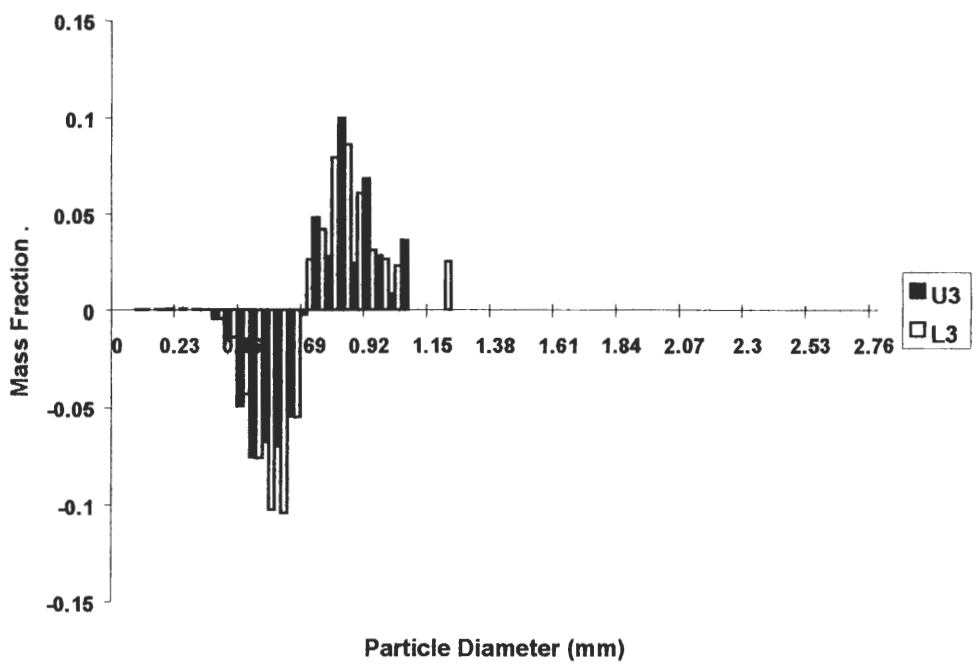

Figure A3.3-8 Experiment 1.3 Several seedbed particles (negative) grew to form larger particles (positive)

3.3-2 Experiment 2

Experimental Conditions: F_o=2.2g/s, u_o=100cm/s, ΔT=260°C

2.1

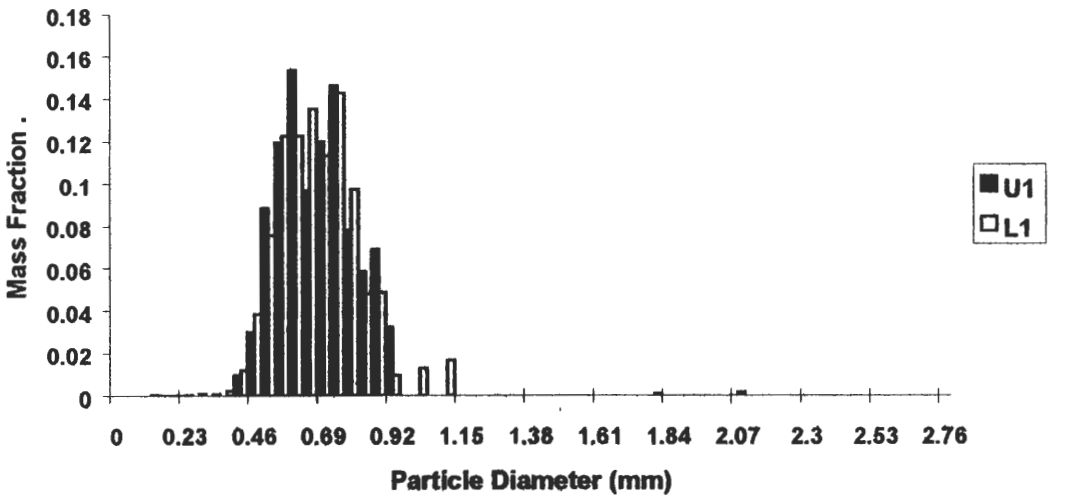

Figure A3.3-9 Experiment 2.1 Upper and lower particle size distribution at 30s

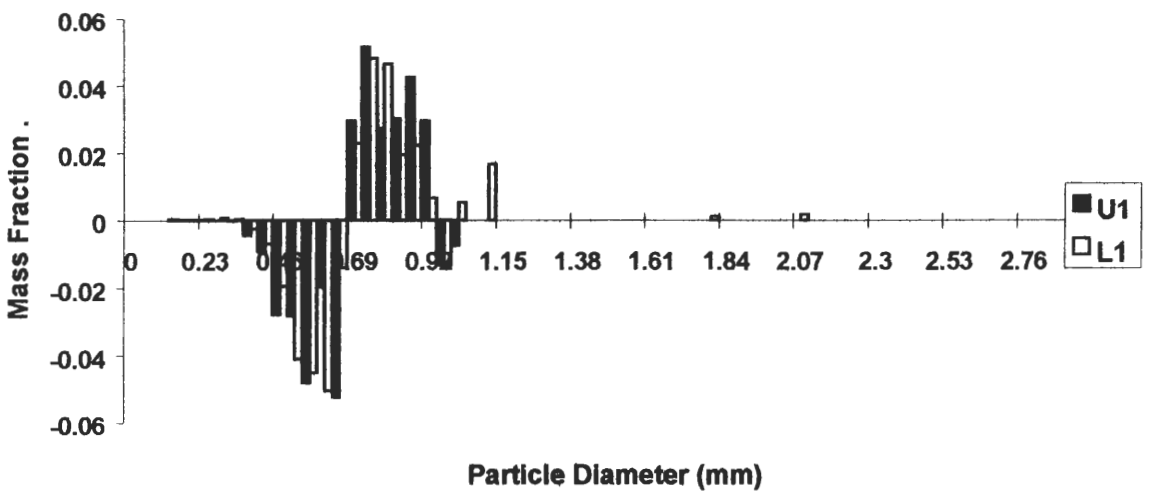

Figure A3.3-10 Experiment 2.1 Several seedbed particles (negative) grew to form larger particles (positive)

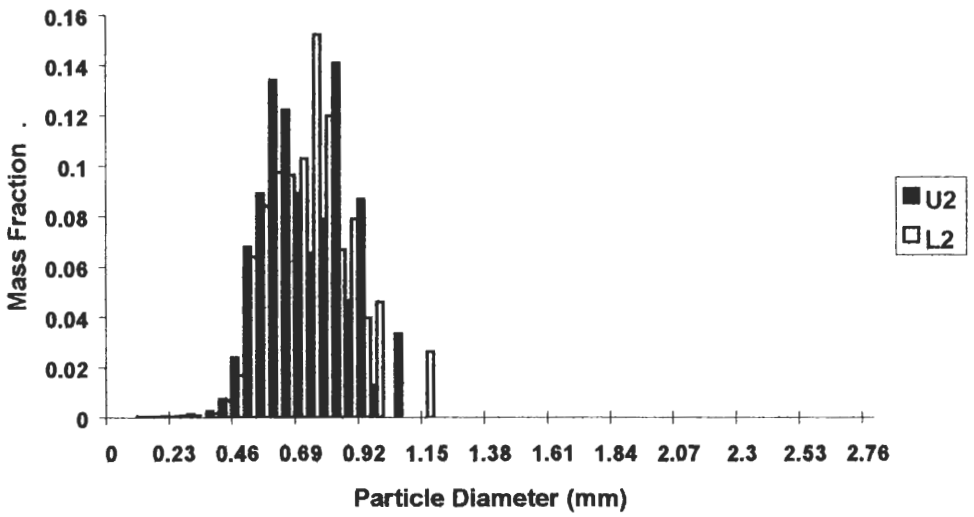

Figure A3.3-11 Experiment 2.2 Upper and lower particle size distribution at 30s

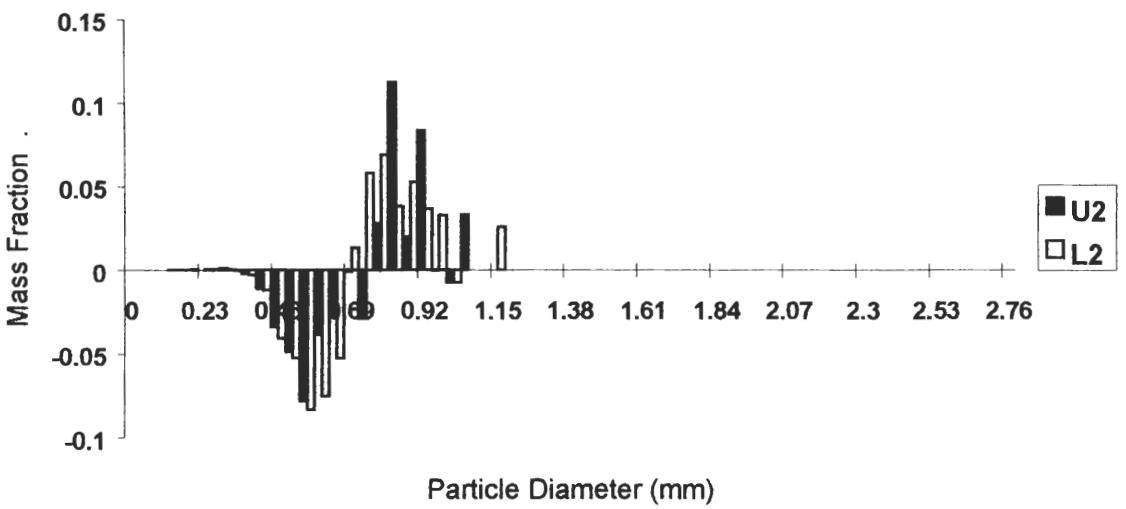

Figure A3.3-12 Experiment 2.2 Several seedbed particles (negative) grew to form larger particles (positive)

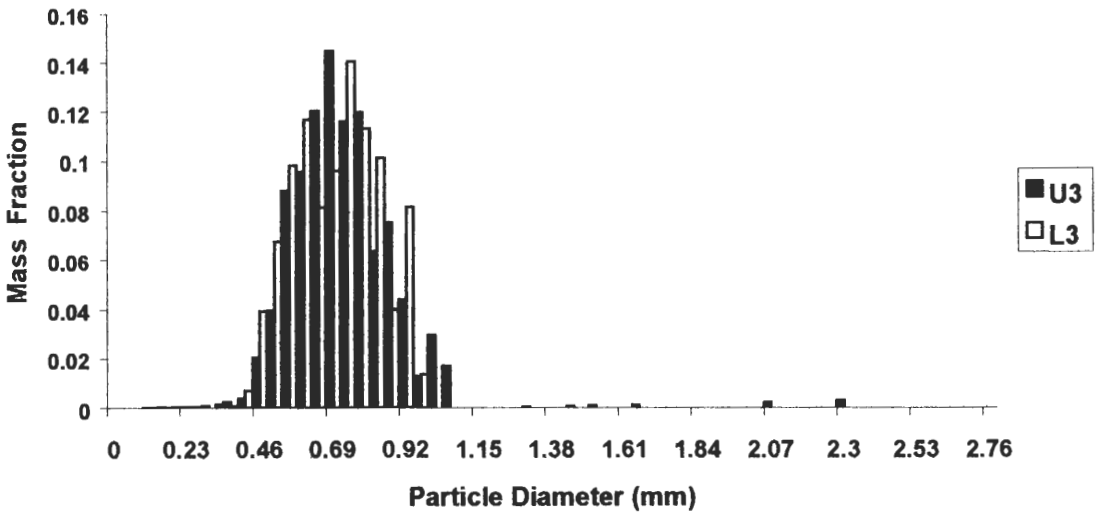

Figure A3.3-13 Experiment 2.3 Upper and lower particle size distribution at 30s

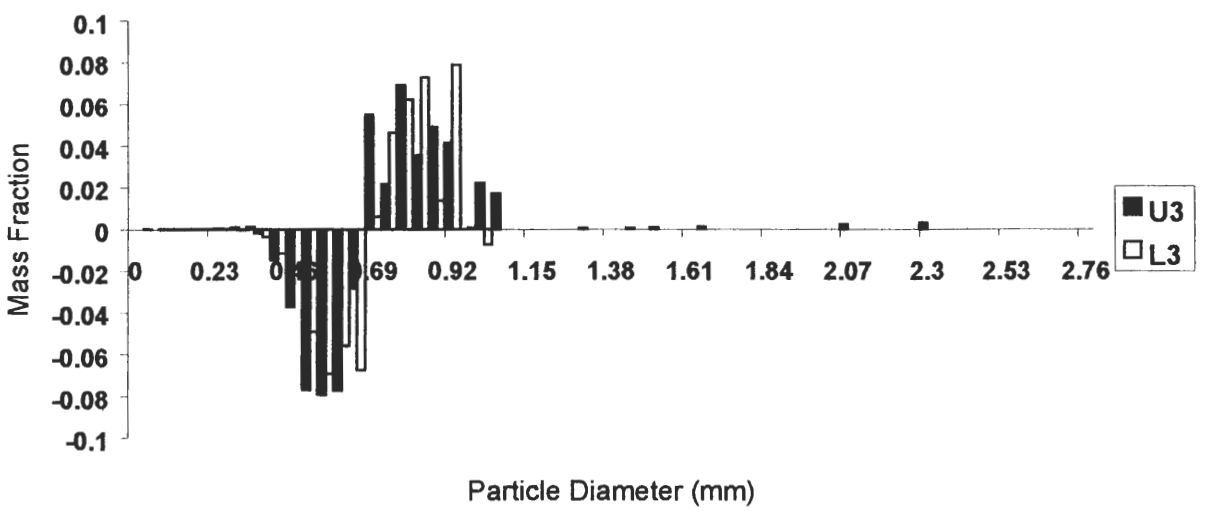

Figure A3.3-14 Experiment 2.3 Several seedbed particles (negative) grew to form larger particles (positive)

3.4.3 Experiment 3

Experimental Conditions: F_o=1.1g/s, u_o=200cm/s, ΔT=260°C

3.1

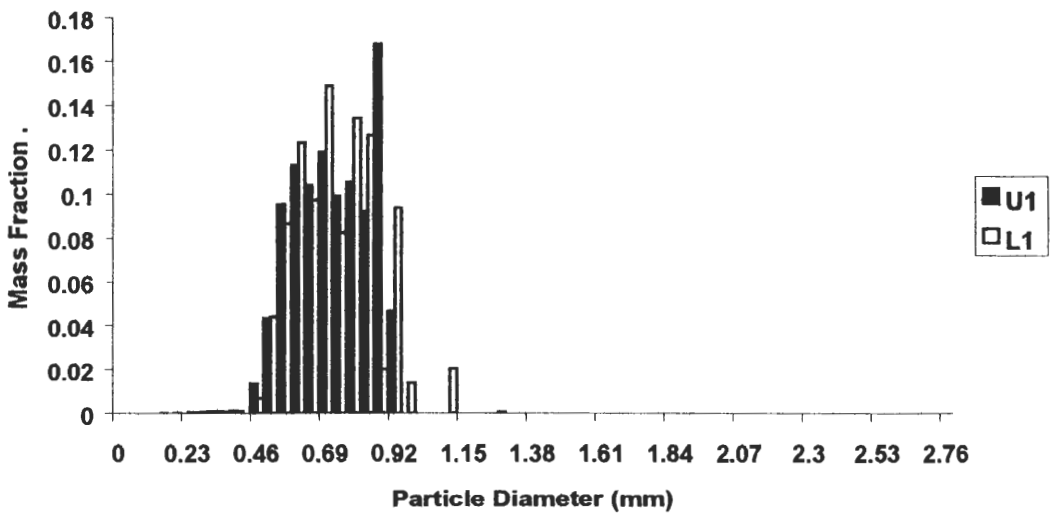

Figure A3.3-15 Experiment 3.1 Upper and lower particle size distribution at 30s

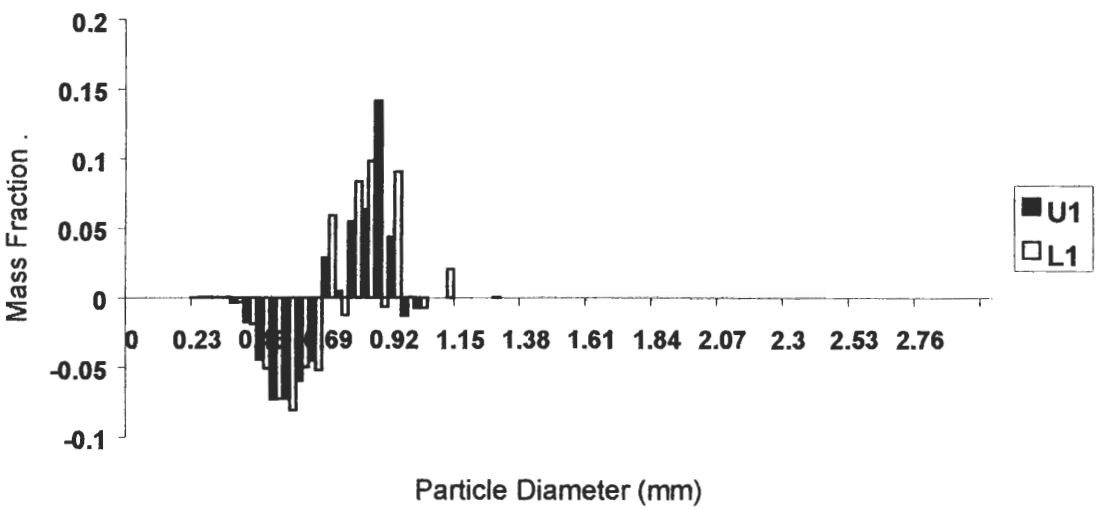

Figure A3.3-16 Experiment 3.1 Several seedbed particles (negative) grew to form larger particles (positive)

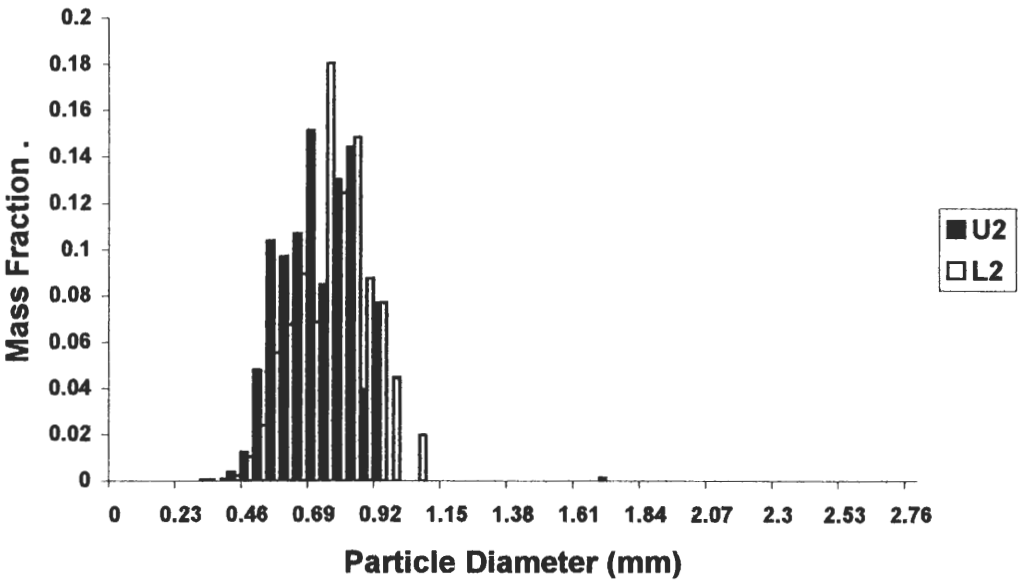

Figure A3.3-17 Experiment 3.2 Upper and lower particle size distribution at 30s

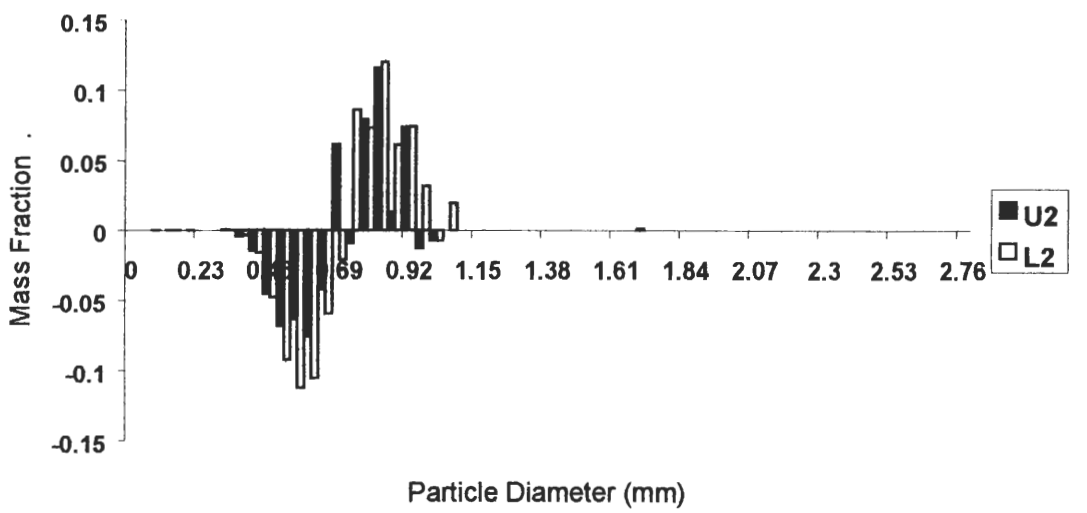

Figure A3.3-18 Experiment 3.2 Several seedbed particles (negative) grew to form larger particles (positive)

3.4.4 Experiment 4

Experimental Conditions: F_o=2.2.1g/s, u_o=200cm/s, ΔT=260°C

4.1

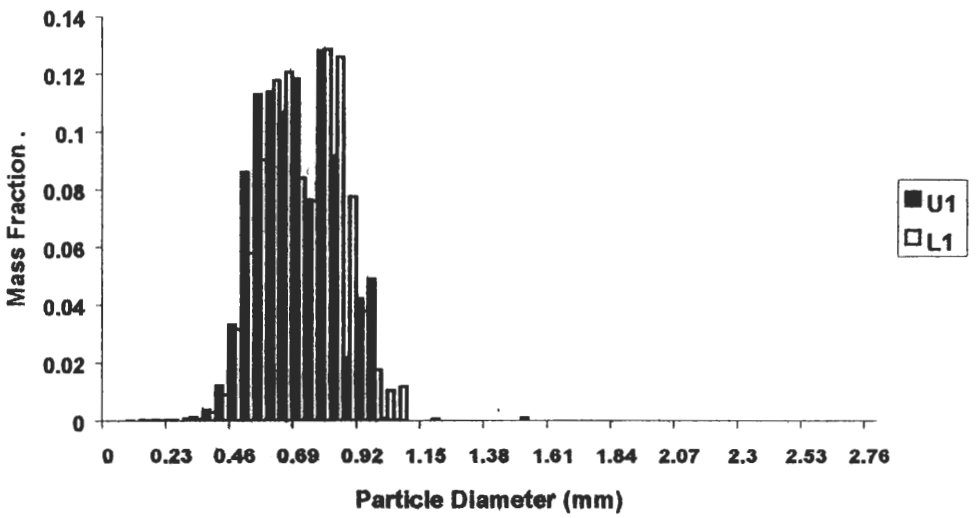

Figure A3.3-19 Experiment 4.1 Upper and lower particle size distribution at 30s

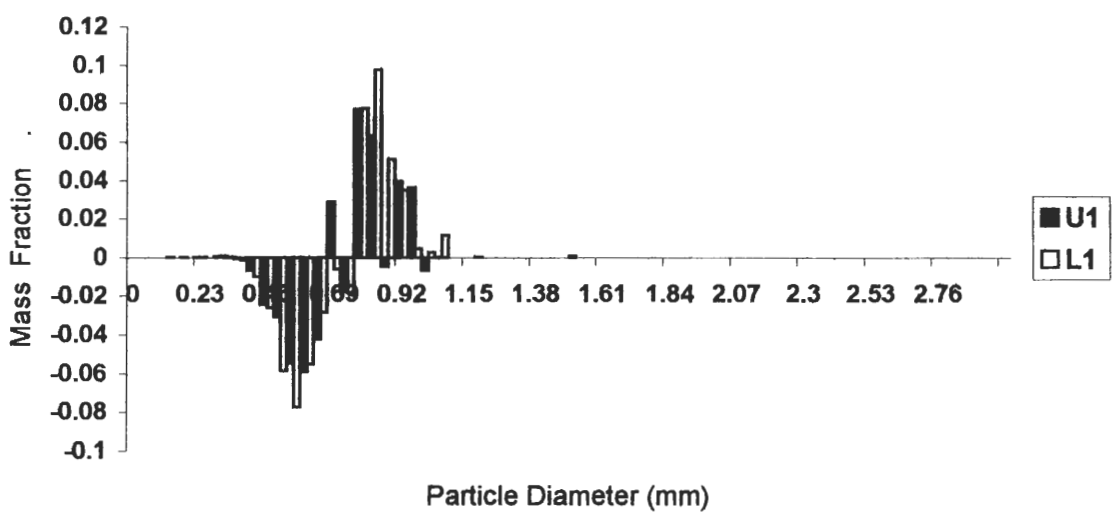

Figure A3.3-20 Experiment 4.1 Several seedbed particles (negative) grew to form larger particles (positive)

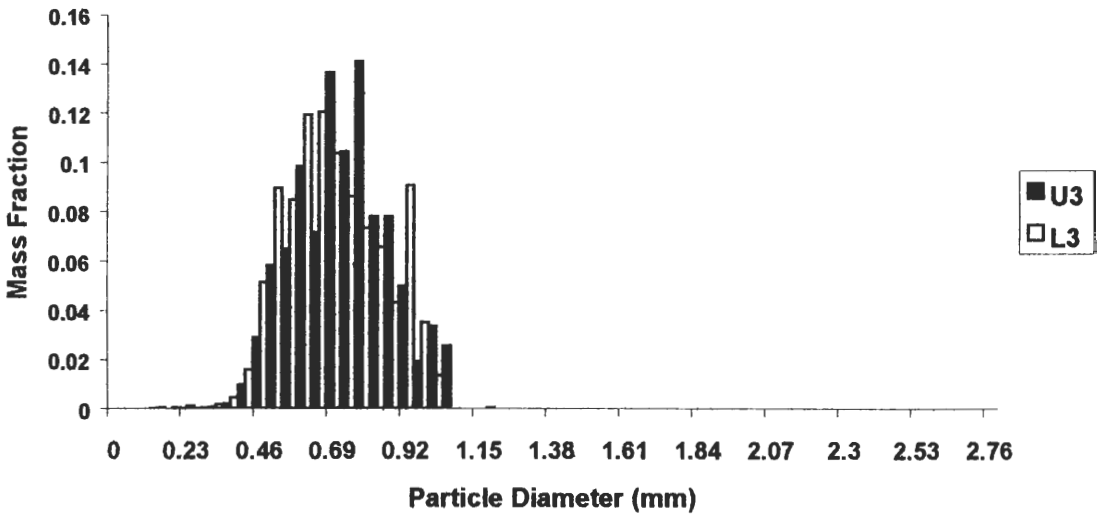

Figure A3.3-21 Experiment 4.3 Upper and lower particle size distribution at 30s

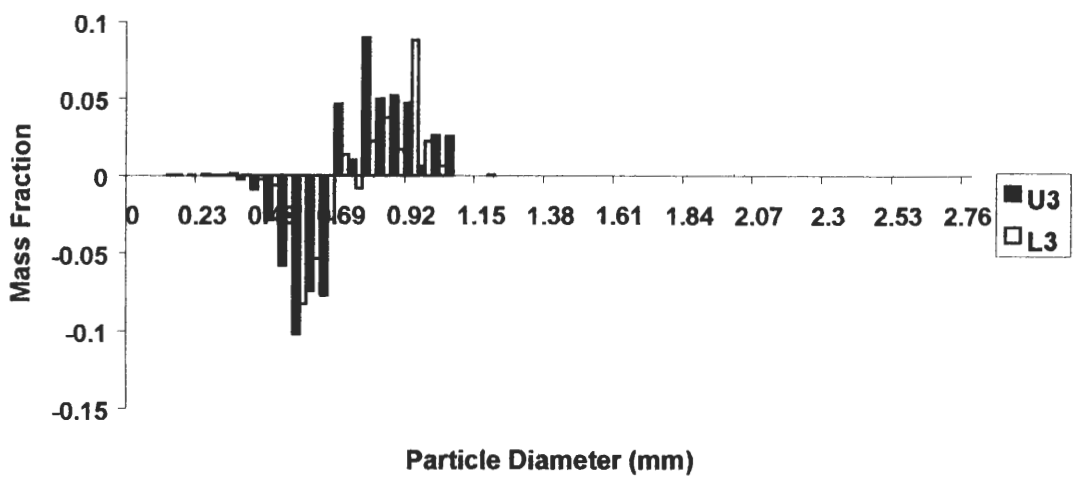

Figure A3.3-22 Experiment 4.3 Several seedbed particles (negative) grew to form larger particles (positive)

3.4.5 Experiment 5

Experimental Conditions: F_o=1.1g/s, u_o=100cm/s, ΔT=260°C

5.1

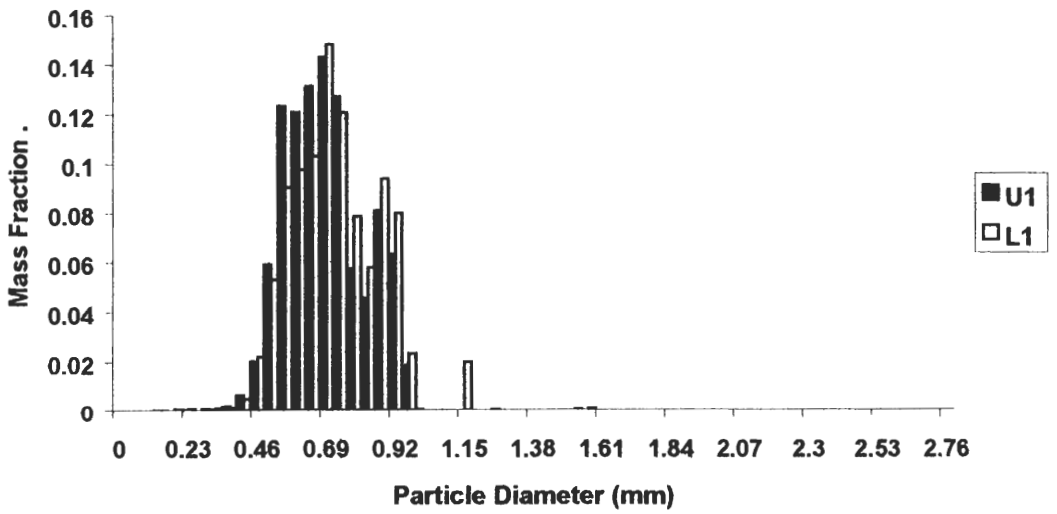

Figure A3.3-23 Experiment 5.1 Upper and lower particle size distribution at 30s

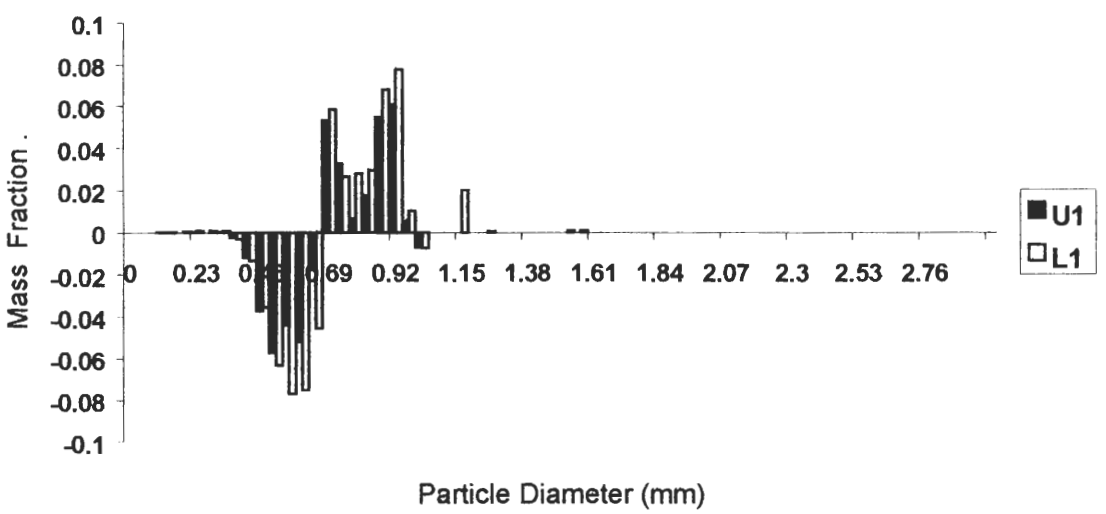

Figure A3.3-24 Experiment 5.1 Several seedbed particles (negative) grew to form larger particles (positive)

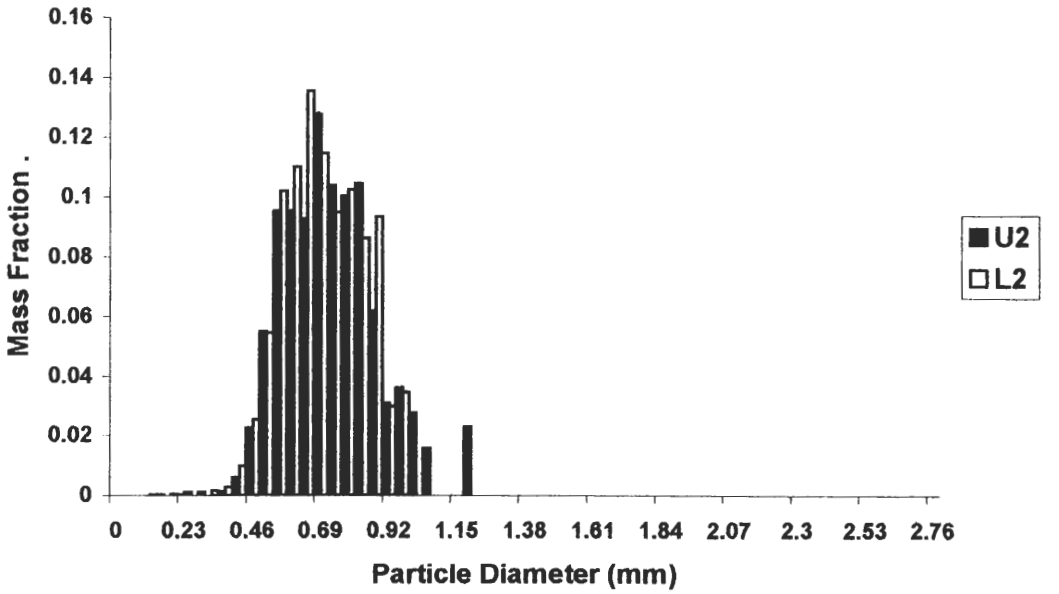

Figure A3.3-25 Experiment 5.2 Upper and lower particle size distribution at 30s

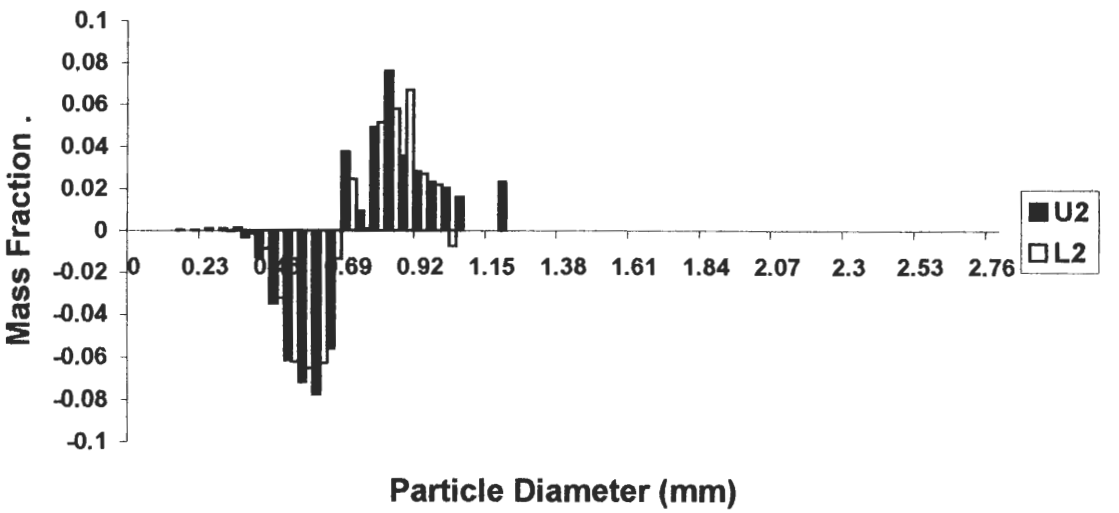

Figure A3.3-26 Experiment 5.2 Several seedbed particles (negative) grew to form larger particles (positive)

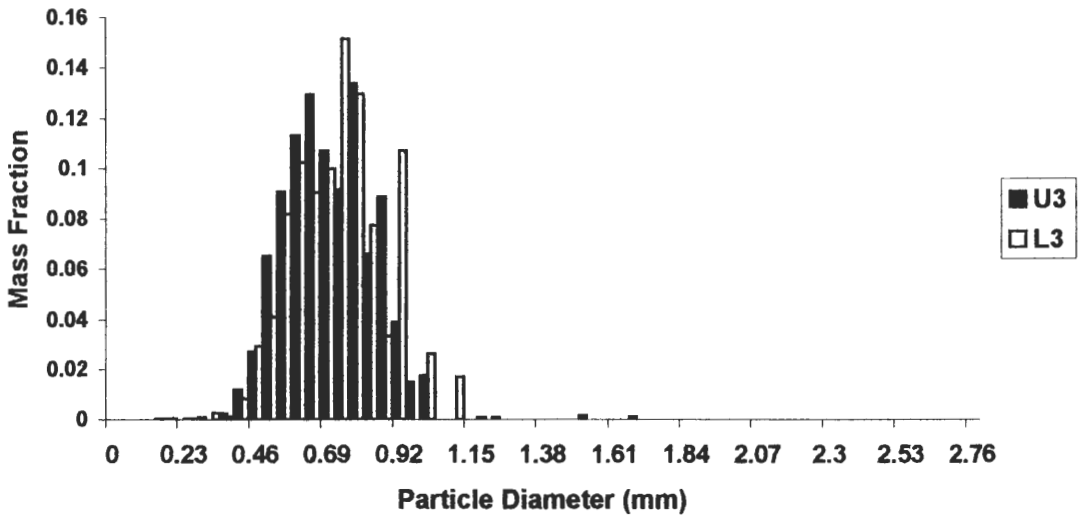

Figure A3.3-27 Experiment 5.3 Upper and lower particle size distribution at 30s

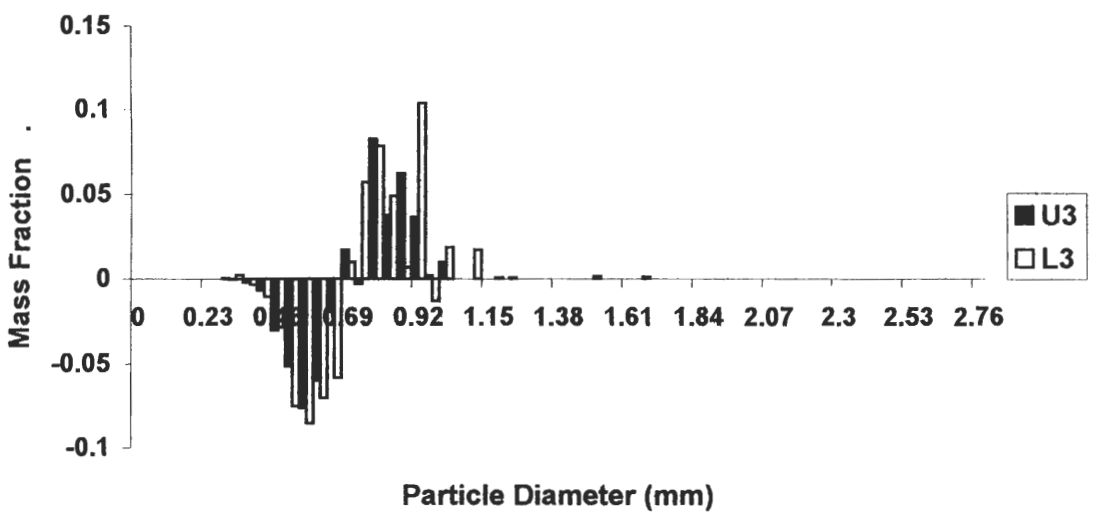

Figure A3.3-28 Experiment 5.3 Several seedbed particles (negative) grew to form larger particles (positive)

3.4.6 Experiment 6

Experimental Conditions: F_o=2.2g/s, u_o=100cm/s, ΔT=300°C

6.1

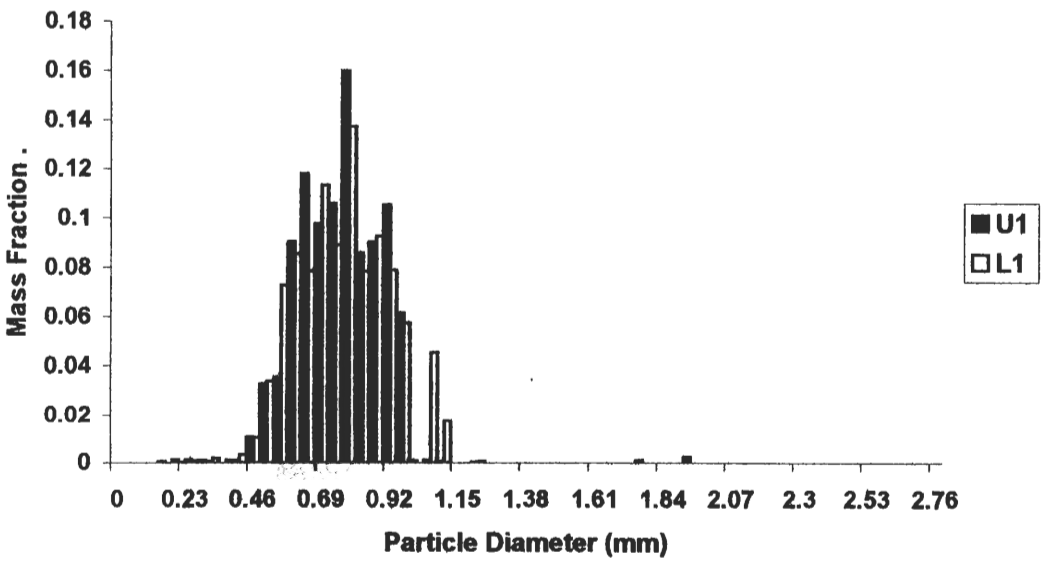

Figure A3.3-29 Experiment 6.1 Upper and lower particle size distribution at 30s

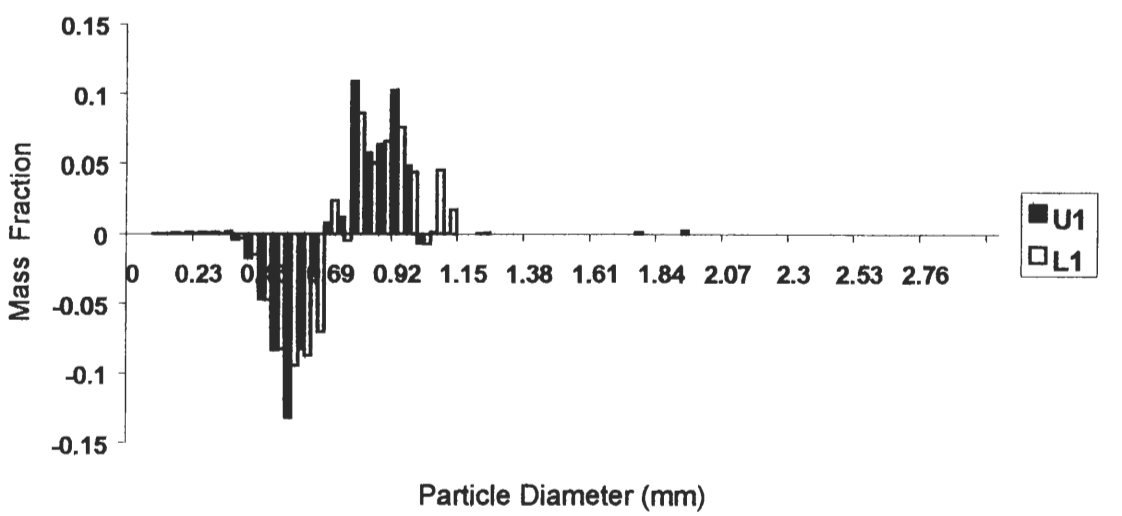

Figure A3.3-30 Experiment 6.1 Several seedbed particles (negative) grew to form larger particles (positive)

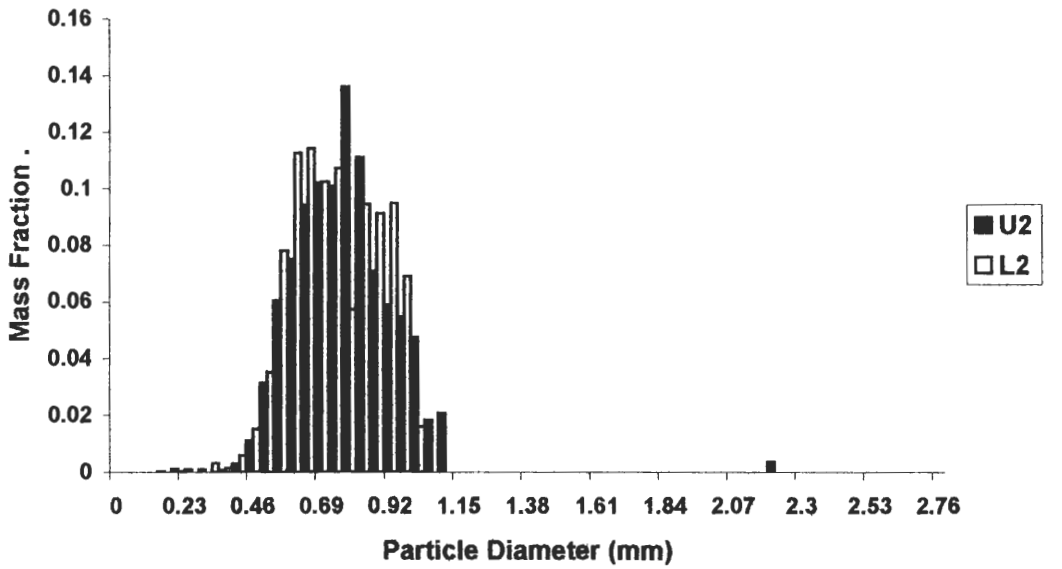

Figure A3.3-31 Experiment 6.2 Upper and lower particle size distribution at 30s

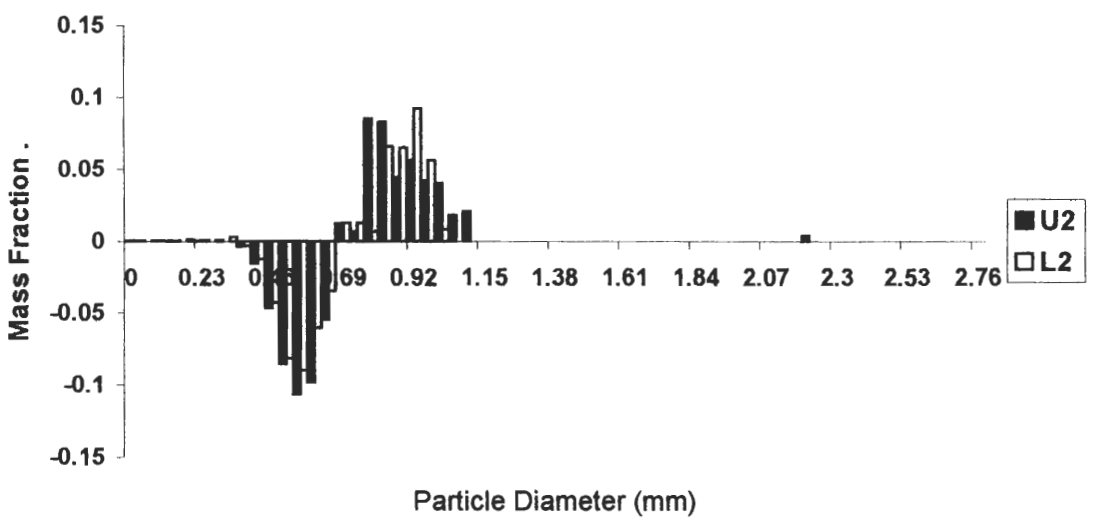

Figure A3.3-32 Experiment 6.2 Several seedbed particles (negative) grew to form larger particles (positive)

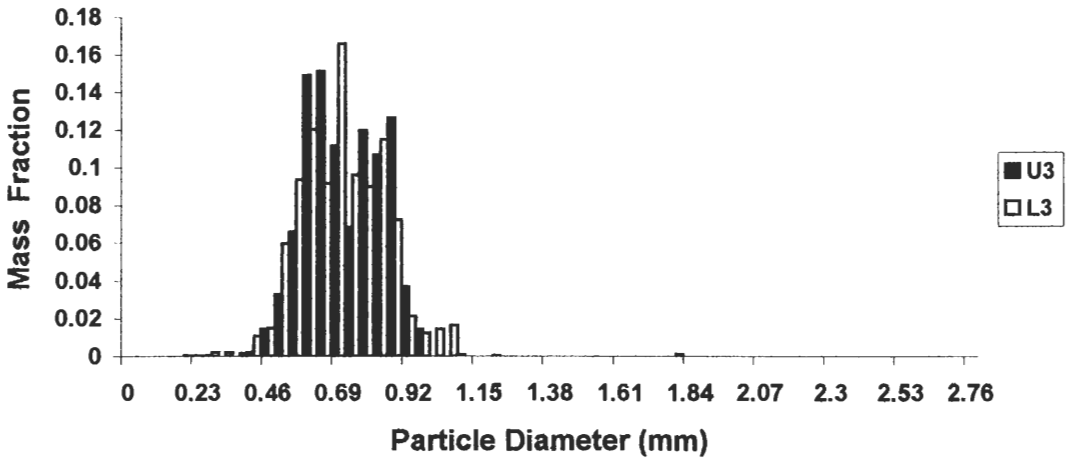

Figure A3.3-33 Experiment 6.3 Upper and lower particle size distribution at 30s

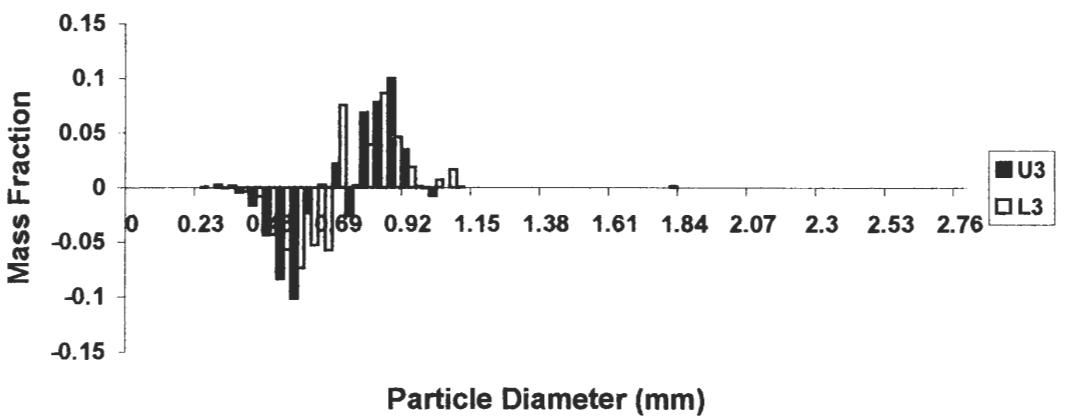

Figure A3.3-34 Experiment 6.3 Several seedbed particles (negative) grew to form larger particles (positive)

3.4.7 Experiment 7

Experimental Conditions: F_o=1.1g/s, u_o=200cm/s, ΔT=300°C

7.1

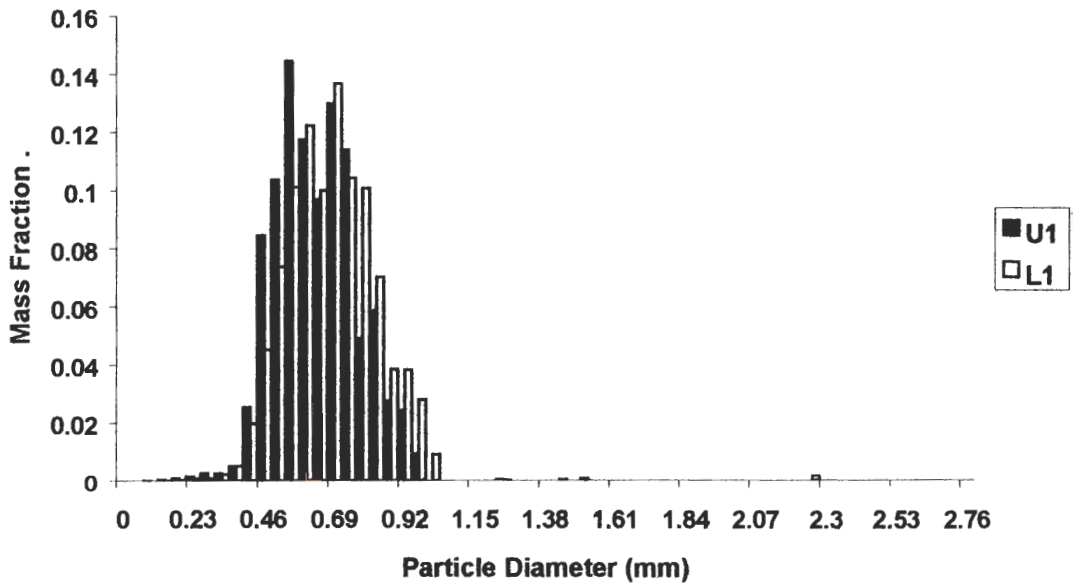

Figure A3.3-35 Experiment 7.1 Upper and lower particle size distribution at 30s

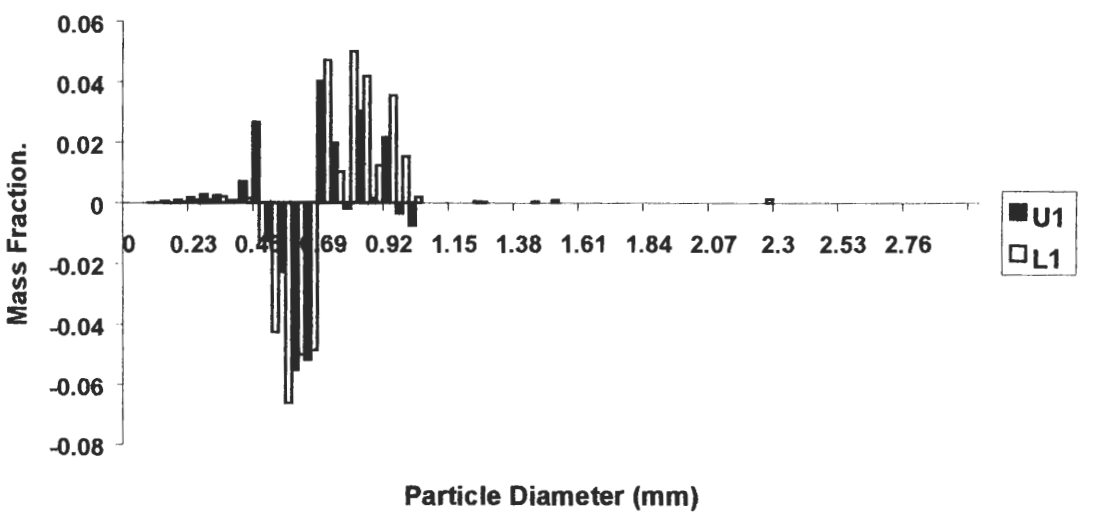

Figure A3.3-36 Experiment 7.1 Several seedbed particles (negative) grew to form larger particles (positive) The positive portion of the histogram on the left side of the distribution is the result of attrition of particles grown in the bed.

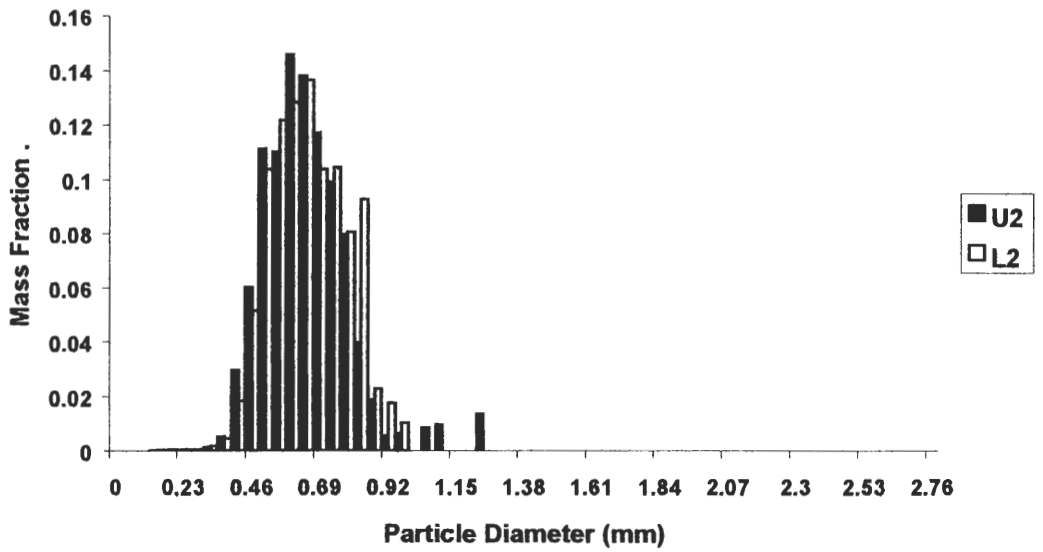

Figure A3.3-37 Experiment 7.2 Upper and lower particle size distribution at 30s

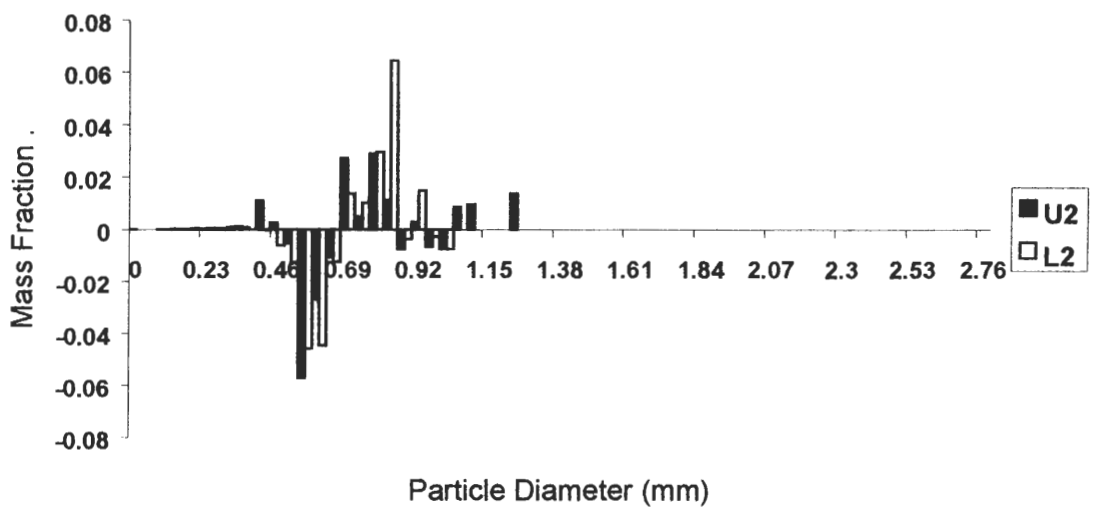

Figure A3.3-38 Experiment 7.2 Several seedbed particles (negative) grew to form larger particles (positive) Particles created to the left side of the distribution are the result of attrition of particles grown in the bed.

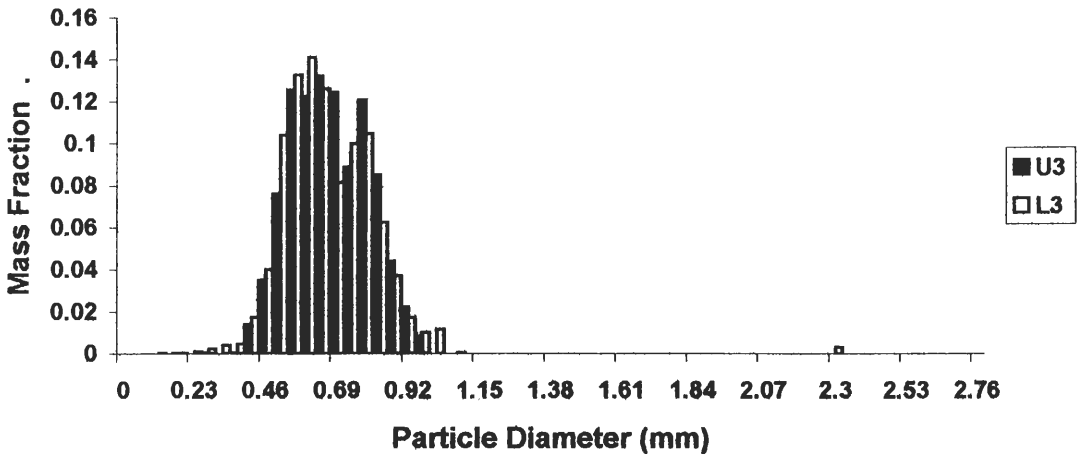

Figure A3.3-39 Experiment 7.3 Upper and lower particle size distribution at 30s

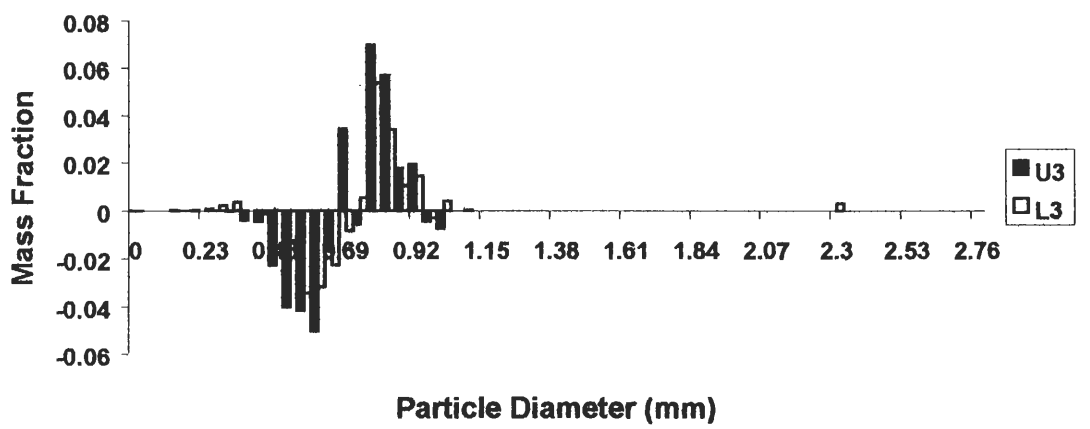

Figure A3.3-40 Experiment 7.3 Several seedbed particles (negative) grew to form larger particles (positive)

3.4.8 Experiment 8

Experimental Conditions: F_o=2.2g/s, u_o=200cm/s, ΔT=300°C

8.1

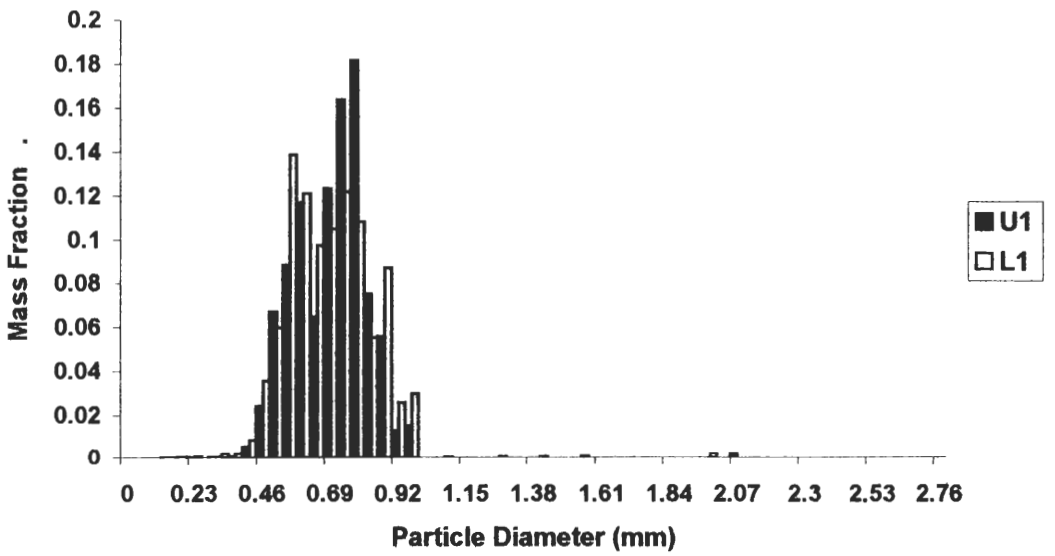

Figure A3.3-41 Experiment 8.1 Upper and lower particle size distribution at 30s

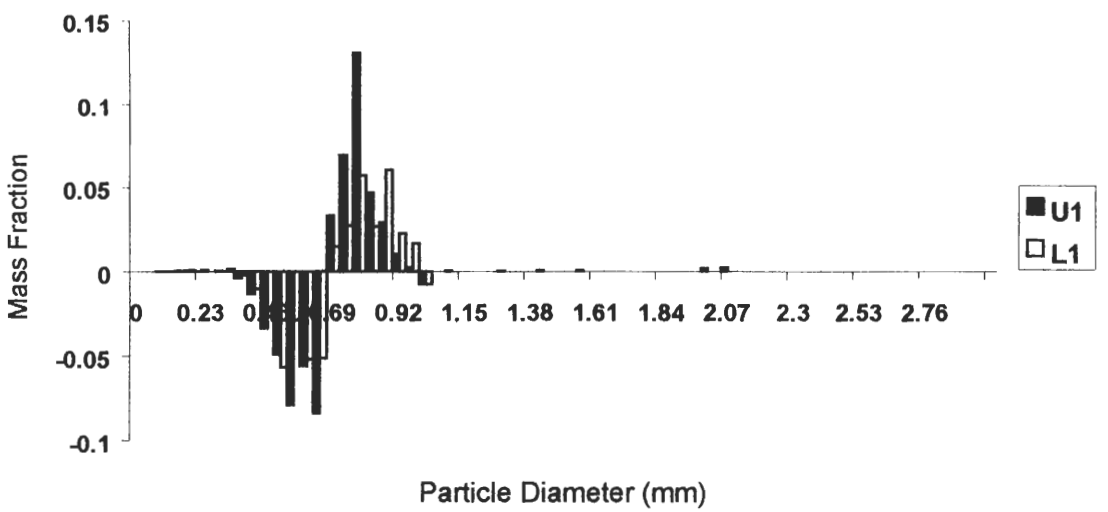

Figure A3.3-42 Experiment 8.1 Several seedbed particles (negative) grew to form larger particles (positive)

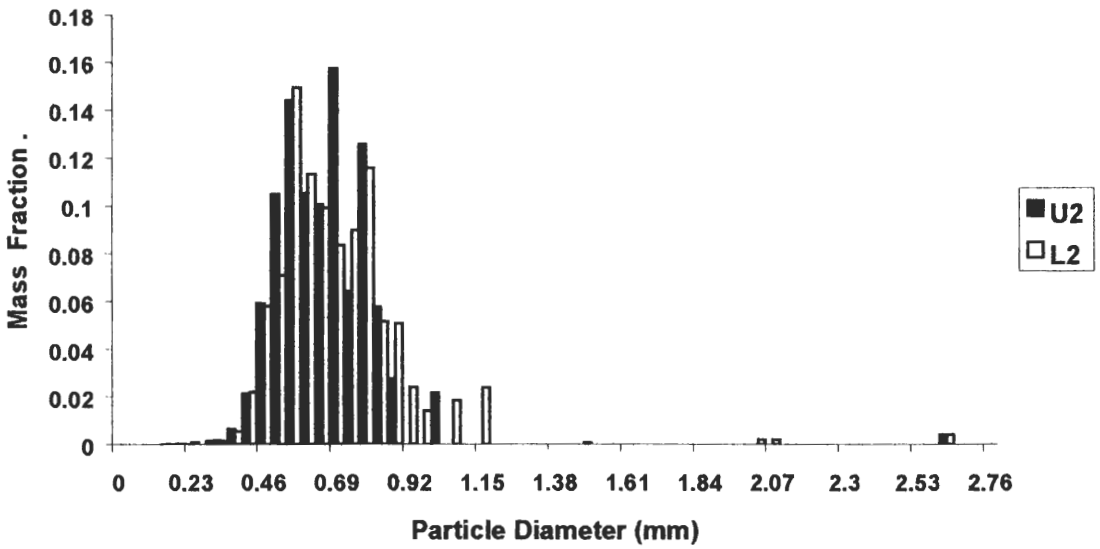

Figure A3.3-43 Experiment 8.2 Upper and lower particle size distribution at 30s

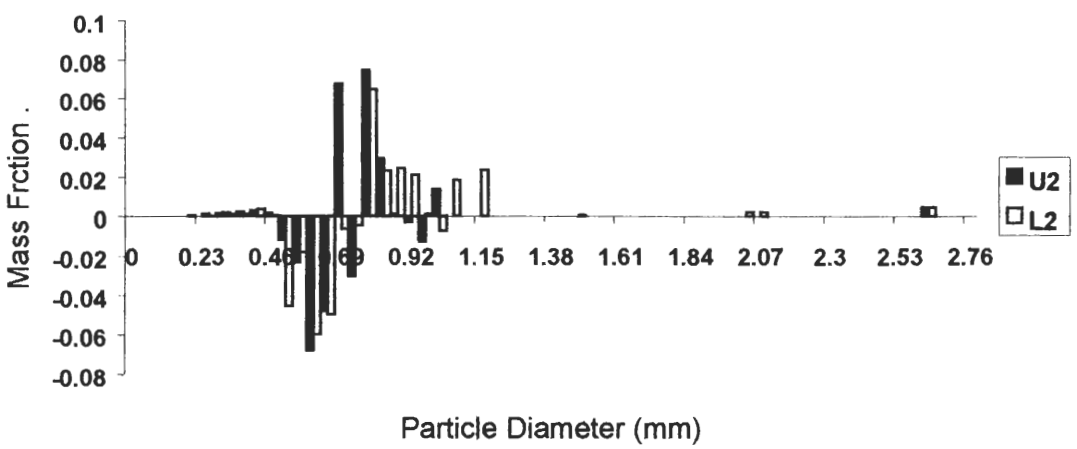

Figure A3.3-44 Experiment 8.2 Several seedbed particles (negative) grew to form larger particles (positive)

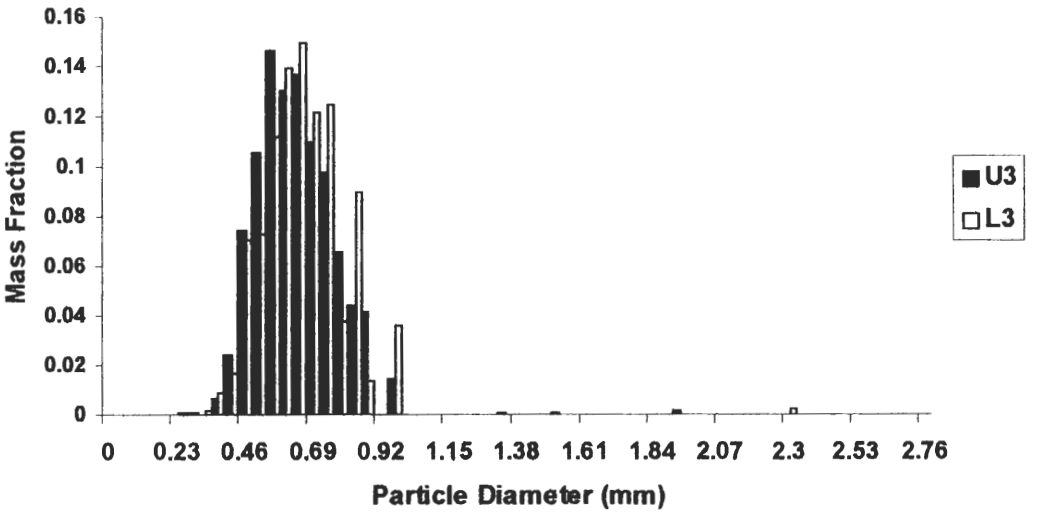

Figure A3.3-45 Experiment 8.3 Upper and lower particle size distribution at 30s

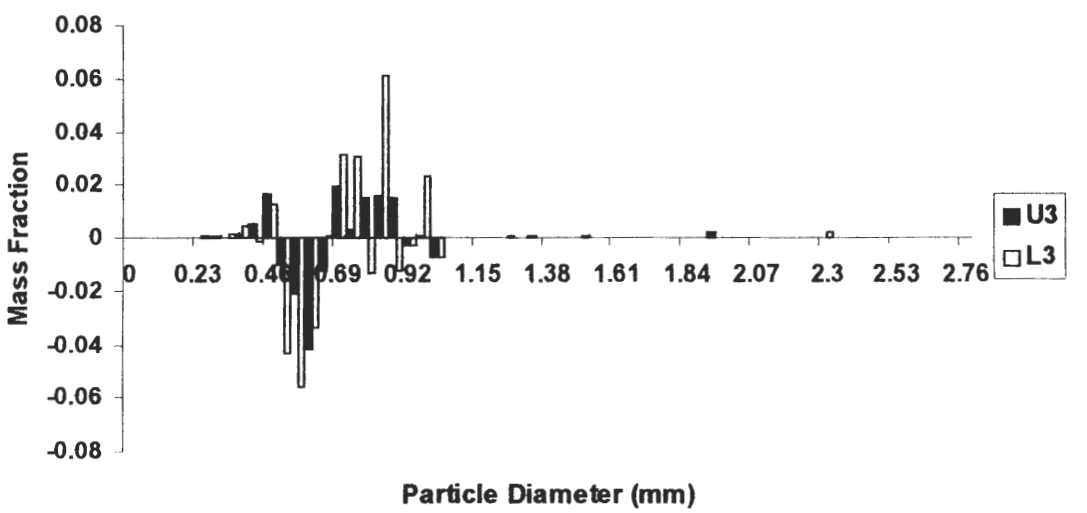

Figure A3.3-46 Experiment 8.3 Several seedbed particles (negative) grew to form larger particles (positive)

Table A3.3-1. Mean particle diameter absorbed to form agglomerates and the mean diameter of agglomerates formed (mm)

EXPERIMENT	SAMPLE POSITION	PARTICLES GROWN		PARTICLES FORMED	
		$\bar{d}_{Pa}$ (mm)	σ (mm)	$\bar{d}_{Pf}$ (mm)	σ (mm)
1	U	0.55	0.06	0.85	0.1
	L	0.56	0.06	0.88	0.1
2	U	0.54	0.06	0.86	0.08
	L	0.57	0.07	0.83	0.06
3	U	0.55	0.06	0.86	0.04
	L	0.56	0.07	0.9	0.07
4	U	0.57	0.06	0.9	0.11
	L	0.59	0.06	0.87	0.06
5	U	0.55	0.06	0.86	0.09
	L	0.56	0.06	0.91	0.07
6	U	0.55	0.07	0.91	0.09
	L	0.56	0.06	0.82	0.09
7	U	0.69	0.05	0.89	0.08
	L	0.58	0.1	0.89	0.14
8	U	0.59	0.1	0.83	0.06
	L	0.58	0.1	0.88	0.15

A3.4 Analysis of Variance Performed on Particle Growth Rates

Table A3.4-1. Analysis of variance results for 2^4 factorial experiment where the main effects and interaction effects of the following parameters was analyzed

		Low	High	
A	Molten Feed Rate	1.1	2.2	g/s
B	Superficial Gas Velocity	1000	2000	mm/s
C	Molten Feed Temperature	38	78	C
D	Sampling Position	-391	-324	mm

Source of Variation	Effects	Sum of Squares	d.o.f.	Mean Square	Computed f	Critical f
A	9.39	470.25	1	470.25	23.47	95%
B	-18.50	2736.52	1	2736.52	136.55	4.21
C	1.84	27.20	1	27.20	1.36	
D	6.15	201.80	1	201.80	10.07	99%
						7.68
AB	-5.15	212.18	1	212.18	10.59	
AC	4.09	89.27	1	89.27	4.45	
AD	0.79	3.32	1	3.32	0.17	
BC	4.14	91.25	1	91.25	4.55	
BD	-2.97	70.51	1	70.51	3.52	
CD	2.25	27.06	1	27.06	1.35	
ABC	0.27	0.38	1	0.38	0.02	
ABD	-1.19	11.31	1	11.31	0.56	
ACD	-3.97	84.06	1	84.06	4.19	
BCD	-1.56	13.02	1	13.02	0.65	
ABCD	1.86	18.40	1	18.40	0.92	
Error		541.07	27	20.04		
Total		4597.59	42			